Characterization of a novel lysine acetylation site in the N-terminal domain of the centromeric histone variant Cse4 in *Saccharomyces cerevisiae*

Dissertation
zur Erlangung des akademischen Grades

doctor rerum naturalium
(Dr. rer. nat.)

im Fach Biologie

eingereicht an der
Lebenswissenschaftlichen Fakultät
der Humboldt-Universität zu Berlin

von

Juliane Pöpsel

Präsident der Humboldt-Universität zu Berlin
Prof. Dr. Jan-Hendrik Olbertz

Dekan der Lebenswissenschaftlichen Fakultät
Prof. Dr. Richard Lucius

Gutachter/innen:

1. Prof. Dr. Ann Ehrenhofer-Murray
2. Prof. Dr. Peter Bayer
3. Prof. Dr. Harald Saumweber

Tag der mündlichen Prüfung:

07.07.2015

Abstract

The centromeric regions of eukaryotic chromosomes are essential for proper chromosome segregation during mitosis. The nucleosomal composition in these regions differs from canonical nucleosomes in that histone H3 is replaced by the conserved centromeric variant CENP-A (Cse4 in *Saccharomyces cerevisiae*), which is the most prominent epigenetic feature of centromeres. The CENP-A N-terminal domain is larger than canonical histone tails as the centromeric histone variants of higher eukaryotes. A functionally critical part of this flexible, positively charged histone tail is the essential N-terminal domain (END). Interestingly, arginine 37 (R37) residing in this region was previously found to be methylated and to act as an epigenetic regulator of kinetochore recruitment and chromosome segregation. Lysine 49 (K49) was defined as an acetylation site, but this modification remained to be characterized in detail.

In this study, it was shown that Cse4K49 acetylation depends on the histone acetyltransferase (HAT) Gcn5, and that in this context the enzyme acts within the SAGA/SLIK complex, whereas an involvement of the smaller ADA complex was not observed. Furthermore, a cell-cycle dependence of the K49 acetylation was found, with acetylation levels increasing in early S-phase and a decreasing in late S-phase, while R37 methylation persisted throughout the entire S-phase. Furthermore, direct protein-protein interactions were investigated via peptide pull-down experiments of Cse4 with kinetochore components. Ctf19 was found to bind both acetylated and unacetylated Cse4K49 with a preference for unacetylated Cse4. The analysis of secondary structural elements of the Cse4 N-terminus via CD-spectroscopy showed that the N-terminus is an intrinsically unstructured domain, which may fold upon binding to interaction partners like Ctf19.

Taken together, the findings presented here show that the transcriptional co-activator complex SAGA functions at centromeric regions in *S. cerevisiae*, and that the Cse4K49 acetylation (Cse4K49ac) has an influence on the recruitment of the kinetochore subunit Ctf19. This suggests an epigenetic regulatory mechanism in chromosome segregation involving a specific acetylation on the N-terminus of Cse4.

Zusammenfassung

Die zentromerischen Regionen eukaryotischer Chromosomen sind notwendig für die Segregation der Schwesternchromatiden während der mitotischen und der meiotischen Zellteilung. In den Nukleosomen in diesen Regionen ist das kanonische Histon H3 durch die in allen Eukaryoten hochkonservierte zentromerische Variante CENP-A (Cse4 in *Saccharomyces cerevisiae*) ersetzt. Indem CENP-A die Assemblierung einzelner Untereinheiten des Kinetochors vermittelt, markiert es die zentromerische Chromosomenregion und ist damit essentiell für die korrekte Segregation der Chromosomen während der Zellteilung. Kürzlich wurde gezeigt, dass Cse4 posttranslational modifiziert wird. Von Bedeutung für diese Arbeit sind die in einer essentiellen Domäne des N-terminus liegende Methylierung von Arginin 37 (R37) und die Acetylierung von Lysin 49 (K49), die durch phänotypische Suppression eine genetische Interaktion und eine antagonistische Funktion bei der epigenetischen Regulation der Assemblierung der Kinetochoruntereinheiten zeigen.

In dieser Arbeit wurde gezeigt, dass die Acetylierung an Cse4K49 von der Histonacetyltransferase (HAT) Gcn5 abhängt, und dass dieses Enzym hierbei Komponenten des SAGA-Komplexes, aber nicht des ADA-Komplexes benötigt. Außerdem konnte in dieser Arbeit nachgewiesen werden, dass die Acetylierung von K49 in der frühen S-Phase zunimmt und am Ende der S-Phase abnimmt. Die Methylierung von R37 hingegen ist während der gesamten S-Phase erhöht. Es konnte weiterhin eine biochemische Interaktion der N-terminalen Domäne von Cse4 mit der COMA-Untereinheit Ctf19, der zentralen Region des Kinetochors, nachgewiesen werden, möglicherweise mit einer Präferenz zu einer nicht acetylierten Form von Cse4K49. Schließlich wurde per CD-Spektroskopie gefunden, dass die N-terminale Domäne von Cse4 intrinsisch unstrukturiert ist.

Zusammenfassend konnte in dieser Arbeit gezeigt werden, dass der SAGA Komplex eine Funktion an der zentromerischen Region in *S. cerevisiae* aufweist. Des Weiteren ist die Acetylierung an Cse4K49 (Cse4K49ac) in der Rekrutierung der Kinetochoruntereinheit Ctf19 involviert, und legt damit einen neuen epigenetischen Regulationsmechanismus während der Chromosomensegregation nahe.

Table of Contents

List of Tables

List of Figures

Abbreviations

5-FOA	5-fluoro-orotic acid
aa	amino acid
ac	acetylation (eg. Cse4 K49 = Cse4 K49ac)
ACN	acetonitrile
ADA	adaptor
AT-rich	adenine thymine-rich
ATP	adenosine triphosphate
bp	base pair
CATD	centromere associated targeting domain
Cbf1	centromere binding factor 1
CDEI/II/III	centromere DNA element I/II/III
CenH3	centromeric histone H3
CENP-A	centromere protein A
Co-IP	co-immunoprecipitation
COMA	Ctf19/Okp1/Mcm21/Ame1
Cse4	chromosome segregation 4
DNA	deoxyribonucleic acid
DTT	di-thiothreitol
END	essential N-terminal domain in Cse4
FACS	fluorescence associated cell sorting
FPLC	Fast Performance Liquid Chromatography
Gcn5	general control nonderepressible 5
HAT	histone acetyltransferase
HDAC	histone deacetylase
HJURP	Holliday Junction Recognition Protein
HML	homothallic mating left
HMR	homothallic mating right
HP1	Heterochromatin Protein 1
HPLC	High Performance Liquid Chromatography
HU	hydroxyurea
IP	immunoprecipitation
LB	Luria-Bertani
Mbp	mega base pair
me	methylation (eg. Cse4R37 = Cse4R37me)
me3	trimethylation

MNase	micrococcal nuclease
MS	mass spectrometry
MTF	methyltransferase
nm	nano meter
NP-40	Nonidet P-40
OD	optical densitiy
ORF	open reading frame
otr	outer repeats
PBS	phosphate buffer saline
PCR	polymerase chain reaction
pmol	pico mole
PTM	posttranslational modification
PVDF	polyvinylidene fluoride
RNA	ribonucleic acid
rpm	rounds per minute
RT	room temperature
SAC	spindle assembly checkpoint
SAGA	Spt–Ada–Gcn5 acetyltransferase
SAM	S-adenosyl-L-methionine
SDS-PAGE	sodium dodecyl sulfate polyacrylamide gel electrophoresis
SLIK	SAGA-like
TE	Tris-HCL/EDTA buffer
TFA	trifluoroacetic acid
ts	temperature sensitive
wt	wild-type
YM	yeast minimal medium
YPD	yeast peptone medium

The nomenclature of yeast (Saccharomyces cerevisiae) proteins was taken from the Saccharomyces cerevisiae genome database (SGD). Amino acids were given in the single-letter code, e.g. K = lysine, R = arginine.

1. Introduction

1.1. Eukaryotic chromatin organization

The DNA of every cell in a eukaryotic organism comprises all the genetic information it requires to perform essential processes. It is organized in the form of genes, which are defined as the coding regions for proteins and the associated regulatory sequences, such as the promoter regions. It is compacted with histones and non-histone proteins to form chromosomes. The entirety of the DNA of one organism is referred to as the genome, and the genome of human somatic cells, the diploid chromosome set, consists of 46 chromosomes, two of which are the sex chromosomes. The DNA is packaged tightly in the nucleus, if one considers that all of the DNA molecules in one human cell consist of 3.27 Gbp, i.e. 3.27 billion base pairs, but fits into a nucleus with 1-5 µm diameter. Unexpectedly, this enormous amount of DNA only comprises about 30,000 – 40,000 genes, which code for about 100,000 proteins. This implies that most of the human genome is composed of non-coding regions (Lander et al., 2001).

Among eukaryotes, vertebrates and higher plants have the largest genomes and numbers of chromosomes per cell. Interestingly, the human genome contains only twice as many protein coding genes than that of the fruit fly *Drosophila melanogaster*, suggesting that more than just the DNA sequence is needed for generating the variety of information that results in a complex eukaryotic organism (reviewed in Jenuwein and Allis, 2001). The DNA is associated in a nucleoprotein complex with non-histone proteins and histones, referred to as chromatin, which provides the compaction of the DNA. DNA packaging is not static but highly dynamic and thus contributes to gene regulation by regulating the accessibility of the genetic information. This additional level of genetic information and regulation, termed “epigenetic”, is defined as heritable changes in phenotype that are not due to changes in the DNA sequence itself.

In comparison to higher eukaryotes, the budding yeast *Saccharomyces cerevisiae* possesses a relatively small genome of only 12.1 Mbp of DNA per cell, carrying about 6.300 genes. On its 16 chromosomes, most of the DNA codes for proteins and

therefore, a comparably small amount of the DNA of this unicellular organism comprises non-coding regions. This simplicity makes the yeast a tractable model system for genetic and biochemical studies. The budding yeast genome was the first eukaryotic genome to be completely sequenced in 1996 (Goffeau et al., 1996).

Each cell has to accomplish a DNA condensation process that demands high accuracy and fidelity. The basic level of condensation is conferred by the canonical nucleosome, a structure of 145-147 bp of the DNA double helix wrapped around one core particle 1.7 times in a left-handed manner. The core particle is composed of histone proteins, with two copies each of H2A, H2B, H3 (in human H3.1) and H4. The structure of this nucleosome core particle was first solved at 2.8 Å resolution by Luger et al., 1997 (Figure 1).

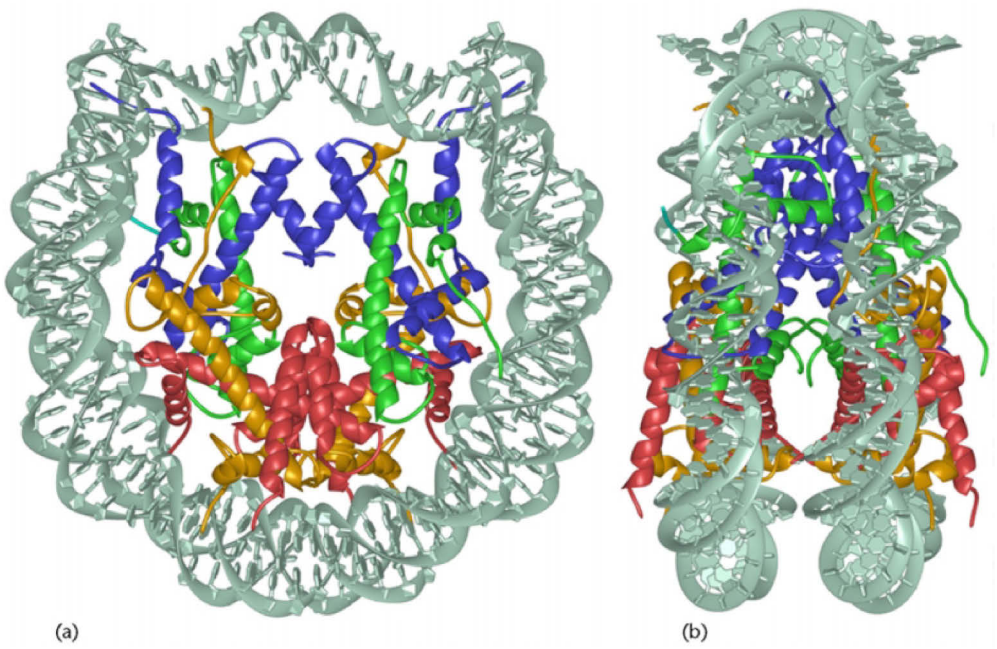

Figure 1: High-resolution crystal structure of the nucleosomal core particle
Core particle structure viewed in two orientations. (a) View down the superhelical axis; (b) 90° rotation of the y-axis to highlight the flat, disc-like shape of the nucleosome. H3 and H4 make up two heterodimers and are shown in blue and green, respectively. H2A and H2B, which also form two heterodimers, are shown in yellow and red, respectively. The DNA double helix is depicted in grey. Taken from (Luger, 2001).

The topology of the nucleosome core particle reflects its function. For example, the histone fold domains (HFDs) allow the association of the eight histones and a left-handed, approximately two fold winding of the DNA around the histone hetero-octamer to constitute an overall globular structure. HFDs are characterized by one

central α-helix flanked by two shorter α-helices. Additionally, there are neighboring β-strands N-terminal to the HFD in H3, at the C-terminal region of H2B and on both sides flanking the globular domain in H2A, shown in Figure 2 (Arents and Moudrianakis, 1995; Luger et al., 1997).

The flexible, less structured histone tails mediate physical interactions with associated proteins and DNA. They can be posttranslationally modified in many ways, which drives the dynamics of chromatin condensation, active transcription, gene silencing and chromosome segregation. Histones can be exchanged, and the newly synthesized and reassembled histones may carry modifications that are distinct from the displaced histone. In other cases, histone variants are recruited to chromatin to replace canonical histones. The concerted placement and the combination of canonical histones and histone variants as well as their covalent modification patterns reflect the epigenetic chromatin status of a cell (reviewed in Jenuwein and Allis, 2001; Kouzarides, 2007).

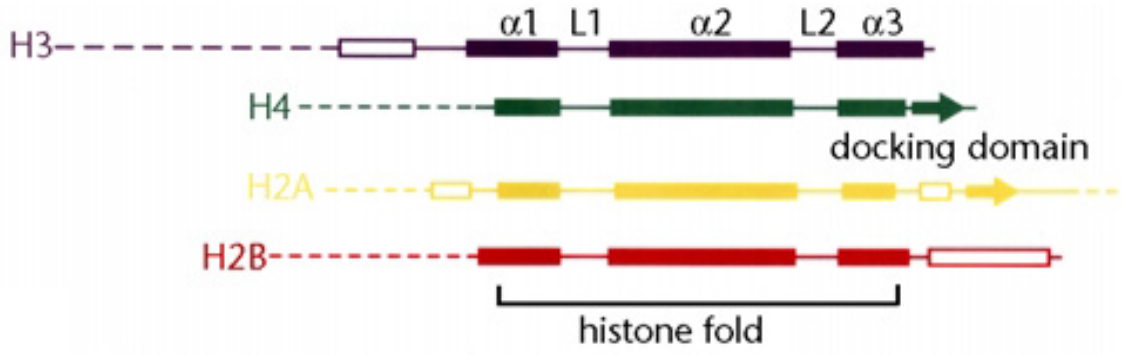

Figure 2: Histone fold architecture

Domain organization of the four canonical histones H3, H4, H2A and H2B. α-helices of the histone fold domains are shown as solid boxes, loops between the helical regions are termed L1 and L2; α-helices and β-strands of the histone fold extensions are shown as open boxes and tails of the histones are shown as dotted lines. Adapted from Luger, 2001.

The first level of DNA compaction are the nucleosomes, which are arranged in a beads-like substructure and are 11 nm in width, shown in Figure 3A (Wang et al., 2008). With the assistance of the highly basic linker histone H1, the next higher order of chromatin structure, the 30 nm fiber, is established. Histone H1, which exhibits no structural homology with core histones, associates at the dyad axis of the nucleosome core engaging a short linker DNA sequence (Allan et al., 1980; Bednar et al., 1998; Richmond and Davey, 2003; Khorasanizadeh, 2004). Histone H1

proteins are conserved among eukaryotes structurally, but not in their amino acid sequence (Maeder and Bohm, 1991). The yeast H1, termed Hho1, and the human H1 are both non-essential proteins, indicating that besides the association of H1 to the nucleosomes, additional processes must be crucial for chromatin condensation. For example, physical interactions of the N-terminal domains of the four core histones could drive the condensation process, while H1 stabilizes higher order chromatin structures (Shen, 1995). Whereas H1 of most species assembles approximately in a 1:1 stoichiometry with nucleosomes, Hho1 is found in yeast chromatin at an average frequency of every 37th nucleosome only and its distribution is restricted to distinct genomic (Patterton et al., 1998; Freidkin and Katcoff, 2001). This observation supports the notion that Hho1 association is auxiliary, but not essential for higher chromatin compaction, or that Hho1 serves a specific purpose yet to be characterized. Experimental data showed that 30 nm chromatin fibers could be assembled *in vitro* in the presence and in the absence of this linker histone H1, but the reconstituted fibers differed in their quaternary structures (Schalch et al., 2005; Huynh et al., 2005; Pepenella et al., 2014).

The structure of the next higher level of compaction, the 30 nm fiber, has long been a matter of debate in the chromatin field, and different models have been proposed. The two prevailing models are the one-start stack solenoid model, and the two-start stack zigzag model, which comprise two subclasses of chromatin structures (Finch and Klug, 1976).

The fiber of the first group is composed of a one-start helical stack of nucleosomes, is shaped like a helical ribbon, and the compaction of this model is higher than in the second group, the cross-linker model (Felsenfeld and McGhee, 1986). The latter group is organized as two-start helix. During the reconstitution process, this structure was generated using long stretches of linker DNA exceeding 217 base pairs, which span the fiber crosswise (Robinson and Rhodes, 2006). With respect to the latter model, the structure prediction depends considerably on the DNA linker lengths that lead to different structures of the 30 nm fiber (Bednar et al., 1998; Wu et al., 2007).

A recently published cryogenic electron microscopy (cryo-EM) structure demonstrated repeating tetranucleosomal units, which coil in a left-handed twist. Here, the nucleosomes zigzag back and forth, with the linker Histone H1 and straight

linker DNA between the core nucleosomes. The whole structure is essentially compatible with the two-start zigzag model (Song et al., 2014; Figure 3 B).

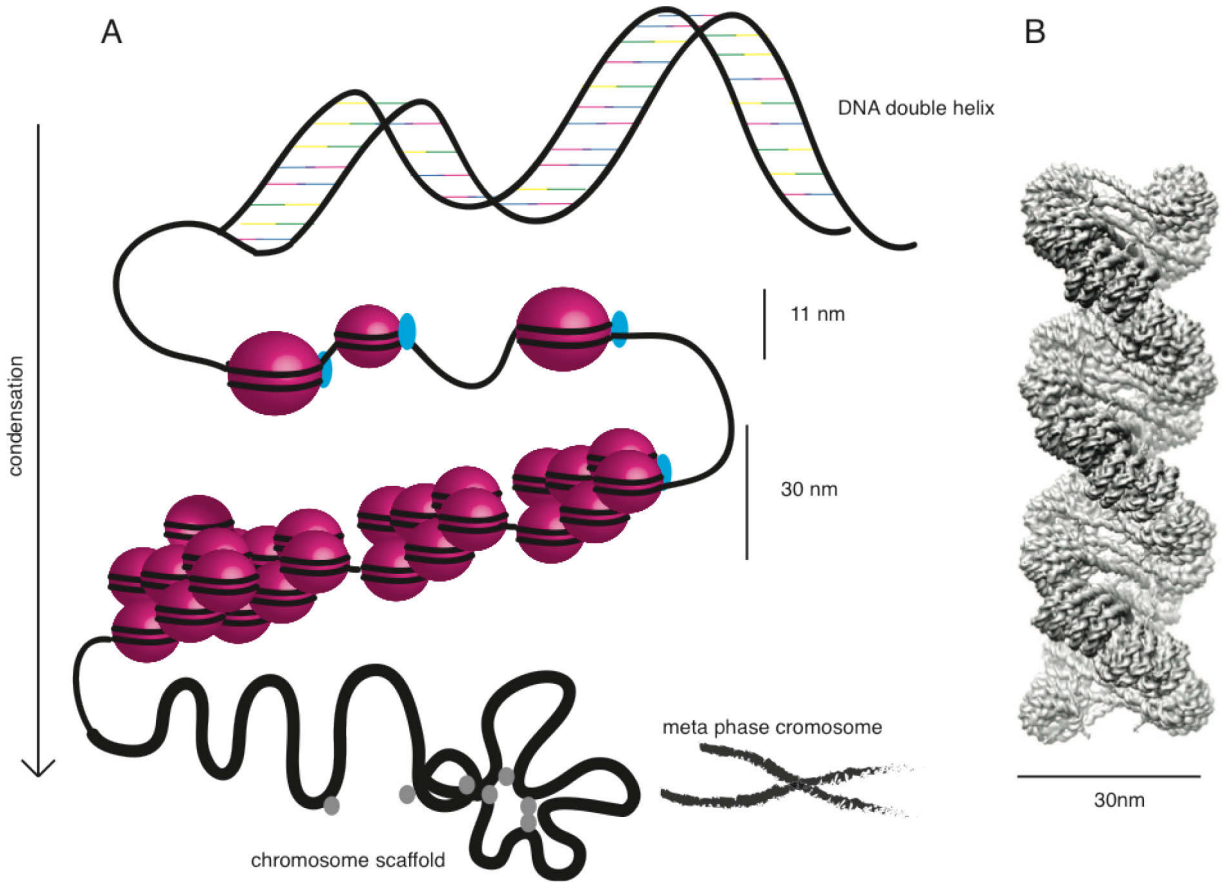

Figure 3: Chromatin organization in eukaryotes.

A: The figure schematically illustrates the successive chromatin condensation levels in eukaryotes. The basis is build by DNA (black lines) and histone octamers (pink bubbles), which assemble into nucleosomes and make up the 11 nm fiber together with histone H1 (light blue). This structure is further organized into the 30 nm fiber. Subsequently and with the help of non-histone proteins, which form the chromosome scaffold, the condensation to higher organized chromatin is achieved. The metaphase chromosome (Modified from http://dellairelab.medicine.dal.ca/research.html) marks the final state of condensation. B: 30nm chromatin fiber model, cryo-EM reconstruction of *in vitro* reconstituted chromatin. Taken from (Song et al., 2014).

Higher order folding occurs in the presence of the two major chromosome scaffold components, topoisomerase II and condensin, and is defined as the further compaction of 30 nm fiber loops which associate on the scaffold. However, whether or not the 30 nm fiber structure persists upon higher order chromatin folding *in vivo* has been a matter of controversy (Maeshima et al., 2010; Nishino et al., 2012). Recent studies have provided new insights into the mode of condensation in mitosis. Condensin shows ATPase activity and binds directly to DNA molecules. It actively

supercoils DNA *in vitro* and is required for establishing the mitotic chromosome structure and for the process of chromosome segregation *in vivo* (Kimura et al., 1999; Hagstrom et al., 2002). Our understanding of higher order chromatin compaction is still lacking detail as compared to the first levels of condensation. The loops of the chromosome scaffold appear to be regularly folded. The localization of genomic loci and the distances between those loci are highly variable in the nucleus and also vary among organisms. The folding processes of interphase and mitotic chromosomes are being investigated in the physical field of complex polymer systems. Along with optical as well as electron microscopic techniques, these approaches promise substantial insights into the mechanisms of chromosome packaging in the future (Berger et al., 2008; Trask et al., 1993; Fudenberg and Mirny, 2012).

1.2. Classes of chromatin

Eukaryotic chromatin can acquire various degrees of compaction, which are generally distinguished into two forms: the closed, highly compacted heterochromatin, and the euchromatic regions (Heitz, 1928; Brown, 1966). The latter can be defined as open, decondensed chromatin marked by a high rate of gene transcription. One mark of active transcription in human cells is the occurrence of the histone variant H3.3, which replaces the replicative H3.1 variant at these sites (Ahmad and Henikoff, 2002). The distribution of functional, protein-coding genes is unequal in favor of the euchromatic regions of the chromosome, shown by the fact that 2.9 Gbp (more than 90% of the whole genome sequence length) of chromatin appears to be euchromatic (Lander, E.S., International Human Genome Sequencing Consortium, 2001).

Two forms of heterochromatin can be distinguished. One is referred to as constitutive, which means that it serves structural purposes important for genome integrity, and it is mostly found at the telomeric or pericentromeric regions of a chromosome (Trojer and Reinberg, 2007; Grewal and Jia, 2007). The second form, termed facultative heterochromatin, is marked by direct gene silencing and the possible switch between active and inactive chromatin. This reversible process is strongly regulated by several chromatin remodeling complexes. Their activity is, in

turn, tightly regulated by the absence or presence of posttranslational modifications (PTMs) of histones mediated by chromatin modifying enzymes, and also by the occurrence of histone variants. For example, it has been shown that H3K4 methylation characterizes actively transcribed gene regions, whereas H3K9 methylation marks heterochromatin (Barski et al., 2007). Upon the latter modification, which functions as a tether, heterochromatin protein 1 (HP1) is recruited as an adaptor for various effector proteins, such as histone modifiers, cohesin and transcription silencing factors (Grewal and Jia, 2007; Trojer and Reinberg, 2007).

A well-known example for the extensively regulated transcriptional silencing in facultative heterochromatin is the inactivation of the mammalian female X-chromosome, a process known as dosage compensation. Here, in each cell of the female organism, one of the two X-chromosomes is silenced in a cascade of heterochromatin establishment and maintenance processes. It is coated by the noncoding RNA Xist, which induces hypoacetylation on histones and, among others, H3K27 methylation (Chow et al., 2005). The subsequent condensation process is necessary to avoid a double X-chromosomal transcription level in females compared to males. Additionally, the inactive X-chromosome is marked by a histone variant; macro-H2A replaces H2A and participates in the maintenance of X inactivation (Costanzi and Pehrson, 1998; Avner and Heard, 2001).

Histone deacetylation of H4K16 earmarks silent chromatin and is mediated by a histone deacetylase (HDAC) complex, which contains the silent information regulator 2, Sir2, in yeast or its homologue SIRT3 in humans (Gottschling et al., 1990; Imai et al., 2000; Pikaart et al., 1998). In facultative heterochromatic structures, H4K16 acetylation has been shown to counteract hypercondensation, and is mediated in *S. cerevisiae* by a specific histone acetyl transferase, Sas2, which acts in the SAS-I complex (Corona et al., 2002; Sutton et al., 2003; Meijsing and Ehrenhofer-Murray, 2001). The interaction between the deacetylated, positively charged H4 tail and the acidic patch of the H2A-H2B dimer of the neighboring nucleosome contributes to the condensation process. These electrostatic interactions are disturbed upon the acetylation of H4K16 (Shogren-Knaak et al., 2006; Gordon et al., 2005; Robinson et al., 2008). This is in agreement with the findings that *Saccharomyces cerevisiae* cells lacking the H4K16 HAT Sas2 show increased silencing at subtelomeric regions (Suka et al., 2002).

1.3. Centromeric chromatin structure

The composition and function of centromeric chromatin differs from euchromatic or heterochromatic chromatin regions in diverse ways. Due to the fact that low transcription levels are present within these regions, it can be defined as a particular form of heterochromatin. It is demarcated as the essential locus at which kinetochores assemble to build the platform for spindle microtubule attachment to ultimately segregate the highly condensed sister chromatids during mitosis. In humans, centromeric chromatin is embedded in regions of pericentromeric heterochromatin and exhibits a distinct pattern of epigenetic marks in the form of histone variants and posttranslational modifications (Sullivan and Karpen, 2004; Allshire and Karpen, 2008).

The histone variant CENP-A (Centromere Protein-A) replaces histone H3 (H3.1 in human) on centromeres and thereby epigenetically marks centromeres in all eukaryotic organisms (Yoda et al., 2000; Palmer et al., 1987; Earnshaw and Rothfield, 1985). It is responsible for the localization of almost all centromere components, basically the kinetochore subunits (Foltz et al., 2006; Liu et al., 2006). In contrast to the assembly of human H3.1 and H3.3 into canonical nucleosomes, which involves the participation of CAF-1 (Chromatin Assembly Factor-1) and the Histone Regulator A, HIRA, the specific histone chaperone HJURP (Holliday junction recognition protein) is necessary for incorporation of CENP-A into centromeric nucleosomes in early G1 phase (Verreault et al., 1996; Foltz et al., 2009; Bodor et al., 2013; Pchelintsev et al., 2013). Despite only minor homology in their amino acid sequence, the mammalian chaperone HJURP and its fungal orthologue Scm3 (Suppressor of chromosomal missegregation) display corresponding chaperone-like roles for centromere specific nucleosome incorporation of newly synthesized CENP-A histones (Dunleavy et al., 2009; Mizuguchi et al., 2007; Stoler et al., 2007; Williams et al., 2009).

In the large centromeric regions of mammalian and *Drosophila* cells, the replacement of the canonical histone H3 occurs partially, whereas in *Candida albicans* and in the point centromeres of budding yeast, nucleosomes exclusively carrying CENP-A are found as shown in Figure 4 (Blower et al., 2002). Distinct posttranslational modification patterns mark the centromeric sites in chromatin. In contrast to

heterochromatic regions, where H3K9 di- or trimethylation occurs, this PTM is lacking on centromeric heterochromatin, whereas H3K4 dimethylation, a mark of euchromatin, is also found in human and *Drosophila* cells as a feature of the centromeres (Figure 4; Blower et al., 2002; Santos-Rosa et al., 2002). An example of a mitotic feature that marks mitosis but does not mark centromeres is Aurora B mediated H3S10 phosphorylation. This PTM has been shown to correlate with mitosis in all eukaryotes. It recruits the histone deacetylase Hst2, which in turn deacetylates H4K16 and permits chromatin hypercondensation during chromosome segregation in mitosis (Wilkins et al., 2014).

The centromeric regions of eukaryotes differ in size, reaching from single nucleosomes in the point centromeres of budding yeasts to large regional centromeres in higher eukaryotes (Henikoff et al., 2001). In the fission yeast *S. pombe*, the centromeric regions encompass 40 - 110 kb. Heterochromatic regions with methylated H3K9 containing nucleosomes, termed outer repeats (otr), flank the innermost repeats (imr) and the central, non-repetitive core region (cnt). Several copies of the centromeric histone H3 variant CENP-A^{Cnp1} are placed at the core domain and, together with the imr regions, they are crucial for kinetochore assembly (Figure 4, mid panel; Pidoux and Allshire, 2004; Allshire and Karpen, 2008).

The regional centromeres found in humans are particularly complex. The DNA sequence possesses homogeneous arrays of chromosome-specific α-satellite repeats, which are 171 bp in length and are arranged in tandem over a genomic region of about 1500 kb (Figure 4 upper panel). The DNA binding protein CENP-B binds specifically to a 17 bp motif, termed CENP-B box and promotes a higher order centromere chromatin packaging. These structures form the basis for kinetochore and microtubule attachment during mitosis and meiosis (Figure 4 upper panel; Choo, 2001; Schueler and Sullivan, 2006; Allshire and Karpen, 2008).

A special centromere was found in the budding yeast *S. cerevisiae*, which possesses a DNA sequence-dependent point centromere, with a single microtubule attaching to one kinetochore. This strict sequence dependency is unusual and, to our knowledge, occurs only in these unicellular organisms. There are 125 bp of DNA wrapped around the centromeric nucleosome-like structure, and the sequence is divided into three consensus elements, CDEI, II and III (centromere DNA element). CDEI consists of the 8 bp motif 5`- RTCACRTG -3` and has been shown to connect the centromeric

nucleosome to the kinetochore via binding of the inner kinetochore component Cbf1 (Cai and Davis, 1989). CDEII is a 78-86 bp AT-rich element, and deletion or shortening of this element results in strong defects in the segregation of sister chromatids. The 25 bp CDEIII element binds directly to the inner kinetochore complex CBF3, a four subunit, sequence-specific DNA binding protein complex, which is crucial for centromere activity, shown in Figure 4, lower panel (Baker et al., 1989; Fitzgerald-Hayes, 1987).

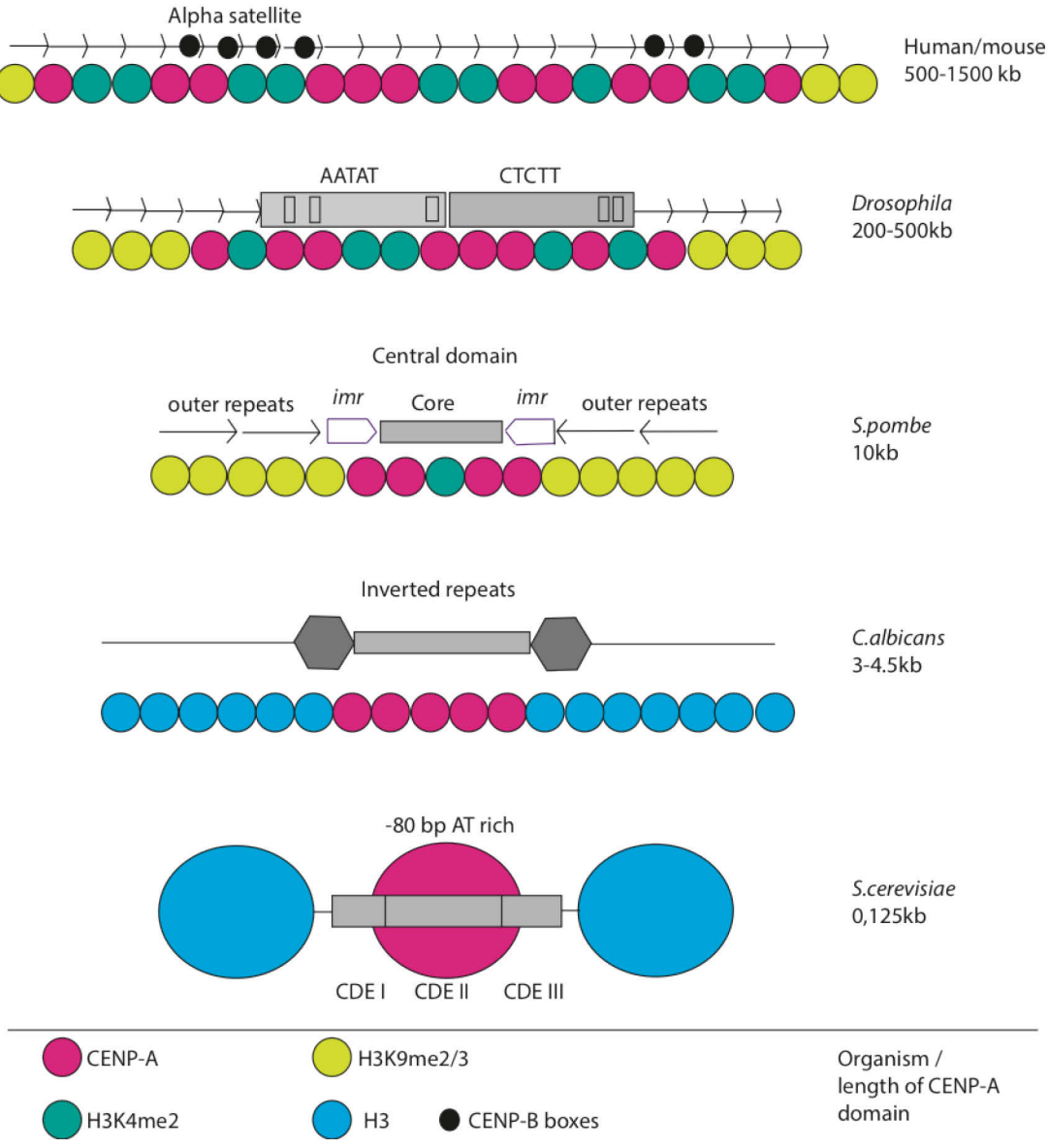

Figure 4: Centromeric regions of eukaryotic organisms.

The centromere diversity among different model organisms is depicted. The yeast *Saccharomyces cerevisiae* contains one CENP-A nucleosome, a `point centromere`, *Candida albicans* and *Schizosaccharomyces pombe* have small regional centromeres. Higher eukaryotes such as insects like *Drosophila melanogaster* up to mammals like *Homo sapiens* show huge and complex centromeric regions. Modified from (Allshire and Karpen, 2008).

1.4. Nucleosome structure at the centromeres

The physical arrangement of centromeric nucleosomes in general has been a subject of controversies for a long time. Several models have been proposed for the nucleosome composition at centromeric regions. The conventional view shows CENP-A nucleosomes in a canonical-like, octameric structure with two copies of H2A-H2B and CENP-A-H4 dimers each and the DNA wrapped around the core in a left-handed manner. This model has been supported by *in vitro* reconstitution studies in budding yeast with its CENP-A homologue CENP-A^{Cse4} as well as by crystal structure analyses using human CENP-A (Figure 5; Camahort et al., 2009; Sekulic et al., 2010) Consistent with these findings, quantitative fluorescence microscopy studies suggested a CENP-A copy number of two per cell (Joglekar et al., 2006; Aravamudhan et al., 2013).

The second proposed centromeric nucleosome structure represents a so-called hemisome, containing a single copy of each histone, and the DNA twisted around each hemisome in a non-canonical, positively supercoiled, right-handed manner. The DNA fragment that is wrapped around the tetramer is about 120 bp in length. This model was recently postulated for the CENP-A^{Cid}-H4-H2A-H2B tetrameric nucleosomes in *Drosophila* (Figure 5; Furuyama and Henikoff, 2009; Dalal et al., 2007).

Interestingly, an additional model different from the classical four-histone composition has emerged. In this model, instead of the two copies of H2A-H2B dimers, the CENP-A specific chaperone HJURP/Scm3 associates with CENP-A^{Cse4}-H4 to form a nucleosome-like structure, indicated in Figure 5 (Mizuguchi et al., 2007; Stoler et al., 2007). The DNA helix is wrapped around this heterohexamer in a conventional, left-handed manner. This model was further supported by crystallographic data of a reconstituted histone-chaperone/histone complex (Zhou et al., 2011). However, recently published live-cell imaging data suggest that nucleosome formation, turnover of CENP-A^{Cse4} and its association with Scm3 are highly dynamic and cell-cycle dependent processes (Wisniewski et al., 2014). According to this study, an Scm3 dimer from a cytoplasmatic pool binds a newly synthesized CENP-A^{Cse4} dimer and assembles with H4 to form a heterohexamer. Subsequently, these Cse4-H4 tetramers are introduced into transient octameric nucleosomes, with Scm3 as an

attached molecule. These results combine and expand the octameric and the heterohexameric models and could explain controversial nucleosome structure predictions of former studies (Wisniewski et al., 2014).

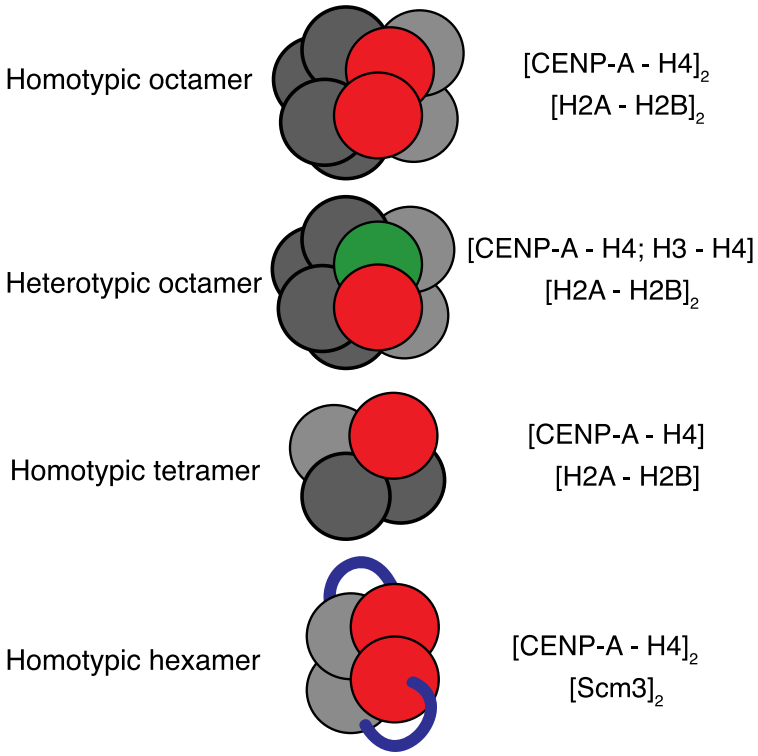

Figure 5: Centromeric nucleosome structures in the budding yeast

In the upper panels, the proposed homotypic and heterotypic octameric structures, similar to that of canonical nucleosomes, are shown. Below, the hemisome structure, which consists of one tetramer of the four histones H2A, H2B, CENP-A and H4, is shown. The lower panel depicts a homotypic hexamer consisting of two Cse4-H4 dimers and an Scm3 homodimer. Taken from (Allshire and Karpen, 2008).

1.5. Kinetochores: Structure and function in chromosome segregation

Amphitelic sister chromatid segregation during mitosis and meiosis depends on the assembly of functional kinetochores on the centromeric regions of each chromosome. Kinetochores are large, stretched multiprotein structures, which are highly conserved throughout all eukaryotes and exhibit a number of functions; one is the specific recognition of centromeric chromatin components, such as the histone variant CENP-A and in budding yeast centromere specific DNA elements (CDEI-III), and the attachment of the centromeric chromatin. Inner kinetochore proteins mediate

these events (Westermann et al., 2007). A second feature is the orientation of the sister chromatids towards the plus ends of the spindle microtubules, which depends on the proper arrangement of the kinetochores. The third function is to connect the centromeres to the microtubules, which generate the force and tension required for the separation of the sister chromatids during anaphase (Figure 6; Hauf and Watanabe, 2004; Santaguida and Musacchio, 2009). An additional function that comes into operation if tension is absent in case of monotelic or syntelic attachment of the kinetochore-microtubule structures, is the induction of a mitotic delay by recruiting signaling proteins of the spindle assembly checkpoint (SAC) to the kinetochore involving the protein kinase Ipl1, i.e. Aurora B (Biggins and Murray, 2001; Burke and Stukenberg, 2008). Besides other factors controlling SAC activation and mitotic delay, such as deficiencies in the spindle pole bodies or the presence of dicentric chromosomes, a mutation of the inner kinetochore subunit Ctf13 has been connected to the recruitment of SAC proteins Bub1 (BubR1) and Bub3, Mad1 and 2 and concomitant mitotic checkpoint activation (Hardwick et al., 1996; Wang and Burke, 1995). Moreover, the large KMN cluster, which is composed of the three sub complexes KNL1, MIS12 and NDC80 and part of the outer kinetochore region, functions in chromosome segregation as an anchor for microtubules and provides a scaffold to generate spindle checkpoint signals (Foley and Kapoor, 2013).

The kinetochore of the budding yeast is composed of about 60 different protein subunits, which are organized in clusters, according to their distance to the point centromere. Using fluorescence labeled kinetochore subunits and high resolution imaging techniques for arrangement and distance analyses, a symmetric organization of the kinetochore around the cylindrical microtubule lattice was predicted and the whole budding yeast kinetochore complex was calculated to be approximately 68 nm in length (Joglekar et al., 2009; Santaguida and Musacchio, 2009; Figure 6).

1.5.1. Inner kinetochore components

The inner components of the yeast kinetochore are responsible for the assembly of the middle and outer kinetochore subunits during mitosis (Westermann and Schleiffer, 2013). The non-conserved CBF3 complex, which is composed of the four

essential subunits Ctf13, Ndc10, Cep3 and Skp1, binds to the CDEIII DNA element (Figure 6). The zinc-finger subunit of Cep3, but also Ndc10 has been shown to be crucial for DNA binding and both bind directly to the CDEIII element (Espelin et al., 1997). Ctf13 is activated upon folding by the molecular chaperone Hsp90 and phosphorylation by Sgt1 kinase. Activated Ctf13 binds Skp1, and subsequently the final complex with Ndc10 and Cep3 is formed, followed by CDEIII binding. In cooperation with CENP-A^{Cse4}, Mif2 (CENP-C in human) and Cbf1 are then recruited to centromeres (Bansal et al., 2004; Kitagawa et al., 1999; Lingelbach and Kaplan, 2004). Cbf1, which is a helix-turn-helix DNA binding protein, interacts with CDEI. It functions as a homodimer and is found only in budding yeasts (Baker et al., 1989; Cai and Davis, 1989). The deletion of *CBF1* results in a growth phenotype and the cells are auxotrophic for methionine. The latter phenotype points at a transcriptional regulation function of Cbf1, which binds to several genomic sites including the promoters of methionine biosynthesis genes (Cai and Davis, 1990; Kent et al., 1994). While Cbf1 has originally been described as a transcription factor, its function has also been linked to kinetochore assembly and chromosome segregation (Masison and Baker, 1992). The exact function of this unique protein in yeast is not well understood, but interestingly, when combined with the non-methylated *CENP-A^{Cse4}R37A* mutant, a strong growth phenotype was observed, indicating a kinetochore-establishing function of Cbf1 (Samel et al., 2012; Figure 6).

1.5.2. Linker kinetochore components

Linker components of the kinetochore are responsible for connecting the inner layer to the outer kinetochore proteins, and they are recruited after the centromeric DNA has been replicated and the inner kinetochore has been assembled to the point centromere in yeast. Most of the middle kinetochore components are highly conserved from unicellular eukaryotes to vertebrates (Westermann and Schleiffer, 2013). One large cluster is the CTF19 complex containing the sub complex COMA (Ctf19-Okp1-Mcm21-Ame1, Figure 6). Okp1, Mcm21 and Ame1 co-purified with Ctf19 and have been functionally linked to centromeres by genetic and biochemical studies. In particular, COMA function has been described in a hierarchical cascade as a recruitment factor of other linker components, such as MIND (Mtw1, Nnf1, Nsl1, Dsn1), Ctf3 and Chl4/Iml3. MIND as well as COMA mutants show unstable spindle

and monopolar attachment phenotypes, and consistent with the activation of the spindle checkpoint, cells show a mitotic delay (De Wulf et al., 2003; Foley and Kapoor, 2013; Ortiz et al., 1999; Scharfenberger et al., 2003; Stoler et al., 1995).

1.5.3. Outer kinetochore components

The attachment to the plus ends of the spindle microtubule is mediated by the outer kinetochore (Foley and Kapoor, 2013). Using fluorescence imaging of labeled Knl1 in *C. elegans* embryos, it was shown that the KNL1 complex acts downstream of CENP-A and is responsible for the assembly of the kinetochore-microtubule interface (Desai et al., 2003). The stretched NDC80 complex is an Spc24 and 25, Nuf2 and Ndc80 containing heterotetramer that binds directly to plus-ends of microtubules (Janke et al., 2001). Using quantitative fluorescence microscopy, the number of NDC80 complexes was determined. Together with the whole KMN network, approximately eight NDC80 complexes associate around one microtubule, resulting in a conical shape (De Wulf et al., 2003; Joglekar et al., 2006; Wigge and Kilmartin, 2001). The MTW1 and SPC105 complexes are associated with spindle pole bodies (SPBs), shown in a co-localization study of outer kinetochore proteins (Nekrasov et al., 2003). The outermost kinetochore region is marked by a large complex termed DAM1. It is most likely a ring, and approximately 16 heterodecameric complexes reaching around one microtubule have been predicted (Joglekar et al, 2006; (Westermann et al., 2006; Figure 6). It has been shown that high tension applied to Dam1 stabilizes the microtubule plus-ends, but its function does not seem to be essential, as Dam1 is not evolutionarily conserved in higher eukaryotes and not essential in fission yeast (Figure 6; Franck et al., 2007; Gachet et al., 2008; Sanchez-Perez et al., 2005).

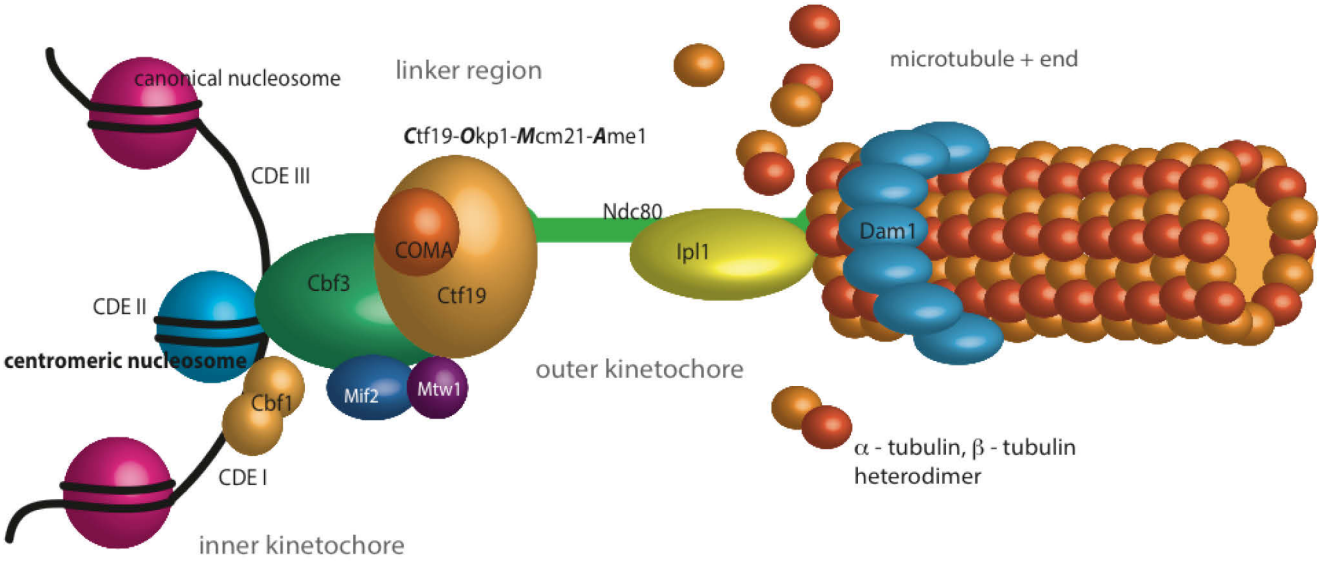

Figure 6: Model of the *Saccharomyces cerevisiae* kinetochore.
All presently known subcomplexes of the yeast kinetochore are arranged according to their distance from the centromeric nucleosome on the left (blue) to the attachment to the microtubules on the right (orange). The composition of the single subcomplexes is depicted, not the numbers of the protein complexes per centromere. Based on (Westermann et al., 2007; Santaguida and Musacchio, 2009).

1.6. Posttranslational modification of histones

The mostly accessible amino acid side chains in the amino-termini of histone are prominent targets for enzymatically mediated, covalent posttranslational modifications. The two main groups that can be distinguished are small chemical modifications, including phosphorylation, methylation and acetylation on one hand, and the attachment of large peptides such as ubiquityl- and sumoyl- moieties to histones on the other hand. Furthermore, there are much less frequent PTMs, for instance ADP ribosylation, proline isomerization and arginine deamination. Acetylation, ubiquitylation and sumoylation occur on lysine residues only. Phosphorylation is restricted to serine and threonine residues, and mono- or dimethylation occurs on arginine or lysine residues whereas trimethylation is exclusively found on lysine residues. Asymmetric or symmetric dimethylation is only found on arginines (Kouzarides, 2007). The large quantity of PTMs that have been discovered so far and their innumerable combinations have led to the idea that PTMs and their patterns epigenetically control biological functions like gene transcription

activation and repression, DNA replication and chromosome segregation (Bannister and Kouzarides, 2011; Kouzarides, 2007). At least three mechanistic models have been proposed to categorize the large number of PTMs. The first concept comprises *cis*-modifying effects by chromatin modifications such as histone phosphorylation or acetylation and refers to the direct structural changes imposed on chromatin conformation. The second group of PTM-induced alterations refers to inhibitory effects on chromatin binding factors. One example is H3S10 phosphorylation, which is mediated by Aurora B. Upon phosphorylation, the binding of HP1 to the nearest trimethylated H3K9 is sterically blocked during heterochromatin formation, keeping the chromatin accessible to the transcription machinery. In the third model, PTMs are involved in mediating chromatin binding factor specificity. For example, the methyllysine-binding domain of HP1, the chromodomain, binds specifically to trimethylated H3K9. Both latter models are *trans*-acting mechanisms (Fischle et al., 2005; Kouzarides 2007).

1.6.1. Acetylation of histones

Histone acetylation typically occurs at multiple lysine residues and is mediated by a variety of histone acetyltransferase complexes (Brown et al., 2000; see chapter 1.8.1). One study showed that the modification patterns are likely to act downstream in the regulation of co-expressed genes (Kurdistani et al., 2004). In another study, a cumulative effect depending on the amount of acetylation on one histone tail was described (Dion et al., 2005). In most of the cases, histone acetylation is associated with transcriptional activation. The attachment of this small chemical group goes along with a partial neutralization of the positively charged histone tail, reducing the affinity of histones to the negatively charged DNA backbone. Consequently, this modification tends to prevent inter- and intranucleosomal interactions with DNA molecules and is therefore likely to play a role in open chromatin formation. Acetylation seems to correlate with transcription, as indicated by many studies including early Chromatin immunoprecipitation (ChIP) experiments in chicken erythrocytes, demonstrating that the active β-globin gene associates with high levels of histone acetylation (Hebbes et al., 1994). Interestingly, histone acetylation is not equally distributed on active genes, but is enriched at promoter regions, where it acts as a recruitment factor for bromodomain containing proteins (see chapter 1.8.2).

Studies showed that the SWI/SNF histone-remodeling complex binds to acetylated histones, which leads to nucleosome displacement at the respective promoter regions (Workman, 2006).

1.6.2. Epigenetic regulation of chromosome segregation

The assumption that chromosome segregation is in part epigenetically regulated has been a matter of debate over many years. Given that histone variants participate in the epigenetic regulation of many cellular processes, it is reasonable that the centromeric histone variant CENP-A is a major subject of epigenetic studies. Surprisingly little is known about the specific function of PTMs on the N- and C-terminal regions of centromeric histones as compared to the abundant knowledge of modification patterns on canonical histones. Sequence differences to canonical H3 suggest distinct modification patterns on the unique N-terminal regions and, consequently, a distinct function of those domains in kinetochore assembly and chromosome segregation (Figure 7A).

In human cells, interspersed H3 blocks mediate the specificity of CENP-A deposition. Following replication of centromeric chromatin, a distinct code of PTMs triggers the recruitment of factors that are required for the replacement of H3 with CENP-A or the deposition of new CENP-A nucleosomes into nucleosomal gaps. H3K4 dimethylation characterizes the canonical histone H3 in the centromeric region in human cells and thereby contributes to centromere specificity (Allshire and Karpen, 2008; Sullivan and Karpen, 2004). Furthermore, genetic studies in fission yeast revealed that mutant alleles of the essential histone deacetylase Clr6 (Cryptic loci regulator 6) disturb epigenetically maintained repression at centromeres and cause chromosome missegregation. These experiments connected the deacetylation of the N-terminal histone tails to centromere function (Grewal et al., 1998).

Recently, it was shown that histone phosphorylation marks the majority of CENP-A nucleosomes in human cells and has a direct influence in chromosome segregation during mitosis. Serines 16 and 18 in prenucleosomal CENP-A N-terminal regions become phosphorylated and form a salt-bridged secondary structure, which leads to intramolecular associations in the CENP-A histones (Bailey et al., 2013). Using phospho-mimetic CENP-A nucleosome arrays in analytical ultracentrifugation

experiments, it was demonstrated that phosphorylation results in larger intranucleosome associations and counteracts the hyper-oligomerized state exhibited by unmodified CENP-A nucleosome arrays. These analyses have shown that two modifications in the N-terminal domain of CENP-A affect the physical and biochemical properties of the chromatin fiber at the centromere during chromosome segregation (Bailey et al., 2013).

1.7. The centromeric histone variant CENP-A^{Cse4}

In the budding yeast, the gene for the centromeric histone variant CENP-A is termed *CSE4*, which stands for Chromosome segregation protein 4. This histone is a 27 kDa protein and was first described in a genetic screen to identify strains with defects in chromosome segregation, as an essential gene that is needed for cell division (Stoler et al., 1995; Chen et al., 2000; Meluh et al., 1998; Baker et al., 1998). Although centromeric histone H3 variants are highly conserved in eukaryotes (CENP-A in humans, CENP-A^{Cid} in *Drosophila*, CENP-A^{Cnp1} in fission yeast), similarities in amino acid sequence are restricted to the histone fold domain in CENP-A^{Cse4}, which shares about 64% sequence identity with canonical histone H3 (Figure 7A); (Wells and McBride, 1989). While all histones exhibit largely unstructured N-terminal regions, the N-terminal tail of CENP-A^{Cse4} is highly unique in that it is almost as large as the histone fold domain, i.e. about 130 aa (Stoler et al., 1995; Meluh et al., 1998). This N-terminus is unusually long as compared to other N-termini, e.g. of human and fission yeast CENP-A, which are only 45 and 20 amino acids in length, respectively.

The N-terminal region of the Drosophila CENP-A^{Cid} is also extended and 120 amino acids in length (Allshire and Karpen, 2008). Interestingly, there is no sequence homology of CENP-A^{Cid} and CENP-A^{Cse4} tails, suggesting a strong evolutionary fluctuations along with species-specific CENP-A interacting proteins (Figure 7A). Overexpression or mislocalization of CENP-A has been connected to strong segregation defects in *Drosophila* and aneuploidy and human cells, which is a hallmark of cancer development (Tomonaga et al., 2003; Heun et al., 2006; Moreno-Moreno et al., 2006).

CENP-A as well as its homologues and H3 are structurally distinct, but both assemble with H4 to build functional heterotetramers. What differentiates CENP-A

from H3 is the centromeric targeting domain CATD, which is located in the α1 helix, loop 1 and α2 helix of the histone fold domain. This motif is 15 aa in length and contains essential hydrophobic amino acids. This domain has been shown to mediate the assembly of rigid and more compact CENP-A-H4 tetramers, which lead to differently arranged higher order centromeric heterochromatic structures. It is also required for the localization of CENP-A-H4 tetramers to centromeres (Black et al., 2004). Recombinant H3 constructs, which were provided with CATD, could be targeted and assembled to centromeres properly. Whereas CENP-A depletion is lethal, this synthetic hybrid could rescue CENP-A function (Black et al., 2007).

Whereas the histone fold domain (HFD) is required for correct centromere targeting, this is not the case for the N-terminus. However, the stretched tail of CENP-A^{Cse4} contains the essential N-terminal domain (END), which extends from aa 28-60 and its deletion has been shown to be lethal in budding yeast (Figure 7B; Chen et al., 2000; Morey et al., 2004).

1.7.1. Posttranslational modifications on Cse4

As outlined above, the N-terminal domains of canonical histones and the histone variants are subject to posttranslational modifications. Recently, the modification pattern of the budding yeast CENP-A^{Cse4} was resolved by mass spectrometric analysis, showing phosphorylation sites on serines 22, 33, 40 and 105, one methylation site on R37 and one acetylation site on K49, which are all positioned at the N-terminus of CENP-A^{Cse4}. Except for serines 22 and 105, all of them are located in the essential N-terminal domain (Samel et al., 2012; Boeckmann et al., 2013). CENP-A histones are necessary for the recruitment and assembly of the kinetochore, and PTMs on their tails may be critical for chromosome segregation (Choy et al., 2012). Although little is known about the involvement of PTMs on CENP-A^{Cse4} in pathways that are crucial for the segregation process, our group showed by genetic interaction studies in yeast that R37 methylation is critical for the recruitment of many kinetochore proteins, e.g. the COMA subunits Ctf19, Ame1, Okp1 and Mcm21 of the linker layer complex CTF19. Mutant alleles of these kinetochore components showed synthetic lethality or synthetic growth defects in combination with *cse4R37A*. Furthermore, this point mutation caused temperature sensitivity in cells that lack Cbf1

and G2/M phase delay at restrictive temperatures, indicating an epigenetic regulatory function of Cse4R37 modifications in kinetochore assembly and cell-cycle progression (Samel et al., 2012).

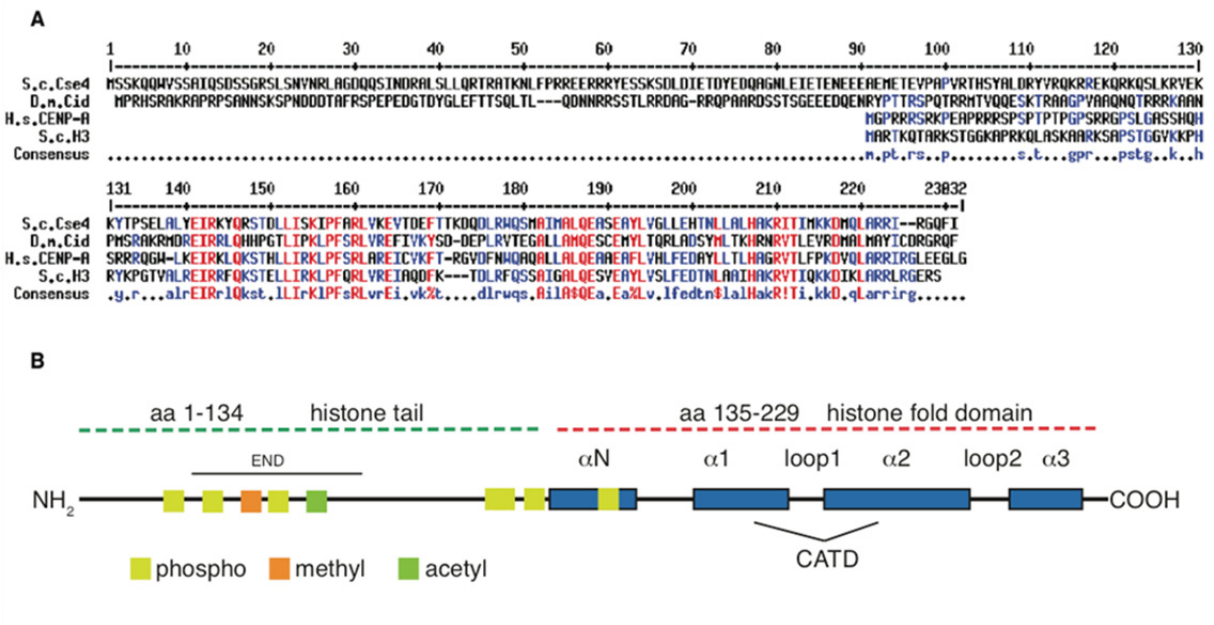

Figure 7: Sequence alignment of CENP-A species and topological view of CENP-A from budding yeast

A: Amino acid sequence alignment of budding yeast (upper panel), *Drosophila* and human CENP-A proteins, compared to budding yeast canonical histone H3 and the consensus sequence (lower panels). Alignment was generated with Multalin (http://multalin.toulouse.inra.fr/multalin). **B**: Topological organization of the *S. cerevisiae* CENP-A molecule. α-helices are shown as blue boxes, CATD indicated the centromeric targeting domain. Phosphorylation sites of serines, methylation of R37 and acetylation of K49 are depicted as yellow, orange and green boxes, respectively. END indicates the essential N-terminal domain. Modified from (Luger et al., 2001; Allshire and Karpen, 2008).

1.8. Histone-modifying enzymes

Several histone-modifying enzyme families are known, including histone acetyltransferases (HATs, see chapter 1.8.1.), arginine and lysine specific methyltransferases, kinases, and ubiquitin conjugating enzymes.

In humans, arginine monomethylation, asymmetric and symmetric dimethylation are catalyzed by specific S-adenosyl-L-methionine dependent protein arginine methyltransferases (PRMTs). These enzymes are classified into type I-III enzymes,

of which type III PRMTs catalyze monomethylations. Type I and II catalyze a monomethylated intermediate, followed by type I mediated asymmetric dimethylation or type II mediated symmetric dimethylation (Bedford and Clarke, 2009; Di Lorenzo and Bedford, 2011). In yeast, three arginine methyltransferases Hmt1, Rmt2 and Hsl7 have been described (Henry and Silver, 1996; Lee et al., 2000a; Niewmierzycka and Clarke, 1999).

Lysine methylation is mediated by members of the large family of KMTs, which share the conserved SET domain harboring the catalytic activity and mediate mono-, di- and trimethylation (Zhang et al., 2012). These enzymes are highly specific, for example the yeast H3K79me2/3 specific methyltransferases Dot1, which has been functionally linked to telomeric silencing (Singer et al., 1998).

Histone deacetylases (HDACs) and arginine and lysine specific histone demethylases (HDMs) remove the methyl and acetyl moieties and convert histones into the initial unmodified state. According to the dynamics of chromatin condensation and decondensation, the outcome of all these modification processes have to be precisely timed to ensure gene transcription regulation, proper DNA replication, sister chromatid separation, DNA damage response and other essential cellular events and to prevent the cell from malignant developments (Butler et al., 2012; Marmorstein and Trievel, 2009).

1.8.1. Histone acetyltransferases (HATs)

Histone acetyltransferases (HATs) are the best described histone modifying enzymes. Such enzymes posttranslationally modify lysines of histone tails by transferring an acetyl group from acetyl-CoA to an ε-amino moiety of the target lysine side chain (Brownell and Allis, 1996). Almost 20 years ago, it was shown that the enzymes p55 as well as the human and yeast Gcn5 proteins have HAT activity, and the list of histone acetyltransferases has been extended since then (Brownell and Allis, 1995; Brownell et al., 1996; Kuo et al., 1996; Wang et al., 1997). Many of the HATs are involved in central processes, like transcriptional activation (Gcn5, Esa1, Sas3 and more), dosage compensation (MOF), DNA repair (Tip60), or histone deposition (Hat1) (Kimura et al., 2005; Marmorstein and Trievel, 2009).

Until today, four HAT families are known, which are grouped according to their amino acid sequence homology and their catalytic mechanisms (reviewed in Marmorstein 2001). The first are the GNAT family (Gcn5-related *N*-acetyltransferases) and their close relatives from the p300/CBP (CREB binding protein; for both see chapter 1.8.2.). Members of the MYST (MOZ, Ybf2/Sas3, Sas2, Tip60) family share the chromodomain and zinc-finger domains as common features. Esa1 acts in the NuA4 complex, which is essential in yeast and specific for the acetylation of H4K8, K12 and K16, but is also able to acetylate the N-terminal tail of H3, and the H2A variant Htz1 on K14 in yeast (Allard et al., 1999; Berndsen and Denu, 2008; Brown et al., 2000). Another MYST complex is SAS-I (something about silencing). It has been demonstrated that its catalytic subunit Sas2 acetylates H4K16 with high specificity, and the deletion of *SAS2* causes silencing phenotypes (Meijsing and Ehrenhofer-Murray, 2001; Osada et al., 2001). Only the MYST and the PCAF/Gcn5 histone acetyltransferases are conserved from yeast to human, and the p300/CBP is conserved among metazoans. The fourth group contains the fungal specific HAT Rtt109, which is specific for H3K56 acetylation and was named for its function as a regulator of Ty1 transposition gene product 109, (Driscoll et al., 2007; Han et al., 2007; Schneider et al., 2006).

1.8.2. Gcn5-related *N*-acetyltransferases (GNATs)

The first member of the protein superfamily of Gcn5-related *N*-acetyltransferases was defined in tetrahymena as p55 histone acetyltransferase, which directly linked histone acetylation of chromatin templates to gene activation (Brownell et al., 1996). Gcn5 (general control nonderepressible 5) was originally described as a co-factor of transcriptional activators, and has been shown to acetylate N-termini of H3 with high affinity, and to a lesser extent, N-termini of H4 (Georgakopoulos and Thireos, 1992; Goodman and Smolik, 2000; Turner, 1991).

Further members of the GNAT protein family are the human P/CAF (p300/CBP associated factor), as well as Hpa2, Hat1 and Elp3, which were first described in *S. cerevisiae*. Most of the enzymes share a bromodomain with the members of the p300/CBP family, which is a highly conserved structural feature composed of a bundle of four α-helices that recognizes acetylated lysine residues and tethers HATs

to specific chromosomal sites (Owen et al., 2000; Zeng and Zhou, 2002). It was shown that the absence of only one allele of P/CAF or p300/CBP causes early embryonic lethality in mice. Additionally, even mice that were heterozygous for both genes died during embryogenesis, indicating an importance of the level of these multifunctional proteins (Yang et al., 1996; Yao et al., 1998). Somatic mutations of p300 and CBP have also been associated with cancer development like leukemia, colon and breast cancers. Thus, these proteins represent promising drug targets in cancer research (Goodman and Smolik, 2000).

In yeast cells, a *GCN5* deletion causes slow growth, a delay in G_2-phase and sister chromatid separation as well as temperature sensitivity. Genetic studies and ChIP experiments showed that Gcn5 function is linked to centromeric DNA and the CBF3 complex of the inner kinetochore, indicating a specific epigenetic role of Gcn5 HAT activity in kinetochore assembly and chromosome segregation (Vernarecci et al., 2008). However, the exact role of Gcn5 at centromeres has not been elucidated so far.

1.9. The Gcn5 containing complexes SAGA/ADA

Extensive research has been performed to understand gene transcription regulation, one of the most accurately regulated processes in eukaryotic cells. Consequently, many factors involved have been characterized. Gcn5, one of the best described among these factors, has been shown to act as a HAT on free histones as an isolated enzyme, but to be unable to acetylate nucleosomal histones (Grant et al., 1997). In budding yeast, Gcn5 is found in at least three distinct high molecular mass protein complexes. One is termed SAGA (Spt-Ada-Gcn5-Acetyltransferase), which is 1.8 MDa in size, and a smaller complex, ADA (Adaptor), which is 800 kDa in size. SAGA is highly conserved from yeast to humans and is composed of four functional modules containing at least 19 protein subunits (Lee et al., 2011; Lee and Workman, 2007). The third HAT complex is a derivate of SAGA and, consequently, this complex was termed SLIK (SAGA-like). Another term has been used, SALSA (SAGA altered, Spt8 absent), which describes the composition of this derivative complex (Lee and Workman, 2007; Sterner et al., 2002).

The functional units of the complexes are categorized in modules. The deubiquitinylation module, termed DUB, is responsible for H2B deubiquitination, which is mediated by the catalytic subunit Ubp8 (Daniel et al., 2004; Henry et al., 2003). The adapter module ADA, also described as the core or acetylation module, contains Ada1, Ada2 and Ada3, which display activator function and are associated with Gcn5 (Balasubramanian et al., 2002; Horiuchi et al., 1997). The SPT (Spt3, Spt7, Spt8, Spt20) module is necessary to ensure the interaction with TBPs (TATA-binding proteins). Spt7 and Spt20 have also been proposed to function in complex architecture and stability (Grant et al., 1997). The fourth module consists of a subset of TBP associated factors, TAFs, which are involved in the initial DNA binding process and transcription activation (Green, 2000).

When the genes coding for *ADA2* or *SPT7* are deleted, the corresponding mutant strains show specific growth phenotypes. *ADA2* null mutants show temperature sensitivity, decreased growth rates and abnormal bud morphology, and it was assumed that these strong phenotypes are caused by the large transcriptional changes in these mutants (Berger et al., 1992; Georgakopoulos et al., 1995; Georgakopoulos and Thireos, 1992; Pina et al., 1993; Watanabe et al., 2009). Similar growth defects were described for *SPT7* null mutants, although these mutants show no abnormal bud morphology (Watanabe et al., 2009). The more severe defects of *ADA2* null mutants may be due to the transcription activator function of Ada2 and its direct association with Gcn5 in the acetylation module of all known complexes, whereas Spt7 functions in the stabilization of the SAGA/SLIK complexes.

It has been suggested to term the SAGA complex the HAT/chromatin interaction module, because of its chromatin interacting and modifying subunits. It has been demonstrated that the subunit Sgf29, which is found in all Gcn5 complexes, includes a TUDOR domain, which binds trimethylated H3K4 with high affinity and acts as a chromatin anchor associated with transcription start sites (Barski et al., 2007; Bian et al., 2011; Lee et al., 2011; Vermeulen et al., 2010). The SAGA derivate SLIK shares the majority of subunits with SAGA, whereas the Rtg2 subunit seems to be a unique feature of SLIK and links it to the yeast retrograde response pathway, a stress response mechanism in which gene expression levels are altered during mitochondrial dysfunction (Pray-Grant et al., 2002). The Spt8 subunit is only present

in SAGA and not in SLIK, and Spt7 occurs in the latter in a C-terminally truncated form (Sterner et al., 2002; Wu and Winston, 2002).

In the budding yeast, SAGA is one of the two co-activator complexes involved in transcriptional activation. The second complex is TFIID (Transcription factor IID), and both act in complementary pathways (Lee et al., 2000b). The latter mediates about 90% of the gene activation, mostly of housekeeping genes. SAGA initiated gene activation facilitates transcription complex assembly at *GAL1* and generally acts at genes that are involved in stress response (Bhaumik and Green, 2001; Huisinga and Pugh, 2004; Larschan and Winston, 2001). In contrast, SAGA has also been shown to play an inhibitory role at promoters of certain *GCN4*-regulated genes, *HIS3* and *TRP3*, mediated through Spt3 and Spt8 subunits. In SLIK/SALSA, Spt8 cannot assemble in the complex due to the presence of a C-terminally processed form of Spt7, which lacks the Spt8 docking site. The altered composition leads to derepression of *HIS3* and *TRP3*, displaying a specific SLIK/SALSA function in gene activation of distinct promoters (Sterner et al., 2002; Lee and Workman, 2007; Daniel and Grant, 2007).

Both Gcn5 HAT complexes share the ADA module with the Ada2 and Ada3 subunits, as well as the enzymatic subunit. The ADA complex is yeast specific and was described as a distinct HAT complex, containing the unique subunits Ahc1 and Ahc2, besides Ada2, Ada3 and Gcn5. The deletion of *AHC1* leads to a loss of the ADA complex, whereas the SAGA complex remains unaffected, which was shown in co-purification experiments (Eberharter et al., 1999; Lee et al., 2011). Interestingly, *AHC1* mutants showed no growth phenotypes, which is in contrast to *ADA2/3* or *GCN5* deleted cells. It has been shown that a functional SAGA complex physically interacts with the acidic activators Gcn4 and VP16, which were not detected for the ADA complex (Utley et al., 1998). Taken together, these data indicate overlapping but distinct functions of both complexes (Eberharter et al., 1999).

1.10. Aim of this work

During cell division, the process of chromosome segregation is initiated by the attachment of spindle microtubules to the kinetochore, which assembles at the centromeric regions of each chromosome and mediates sister chromatid separation and their orientation towards the spindle poles. A crucial epigenetic mark of centromeres is the presence of the centromeric histone H3 variant CENP-A, which is essential for proper chromosome segregation. Studies using cultured human cells have shown that PTMs on CENP-A prevent the misalignment of chromosomes during mitosis (Kunitoku et al., 2003; Zeitlin et al., 2001).

The function of many PTMs such as acetylation is well understood on canonical histones, and knowledge is expanding of epigenetic mechanisms regulating physiological and pathological cellular processes during development and differentiation. However, less is known about epigenetic regulatory mechanisms involving the centromeric histone variant CENP-A, despite substantial biomedical relevance of understanding its function in cell cycle and chromosome segregation regulation. Recently, work on the budding yeast CENP-A^{Cse4} led to new insights into the epigenetic regulation of the recruitment of kinetochore components. Novel modification patterns of the extended N-terminal domain of CENP-A^{Cse4} were identified by mass spectrometry and functionally linked to kinetochore assembly and chromosome segregation. The methylation of R37 was proposed to positively regulate the recruitment of linker kinetochore subunits of the COMA complex to the point centromeres. In contrast, K49 acetylation was found to most likely act antagonistically to R37 methylation (Samel et al., 2012 and unpublished data).

To understand the epigenetic basis of kinetochore assembly regulation, which likely depends on several specific PTMs on CENP-A^{Cse4}, the identification of the responsible histone modifying enzymes and the complexes in which they are engaged is essential. Consequently, the aim of this study was to identify the histone acetyltransferase (HAT) that acetylates lysine 49 on CENP-A^{Cse4} in *S. cerevisiae*. To obtain further insight into HAT function on centromeric chromatin, biochemical and genetic experiments that aimed at defining the corresponding HAT complex were designed and performed in the course of this study. The results of these investigations helped to shed light on the mechanisms of the epigenetic regulation of

kinetochore attachment and chromosome segregation and link HAT complexes to centromeric chromatin.

PTMs have been shown to be cell-cycle dependent in many cases and by these means help to epigenetically regulate chromatin according to the particular requirements of distinct cell cycle stages. In particular, chromosome segregation is an eminent part of mitosis, which raises the question of the possible dynamics of CENP-A PTMs throughout the cell cycle. Such dynamic regulation of PTM levels could provide a basis for the concerted recruitment of kinetochore subunits as well as the concomitant kinetochore assembly.

As these processes are based on the kinetochore-chromatin interface, the investigation of the protein-protein interactions between different subunits of kinetochore components and the N-terminus of CENP-A^{Cse4} could yield important insights into the regulation of kinetochore establishment. Furthermore, the dependence of these interactions on PTMs of the N-terminus of CENP-A^{Cse4} was investigated. Initial structural approaches will help pointing at the relationship between its structural properties of CENP-A^{Cse4} and its biological function. This was hoped to extend our understanding of centromere function and regulation in eukaryotic chromosome segregation.

2. Material and Methods

2.1. *Escherichia coli* strains

Table 1: *E. coli* strains used in this study

ElectroShox	F^- *mcr*A Δ (*mrr-hsd*RMS-*mcr*BC) Φ80*lac*ZΔM15 Δ*lac*X74 *rec*A1 *end*A1 *ara* Δ139 Δ (*ara*, *leu*) 7697 *gal*U *gal*K *rps*L (Str^R) *nup*G λ^-
TOP10	F^- *mcr*A Δ (*mrr-hsd*RMS-*mcr*BC) Φ80*lac*ZΔM15 Δ*lac*X74 *rec*A1 *AraD139Δ* (*ara-leu*) 7697 *gal*U *gal*K *rps*L (Str_R) *end*A1 *nup*G (Invitrogen)
DH5α	F^- Φ80d*lac*ZΔM15 Δ (*lac*ZYA-*arg*F) U169 *rec*A1 *end*A1 *hsd*R17 (r_k^-, m_k^+) *pho*A *sup*E44 *thi*-1 *gyr*A96 *rel*A1 λ^- (Invitrogen)
Rosetta (DE3) pLysS	F^- *omp*T *hsd*S_B (R_B^- m_B^-) *gal dcm* λ (DE3 [*lac*I *lac*UV5-T7 gene 1 *ind*1 *sam*7 *nin*5]) pLysSRARE (Cam^R)

2.2. *Escherichia coli* media and growth conditions

All bacterial strains (Table 1) used for plasmid amplification or expression of recombinant proteins were cultured according to standard procedures (Sambrook et al., 1989) at 37°C in Luria-Bertani (LB) Medium (5 g/L yeast extract, 5 g/L NaCl and 10 g/L tryptone) supplemented with either kanamycin or ampicillin at 50 µg/ml. For protein expression in Rosetta cells, cultures were additionally supplemented with 50 µg/ml chloramphenicol.

2.3. *Saccharomyces cerevisiae* strains

Yeast strains and plasmids used in this study are listed in Table 2 and Table 3, respectively. The strains were either generated during this study by direct gene deletion, transformation with plasmids or crossing of yeast cells, or they were taken

from the laboratory strain collection, and are isogenic to W303 (AEY1-4). Unless indicated otherwise, plasmids were generated during this study or taken from the plasmid library.

Table 2: *Saccharomyces cerevisiae* strains used in this study

Strain [a]	***Genotype***	***Source*** [b]
AEY1	*MATα ade 2-101 his3-11,15 trp1-1 leu2-3,112 ura3-1* (W303)	J. Rine
AEY2	AEY1, but *Mat* **a**	J. Rine
AEY4	AEY2, but *ADE2 lys2Δ*	J. Rine
AEY264	*MAT***a** *his4*	
AEY265	*MATα his4*	
AEY266	AEY2 *sas2Δ::TRP1*	
AEY468	AEY2, but *ADE2 lys2Δ, hat1Δ::HIS3*	
AEY921	AEY1 *HMR***a**-*e*** *sas3Δ::HIS3*	
AEY1404	*MAT***a** *gcn5Δ::TRP1 hmrΔ::URA3 ade2 LYS2*	
AEY2781	*MATα cse4Δ*:: KanMX *ade2-1 lys2Δ* pRS426-3xHA-*CSE4* (pAE977)	
AEY2960	*MATα HMR cse4Δ*::KanMX *pRS423 3xHA-cse4-K49R (pAE941) ade2 lys2*	
AEY3735	*MAT***a** *esa1Δ*::*HIS3 esa1-L327S::URA3 LYS2 ade2 trp1 leu2*	L.Pillus
AEY4217	*MAT***a** *his3 200 trp1-901 leu2-3,112 ade2 LYS2::14lexAop-HIS3 URA3::8lexAop-lacZ-GAL4*	
AEY4985	*MAT***a** *cbf1Δ::*NatMX *cse4-R37A LYS2 ADE2*	
AEY4986	*MATα cbf1Δ::*NatMX *cse4-R37A LYS2 ADE2*	
AEY4987	*MATα cbf1Δ::*NatMX *cse4-R37A lys2 ADE2*	
AEY5040	AEY2781 + pRS423 -3xHA-*cse4-R37A*	
AEY5095	AEY2 *rtt109Δ*::KanMX	
AEY5096	AEY2 *elp3Δ*::KanMX	
AEY5097	AEY2 *hpa2Δ*::KanMX	
AEY5098	AEY2 *spt10Δ*::KanMX	
AEY5100	*MATα hat1Δ*::*HIS3 cbf1Δ::*NatMX *cse4-R37A LYS2 ADE2*	
AEY5101	*MATα sas2Δ*::*TRP1 cbf1Δ::*NatMX *cse4-R37A lys2 ADE2*	
AEY5102	*MATα hat1Δ*::*HIS3 cbf1Δ::*NatMX *cse4-R37A lys2 ADE2*	
AEY5122	*MATα esa1Δ*::*HIS3 esa1-L327S::URA3 cbf1Δ::*NatMX *cse4-R37A lys2 ade2*	
AEY5123	*MAT***a** *esa1Δ*::*HIS3 esa1-L327S::URA3 cbf1Δ::*NatMX *cse4-R37A LYS2 ADE2*	
AEY5124	*MATα sas3Δ*::*HIS3 cbf1Δ::*NatMX *cse4-R37A LYS2 ADE2*	

AEY5125	*MAT*α *rtt109Δ*::KanMX *cbf1Δ::*NatMX *cse4-R37A lys2 ADE2*
AEY5126	*MAT***a** *rtt109Δ*::KanMX *cbf1Δ::*NatMX *cse4-R37A LYS2 ade2*
AEY5127	*MAT***a** *elp3Δ*::KanMX *cbf1Δ::*NatMX *cse4-R37A LYS2 ade2*
AEY5128	*MAT*α *elp3Δ*::KanMX *cbf1Δ::*NatMX *cse4-R37A LYS2 ADE2*
AEY5129	*MAT***a** *hpa2Δ*::KanMX *cbf1Δ::*NatMX *cse4-R37A LYS2 ade2*
AEY5130	*MAT*α *hpa2Δ*::KanMX *cbf1Δ::*NatMX *cse4-R37A LYS2 ade2*
AEY5131	*MAT***a** *spt10Δ*::KanMX *cbf1Δ::*NatMX *cse4-R37A LYS2 ade2*
AEY5136	*MAT***a** *elp3Δ*::KanMX *cbf1Δ::*NatMX *LYS2 ADE2*
AEY5137	*MAT*α *sas3Δ*::*HIS3 cbf1Δ::*NatMX *LYS2 ADE2*
AEY5138	*MAT***a** *hpa2Δ*::KanMX *cbf1Δ::*NatMX *LYS2 ADE2*
AEY5139	*MAT***a** *esa1Δ*::*HIS3 esa1-L327S::URA3 cbf1Δ::*NatMX *LYS2 ADE2*
AEY5140	*MAT*α *rtt109Δ*::KanMX *cbf1Δ::*NatMX *LYS2 ADE2*
AEY5141	*MAT*α *spt10Δ*::KanMX *cbf1Δ::*NatMX *LYS2 ADE2*
AEY5267	AEY266 + pRS426-3xHA-*CSE4 (*pAE977)
AEY5268	AEY468 + pRS426-3xHA-*CSE4 (*pAE977)
AEY5269	AEY921 + pRS426-3xHA-*CSE4 (*pAE977)
AEY5270	AEY1404 + pRS425-3xHA-*CSE4 (*pAE976)
AEY5271	AEY3735 + pRS425-3xHA-*CSE4 (*pAE976)
AEY5272	AEY5095 + pRS426-3xHA-*CSE4 (*pAE977)
AEY5273	AEY5097 + pRS426-3xHA-*CSE4 (*pAE977)
AEY5274	AEY5098 + pRS426-3xHA-*CSE4 (*pAE977)
AEY5279	AEY1 + pRS425-3xHA-*CSE4 (*pAE976)
AEY5280	AEY5096 + pRS425-3xHA-*CSE4 (*pAE976)
AEY5298	AEY921 + pRS426-3xHA-*CSE4 (*pAE977)
AEY5299	AEY2 *sas3Δ::*NatMX
AEY5300	AEY2781 *sas3Δ::*NatMX
AEY5302	AEY2781 *elp3Δ::*NatMX
AEY5304	AEY2781 *spt10Δ::*NatMX
AEY5306	AEY2781 *rtt109Δ::*NatMX
AEY5308	AEY2781 *hpa2Δ::*NatMX
AEY5310	*MAT*α *gcn5Δ::TRP1 cse4 Δ* ::KanMX *ade2 lys2* + pRS426-3xHA-*CSE4* (pAE977)
AEY5312	*MAT*α *sas2Δ::TRP1 cse4Δ*::KanMX *ade2 LYS2* + pRS426-3xHA-*CSE4* (pAE977)
AEY5314	*MAT***a** *hat1Δ::HIS3 cse4Δ*::KanMX *ade2 lys2* + pRS426-3xHA-*CSE4* (pAE977)

AEY5316	*MAT***a** *esa1Δ::HIS3 esa1-L327S::URA3 cse4Δ*::KanMX *ade2 LYS2* + pRS426-3xHA-*CSE4* (pAE977)
AEY5478	*MAT***a** *cse4 Δ*::KanMX + pRS426-3xHA-*CSE4 ade2 lys2 ahc1Δ::*HISMX
AEY5538	AEY2781 *ubp8Δ::*NatMX
AEY5617	AEY2781 but *MAT***a** *spt7Δ::*NatMX
AEY5618	AEY2781 *spt7Δ::*NatMX
AEY5619	AEY2781 but *MAT***a** *spt7Δ::*NatMX *ADE2*
AEY5620	AEY2781 *spt7Δ::*NatMX *ADE2*
AEY5621	*MATα spt7Δ::*NatMX *ADE2 lys2*
AEY5622	*MAT***a** *spt7Δ::*NatMX *ADE2 lys2*
AEY5623	AEY4 x AEY2781 *spt7Δ::*NatMX diploid strain
AEY5624	AEY2781 *ada2Δ::*NatMX
AEY5688	AEY2781, but *MAT***a**
AEY5689	AEY5688 *bar1Δ::*HisMX
AEY5690	*MAT***a** *cbf1Δ::*NATMX *cse4-R37A::*HisMX *ade2 LYS2*
AEY5691	*MATα cbf1Δ::*NATMX *cse4-R37A::*HisMX *ade2 LYS2*
AEY5692	*MATa adaΔ::*NATMX *ade2 LYS2*
AEY5735	*MATa spt7Δ::*NATMX *cse4R37A::HisMX ade2 lys2*
AEY5736	*MATα spt7Δ::*NATMX *cbf1Δ::*NATMX *ADE2 lys2*

[a] Strains are isogenic to W303 except those which are underlined.

[b] Unless indicated otherwise, the strains were constructed during this study or were taken from the laboratory strain collection.

Table 3: Plasmids used in this study

Plasmid	***Description***	***Source*** [a]
pAE240	*YEp351-GPDp-SAS2-PGKt*	
pAE524	pACT2	
pAE525	pBTM117c	
pAE615	pRS313-3x HA-*CSE4*	
pAE686	pACT2-N-term.-*CSE4* (aa 11-139)	
pAE688	pBTM117c-N-term.-*CSE4* (aa 11-139)	
pAE906	pRS313-*CSE4*	
pAE956	pBTM 117c-*CTF19*	
pAE794	pBTM117c-*CSE4*	
pAE976	pRS426- 3x HA-*CSE4*	

pAE977	pRS423- 3x HA-*CSE4*	
pAE1996	pAE1512 pET41b$^+$ -*GST*	Prof. P. Bayer, University Duisburg-Essen
pAE1998	pAE1512 pET41b$^+$ -*GST-CSE4 (1-100)*	
pAE2000	pAE1512 pET41b$^+$ -*GST-CSE4 (14-134)*	
pAE2002	pAE1512 pET41b$^+$ -*GST-CSE4 (33-132)*	
pAE2004	pAE1512 pET41b$^+$ -*GST-CSE4 (1-134)*	
pAE2128	pET41b$^+$ -*OKP1full length*	
pAE2130	pET Duet -*CTF19(35-363)*	
pAE2132	pET Duet -*CTF19 (35-363)-MCM21 (41-368)*	
pAE2142	pET41b$^+$ -*okp1 R164C full length*	

[a] Unless indicated otherwise, plasmids were constructed during this study or were taken from the laboratory plasmid collection.

The oligonucleotides used in this study were taken from the laboratory's common primer collection or synthesized by Metabion (Martinsried) and dissolved with A. dest to a concentration of 100 pmol/µl. Primer design was accomplished with genome sequences derived from the *Saccharomyces* Genome Database (www.sgd.com).

Table 4: Oligonucleotides used in this study

Primer labeling	***Primer sequence (5`- 3` direction)***
ADA2-300bp-fw	GCGTCTTCCAGATGAAATTCTTCG
ADA2-300bp-rev	GAAAAATGAGTATCGTTCATATTTACAAGAC
ADA2-S1-fw	GCGTAGTCTGAAAATATATACATTAAGCAAAAAGAATGCGTACGCTG CAGGTCGAC
ADA2-S2-rev	CTAGTGACAATTGTAGTTACTTTTCAATTTTTTTTTTGTTAATCGATGA ATTCGAGCTCG
SPT7-300bp-fw	GGAATGCTTGTTGGGACTAAC
SPT7-300bp-rev	GCTCTTATCTTTGAGAGAAACAACG
SPT7-S1-fw	CTTTAAACTGTAACACTACAAAGAAATTAAGTCTGAATAATGCGTAC GCTGCAGGTCGAC
SPT7-S2-rev	GATAAAATATTCAACTATTTAGCGCGCTCATTAATCGATGAATTCGA GCTCG
UBP8-300bp-fw	GTGAAAAAAAATCCTCGATTATAGTG
UBP8-300bp-rev	CTTTAATTATTACTATATATAAACTCAC
UBP8-S1-fw	CCCTGCTTTTTTTATTTGTTATTAATAATTATGCGTACGCTGCAGGTC GAC

UBP8-S2-rev	GTTTTATTATTATTGTTGAATGCTATTTGCTGAATCAATCGATGAATT CGAGCTCG
SAS3-S1-fw	CTTCCTTCTTCATTAATTAGTCTCCGTATAATTTGCAGATAATGCGTA CGCTGCAGGTCGAC
SAS3-S2-rev	CATGTATATGCTTATATCCAATATATACCCATCGCCGCTTAATCGATG AATTCGAGCTCG
SAS3-300bp-fw	CGTTCAGGCCAATTGAACAAGAAA
SAS3-300bp-rev	GCTTTCTTCTATGACCAGCGC
RTT109-S1-fw	CCAGTAGAGTTAAAAGGTCAATTCAACCGGTCTTCAATAAGACATGC GTACGCTGCAGGTCGAC
RTT109-S2-rev	CGATGCTACATACGTGTACTAAATAATAAATATCAATATGTATCAATC GATGAATTCGAGCTCG
RTT109-300bp-fw	CCTAAAATCGATCAAGATATGG
RTT109-300bp-rev	CTAAACTAGCCATTCTTTATCC
HPA2-S1-fw	CTTAGTATTTTATATGCCAAGAAAGCAAACAGCCCTTTCTGTGTAGC ATGCGTACGCTGCAGGTCGAC
HPA2-S2-rev	TTTTTTTTTTTCTATACATCCATACTACTGAGGTAATTAGTGTTTTCAA TCGATGAATTCGAGCTCG
HPA2-300bp-fw	CTTTATAAGACGTTTGCGAAATAC
HPA2-300bp-rev	CTGGATTTATTGGATTGGC
ELP3-S1-fw	CAAGTCCTAAAAGCACCTAAGGAAAATCGAAGAACACCCTGACAAA GATGCGTACGCTGCAGGTCGAC
ELP3-S2-rev	CTTGGAAAACCGGCCATGTCGGCGGCACATAAAAGTTCTATTTACC TTCAATCGATGAATTCGAGCTCG
ELP3-300bp-fw	CAGCGATAAGACAGTGAG
ELP3-300bp-rev	CGTATATGTTATGTATGTATATAAATTGT
SPT10-S1-fw	CTTCCGCCAAAGTGATTATCAACAAAAATCGTAATAATTAGCTTCAAT GCGTACGCTGCAGGTCGA
SPT10-S2-rev	CTTTATAGTTTCTAGGGTTGGTGATGTGACCGTCTCTGGCAGAGTC GCAATTCAATCGATGAATTCGAGCTCG
SPT10-300bp-fw	GCAACCCGTTTTAATTTACTAG
SPT10-300bp-rev	CTAATCTGGAAAATTTTGCAGC
HAT1-S1-fw	GCAAAATTATGCTTAAGCTATAACTATAGTGAGAATCAAGAATATGC GTACGCTGCAGGTCGAC
HAT1-S2-rev	CAGGCTTGTTAAACAAATAAATATGTTATTATATATTTAATAAACAGTT AATCGATGAATTCGAGCTCG
HAT1-300bp-fw	GCCAGTCCAAACTGTTTCATG
HAT1-300bp-rev	GATCTATTTGTGATCACTACCATG
CSE4 1-134 fw	GGGCCCATGTCAAGTAAACAACAATGG
CSE4 1-134 rev	CTCGAGTTAAGGAGTATATTTCTTTTCGAC

CSE4 14-134 fw	GGGGCCCATGAGTGATTCGAGTGGAAG
CSE4 33-132 fw	GGGCCCATGTCTATTAACGATCGTGCG
CSE4 33-132 rev	CTCGAGTTAATATTTCTTTTCGACGCG
CSE4 1-100 rev	GCTCGAGATTATGGTGCAGGTACTTCAGT
CTF19 fw	GCGGATCCGATGAACATTGATGGGGAC
Ctf19 rev	GGCGGCCGCTCAGAATAGGCAAAC
MCM21 fw	GCCATATGAGCGCTAATCCTATAGTACAAGAA
MCM21 rev	GCGGTACCTCACTTGAATATTGTCGCGAA
KanMX fw K3	CCCAGATGCGAAGTTAAGTGCGC
KanMX rev K2	GCCCCTGAGCTGCGCACGTC
NatMX fw	CCCAGATGCGAAGTTAAGTGCGC
NatMX rev	TTCCGCGTCAACCGCCACCGGGGAC
Cbf1-300bp-fw	GTACATCGATGTACGTGATC
Cbf1-300bp-rev	GAAAACGGAGGTTGTGC

2.4. *Saccharomyces cerevisiae* media and growth conditions

Yeast cells were cultured as described previously (Sherman, 1991) in rich medium YPD (10 g/l yeast extract, 20 g/l peptone, 20 g/l glucose) or minimal medium YM (6.7 g/l yeast nitrogen base w/o amino acids and 2 % glucose) at 30°C unless indicated otherwise. YM was supplemented according to the required auxotrophic markers (20 µg/ml adenine, histidine, methionine, tryptophan and uracil or 30 µg/ml leucine and lysine).

2.5. Construction of *Saccharomyces cerevisiae* strains

2.5.1. Crossing, sporulation and dissection of asci

For the crossing of two parental strains carrying complementary mating types, the strains were mixed on YPD plates in a drop of YPD medium and incubated for at least 8 h at 30°C. Subsequently, the mixture was plated on selective YM plates to select for diploid cells. Sporulation was induced by plating the cells on sporulation medium (20 g/L agar, 19 g/L KAc, 0.675 mM ZnAc) and incubation for two to three

days at 23 or 30°C. For ascus digestion, a small amount of cell material was incubated in zymolyase buffer (1 M sorbitol, 0.1 M sodium citrate, 60 mM EDTA, pH 8.0, 5 mg/ml zymolyase) for 5 min at RT. The reaction was stopped by addition of A. dest. Subsequently, the digested ascospores were dissected using a Zeiss AxioscopeFS microscope connected to a Narishige micromanipulator. The plates were incubated for three days at 30°C. To follow the segregation of markers, plates were replicated on selective YM medium for each marker.

2.5.2. DNA techniques in Saccharomyces cerevisiae

Gene knock- out constructions with NatMX or KanMX cassettes, were performed as described (Wach et al., 1994). Correct integration of each gene deletion was verified by colony-PCR analysis. The double knock-out mutant strains were generated by isogenic crosses, followed by tetrad dissection and analysis of marker segregation. For this purpose a small quantity of cells of each colony was transferred to a PCR tube and the DNA was released from the cells at 100°C for 2 min, before adding the PCR mix and starting the standard PCR reaction.

2.5.3. Preparation of Saccharomyces cerevisiae lysates

For immunoprecipitation experiments, yeast cells were pre-cultured over night and diluted to a starting OD_{600} of 0.1 in 500 ml YPD medium. Cells were grown to exponential phase OD_{600} 0.8, or for cell cycle experiments 0.6- 0.7, and harvested by centrifugation at 4000 rpm for 5 min. Pellets were suspended in 5 ml cell lysis buffer (150 mM NaCl, 50 mM Tris-HCl, 1% Nonidet P-40, protease inhibitors (Roche)), transferred to a porcelain mortar and flash frozen in liquid nitrogen. Subsequently, cells were pestled until a fine-grained powder was generated. After thawing, the lysate was cleared from cell debris by centrifugation at 5000 rpm for 15 min at 4°C. The supernatant was frozen in liquid nitrogen for storage at -20°C or freshly used for immunoprecipitation procedures.

2.6. Molecular cloning

Cloning was carried out according to standard techniques (Sambrook et al. 1989). The oligonucleotides (Table 4) and plasmids (Table 3) used in this study were taken from the laboratory's common primer collection or synthesized by Metabion (Martinsried) and dissolved to a final concentration of 100 pmol/µl. Primer design was accomplished with genome sequences derived from the *Saccharomyces* Genome Database (www.sgd.com). Kits for plasmid isolation were purchased from Qiagen or Macherey and Nagel. Restriction endonucleases and appropriate buffers were purchased from New England Biolabs, pGEMT vector systems Kit from Promega and T4 DNA Ligase from Thermo Scientific.

For preparative protein purification, GST-tagged N-terminal regions of Cse4 were constructed with a modified pET41b$^+$ vector (Novagen; modified by AG Bayer, University of Duisburg-Essen). The vector was provided with a PreScission Protease cleavage site introduced C-terminal of the *GST* gene (Figure 8). Second, an *Apa*I cleavage site was deleted at position 2135. Four different N-terminal *CSE4* fragments were constructed, one fragment spanning almost the whole N-terminal tail (aa 1-134) and three shorter fragments (aa 1-100, 14-134 and 33-132), all four containing the essential N-terminal domain (END).

DNA sequences of the *CSE4* fragments were amplified via PCR using pAE906 as template, introducing an N-terminal *Apa*I and a C-terminal *Xho*I cleavage site, and were ligated into pGEMT. For further cloning steps, correct clones were confirmed by control restriction digests or sequencing and transformed into *E. coli* SHOX cells, a dam- strain to avoid the blocking of the *Apa*I recognition site by overlapping Dam methylation at the specific site. Subsequently, pGEMT-*CSE4* clones were digested with *Apa*I and *Xho*I and fragments were isolated using gel elution. The N-terminal *CSE4* fragments and the *Apa*I/*Xho*I linearized pET41b$^+$ vector were ligated, and correct clones were identified via restriction digestion or sequencing and subsequently transformed into *E. coli* Rosetta. Finally, the correct gene products were tested for expression and solubility.

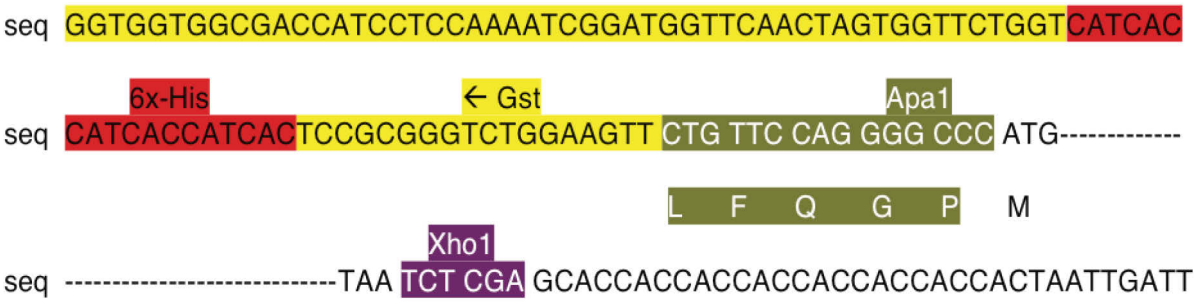

Figure 8: Modified cloning site of the pET41b$^+$ vector.
Illustrated is a cutout of the DNA sequence of the pET41b$^+$ vector-cloning site, which codes for a GST-tag (highlighted in yellow), including a 6x-His-tag indicated in red. The vector was also provided with a PreScission Protease cleavage site (olive), with an overlapping *Apa*I cleavage site. *Xho*I cleavage site is shown in purple. In the resulting target proteins, the tags are located N-terminal of the protein sequence.

For co-expression of the two target genes *CTF19* and *MCM21*, the pETDuet vector system (Novagen) was used. PCR products of the target genes carrying the corresponding cleavage sites were gained by standard PCR methods using yeast genomic DNA isolated by Winston DNA preparation as the template (Hoffman and Winston, 1987). According to its assumed insolubility when expressed alone (Schmitzberger and Harrison, 2012), *CTF19* 35-363 was cloned to multiple cloning site 1 (MSC1), C-terminal of a 6x-His tag. Its putative interaction partner *MCM21* 41-368 was cloned to multiple cloning site 2 (MSC2), without a tag. The *CTF19* gene was inserted via *Bam*HI/ *Not*I; the *MCM2*1 gene was inserted using *Nde*I/ *Asp*718 into the target vector, and correct clones were identified via restriction digestion and sequencing. Vectors were transformed into *E. coli* Rosetta and tested for expression level and solubility of the target proteins.

2.7. Purification of recombinant proteins

2.7.1. Recombinant protein expression

For heterologous expression of recombinant yeast proteins in *E. coli*, Rosetta cells carrying the corresponding plasmids were pre-cultured overnight and used to inoculate the expression culture starting at an OD_{600} of 0.1. Cells were grown to

exponential phase (OD_{600} 0.8) at 37 or 30°C. To induce protein expression, 0.1 mM IPTG was added and the cells were shifted to 18, 20 or 30°C as indicated, followed by protein expression for six hours at 30°C or 18-20°C over night. Cells were harvested at 7000 rpm for 10 min, frozen in liquid nitrogen and stored at -20°C, if not freshly used.

For protein expression tests Rosetta cells carrying the corresponding plasmids were inoculated with overnight pre-cultures starting at an OD_{600} of 0.1. Cells were grown to an OD_{600} of 0.8 and separated into four cultures of equal volume and transferred to 18, 23, 30 or 37°C. Expression was induced with 0.1 mM IPTG. Cultures were incubated for 6 hours or over night, and samples were taken after 2, 4, 6 and 18 hours of expression. The samples were subjected to SDS-PAGE and the protein amount in the soluble fraction was compared to that of the pellet fraction based on Coomassie blue staining. The expression conditions yielding the highest expression levels and solubility of the N-terminally GST-tagged Cse4 fragments were used.

2.7.2. Preparation of *E. coli* cell lysates

Harvested Rosetta cells were suspended in sonication buffer (150 mM NaCl, 50 mM Tris-HCl pH 7.5, a spatula tip of DNAse I, 2 mM DTT, 10% glycerol, 1% NP-40 and protease inhibitors (Roche)), and subsequently sonicated using a Bransonic Digital Sonifier S450D. To clear the lysate from cell debris, whole cell extracts were centrifuged at 48.000 x g for at least 60 min and supernatant was retained. Lysates were frozen in liquid nitrogen and stored at -20°C, or freshly used for further purification steps or pull-down experiments.

2.7.3. Affinity purification of GST- and 6x His-tagged proteins

Lysates containing the tagged target proteins were passed through 0.45 µm filter and incubated with equilibrated Glutathione agarose resin (Qiagen) or Ni^{2+}-NTA (BioRad) for two hours on ice and packed on Poly-Prep chromatography columns (BIO-RAD), followed by three washing steps, one of them a high salt wash (0,5 M NaCl, 50 mM Tris-HCl pH 7.5). The beads-protein-mixture was either directly used for subsequent pull-down experiments, or target proteins were eluted from the column using elution

buffers for GST-tagged proteins (20 mM glutathione, 150 mM NaCl, 50 mM Tris-HCl, pH 7.5), or for His-tagged proteins (150 mM imidazole, 150 mM NaCl, 50 mM Tris-HCl, pH 7.5). In case of His-tag affinity purification, an additional washing step using 10 mM Imidazole was used before the elution.

For further purification, eluted proteins were concentrated with Amicon Ultra centrifugal filters with molecular weight cutoffs between 3 – 30 kDa, and the final protein concentration was determined using the Nano Drop Spectrophotometer ND-1000 (PeqLab). The GST-tag was cleaved off using the PreScission Protease. Cleavage of the target protein was carried out using 0.16 µl/mg protease in cleavage buffer (150 mM NaCl, 50 mM Tris-HCl, 1% TritonX-100, pH 7.5) o/n at 4°C.

2.7.4. Gel Filtration

Size exclusion chromatography via gel filtration was used to separate target proteins from free GST and the PreScission Protease, and was carried out using an ÄKTA FPLC purification system (GE Healthcare). Protein solutions were adjusted to a final volume of 5 ml with 50 mM Tris-HCl, 150 mM NaCl, pH7.5, passed through a 0.45 µm filter and loaded onto a HiLoad 26/600 Superdex 75 pg column (GE Healthcare). Separated proteins were fractionated and collected at a flow rate of 0.5 – 1 ml/min, adjusted to the maximum allowed column pressure. Complete sample chromatography was carried out in one column volume (i.e., 320 ml) in 2 ml fractions, each peak was concentrated using Amicon Ultra centrifugal filters and analyzed by SDS-PAGE and Coomassie staining.

2.8. Immunoprecipitation

For immunoprecipitation experiments, 400 OD yeast cells were harvested and lysates were prepared as described above. The total protein concentration of each lysate sample was verified via Nano drop and adjusted with IP buffer to achieve equal protein amounts of wild type and mutant lysates. The protein concentration of the lysates was approximately 20 mg/ml. 20 µl of each lysate was frozen in liquid nitrogen as a loading control. Samples were then divided into three aliquots of equal size (approximately 1 ml of each sample), and incubated with 40 µl Protein G

Agarose (Pierce) at constant rotation for one hour at 4°C. Beads were pelleted at 1000 rpm for 30 sec, and the supernatant was supplemented with the α-Cse4 modification antibody (10 µl), or α-HA antibody (2 µl) or without antibody as controls. Aliquots were incubated rotating o/n at 4°C. Subsequently, 100 µl Protein G Agarose was added to the samples, incubated for 2.5 hours and, finally, the beads were washed 3 times with lysis buffer and suspended in 50 µl 4x Laemmli buffer (final concentration 62.5 mM Tris pH 6.8, 2% SDS, 10% glycerol, 5% 2-mercaptoethanol, 0.001% bromophenol blue). SDS-PAGE and Western blotting were performed as described below.

2.8.1. Synchronization of *Saccharomyces cerevisiae* cells

For cell cycle experiments, 1 l of yeast cells in YPD were grown at 30°C to exponential phase (OD_{600} 0.6- 0.7) and divided into four cultures of equal volumes. To arrest cells in S-phase, they were treated with hydroxyurea (10 mg/ml) and incubated for three hours at 30°C. For a G2/M cell cycle arrest, cells were incubated with nocodazole (10 µg/ml) for three hours. To obtain cells in G1 phase, the culture was incubated with nocodazole (10 µg/ml) for three hours and harvested in a sterile beaker. Subsequently, cells were suspended and further incubated in YPD to release them into G1 phase. To monitor the cell cycle arrest, 50 µl of the culture were sonicated 3 times for 10 s and checked under the light microscope for characteristic properties of each cell cycle phase. As a control, one population was left asynchronous. Accordingly, 0.1 OD of the cells were taken for fluorescence activated cell sorting (FACS) analysis and cells were frozen in liquid nitrogen and stored at -20°C.

For S-phase release, 1 l of MATa *bar1Δ* yeast cells were cultured to exponential phase (OD_{600} 0.6 -0.7) at 30°C. Subsequently, 200ml of the culture was separated and left asynchronous as control. The remaining culture was incubated with α-factor (25 ng/ml) for at least one hour. G1 arrest was checked under the microscope repeatedly, until the majority of the cells displayed G1 typical morphological characteristics. G1-arrested cells were harvested and washed once with YPD. Sample “0” was taken and the pellet was suspended in YPD containing Pronase E (100 µg/ml) to release cells into S-phase. The culture was incubated at 30°C for 1.5

hours, and 0.1 OD samples were taken after 20, 40, and 60 minutes for FACS analysis. 200 ml of the asynchronous control cells and 200 ml of each of the corresponding time points were harvested and cell lysates for subsequent immunoprecipitation experiments were prepared as described above.

2.8.2. FACS analysis

For FACS analysis, 0.1 OD of yeast cells were harvested, washed once in H_2O and fixed in 70% ethanol o/n at 4°C. Samples were then washed twice with 20x TE (0.2 M Tris pH 8.0, 0.02 M EDTA pH 8.0), suspended in 100 µl 20x TE/ RNase A (1 µg/µl) and incubated for 4 h at 37°C. Subsequently, cells were washed twice with PBS and stained in 50 µl PBS with propidium iodide (PPI, 100 µg/ml) o/n at 4°C. Finally, cells were diluted 10-fold using PBS and sonicated 3 times for 5 s on the Bioruptor and transferred to falcon polystyrene tubes for the FACS measurements. DNA contents of the samples were measured at a BD FACSCalibur or at a BD FACSAriaII and analyzed using FlowJo.

2.9. Protein- protein interaction assays

2.9.1. Peptide pull-down assay

To ensure equal amounts of target proteins incubated with the beads, the total protein concentration of each lysate was measured at the Nano drop Spectrophotometer ND-1000 (PeqLab), and adjusted to a final protein concentration of 20mg/ml. 50 µl of peptide coupled sulfolink beads (described in 1.12.1) were incubated rotating with 1.5 ml adjusted *E. coli* protein lysates o/n at 4°C. Control samples were incubated accordingly, but with uncoupled beads. Subsequently, beads were pelleted at 1000 rpm for 30 sec and washed twice with washing buffer (50 mM Tris-HCl pH 7.5, 150 mM NaCl, 1% Triton X-100). The beads were suspended in 50 µl 1x Laemmli buffer and SDS-PAGE and western blotting were performed as described above.

2.9.2. Pull-down assay

For pull-down experiments, GST-Cse4 aa 14-134 and 6x His-Ctf19, were affinity purified as described above (2.7.3). 6x His-Ctf19 was eluted from the Ni^{2+}-NTA resin using 150 mM imidazole and concentrated in pull-down buffer (50 mM Tris-HCl pH 7.5, 150 mM NaCl, protease inhibitors (Roche), 0,5% NP 40). Matrix-bound GST-Cse4 aa 14-134 was not eluted and functioned as “immobilized bait“. 1 ml of Ctf19 (prey protein) was incubated with 100 µl immobilized bait matrix o/n at 4°C, and successively washed with low salt (150 mM NaCl, 50 mM Tris-HCl, pH 7.5) and high salt buffer (0.5 M NaCl, 50 mM Tris-HCl, pH 7.5). As controls, prey proteins were incubated with the equilibrated matrix in the absence of GST-Cse4. SDS-PAGE analysis followed by Coomassie blue staining was performed to assess protein-protein interactions.

2.9.3. Yeast two-hybrid assay

Two-hybrid interactions were tested by transformation of the plasmids (pBTM117c and pACT2 derivates) containing the genes for expression of the bait and the prey proteins, respectively, in the two-hybrid test strain (AEY4217). Full-length and N-terminal *CSE4* (aa 11-139) were tested using *CTF19* as a control. The reporter strain contained two reporters under the control of the Gal4 promoter, the *HIS3* gene and a *lacZ* reporter. The activation of the *lacZ* reporter was analyzed by incubating the strains on a nitrocellulose membrane, which was frozen in liquid nitrogen and incubated with buffer Z (60 mM Na_2HPO_4, 40 mM NaH_2PO_4, 10 mM KCl, 1 mM $MgSO_4$, pH 7.0 and freshly added 0.1% X-Gal) at 30°C o/n to induce the color reaction. The appearance of blue color indicated the activation of the *lacZ* gene in the respective clones. Activation of the *HIS3* reporter gene was tested by incubating the strains on plates lacking histidine for three days at 30°C.

2.10. SDS-PAGE and immunoblotting

SDS-PAGE was carried out according to standard procedures (Laemmli, 1970) in 12.5% SDS gels. Gels were stained in Coomassie brilliant blue G-250 for at least one hour or o/n at RT, and destained with 20% methanol, 25% acetic acid. Transfer to

nitrocellulose membranes (Amersham Hybond ECL, GE Healthcare) was accomplished by blotting with 5.5 mA x h/cm^2 in the BIO-RAD Tank Transfer System in transfer buffer (48 mM Tris base, 0,037% SDS, 39mM Glycine and 20% methanol). Subsequently, the membrane was blocked in 5% milk/TBS-T (50 mM Tris-HCl, 150 mM NaCl, 0,001% Tween-20, pH 7.6) for 30 min to 1 h at RT.

Antibodies used in this study are listed in Table 5. Membranes were incubated with the primary antibodies in 5% milk/TBST for 2 h at RT or o/n at 4°C, and washed 3 times for 5 min in TBST. Secondary antibodies were incubated with the membranes in 5% milk/TBST for 1 h at RT followed by washing for one or two hours in TBST. Strong signals were detected by the use of freshly made ECL reagents (Luminol, enhancer: Horse radish peroxidase, 1,5 M Tris-HCl pH 8.8) or Amersham ECL Western Blotting Analysis System (GE Healthcare). Weak signals were detected using the Amersham ECL Select System (GE Healthcare). Amersham Hyperfilm ECL chemiluminiscence films (GE Healthcare) were used to develop western blots and dot-blots.

Table 5: Antibodies used in this study

Antibody	***Application***	***Concentration***	***Source***
α-HA mouse	Western blotting,	1:1000	Covance
	Immunoprecipitation	1:500	
α-poly-His mouse	Western blotting	1:3000-1:5000	Sigma
α-GST mouse	Western blotting	1:1000-1:3000	Sigma
α-mouse HRP	Western blotting	1:1000	Sigma
α-rabbit HRP	Western blotting	1:5000	Sigma
α-Cse4-K49ac rabbit	Immunoprecipitation	1:100	A. Samel (AG Ehrenhofer-Murray)
	Dot blot analysis	1:1000	
α-Cse4-R37me rabbit	Immunoprecipitation	1:100	A. Samel (AG Ehrenhofer-Murray)
	Dot blot analysis	1:1000	

2.11. Dot-blot analysis

For analysis of HPLC fractions of analytical purification of 3x HA-Cse4, 5 µl of every second to fifth fraction were spotted on a PVDF membrane (GE Healthcare), dried at RT and blocked in 5% milk/TBST for 1 h. The α-HA antibody was incubated with the membrane at a dilution of 1:1,000 in 5% milk/TBST o/n at 4°C. The α-mouse HRP antibody and TBST washing buffer were used as described above. Signal detection was performed in Amersham ECL Western Blotting Analysis System (GE Healthcare).

For test of affinity purification of antibodies against acetylated and methylated Cse4 peptides, unmodified and modified peptides of each species (Table 6) were serially diluted and 5 µl spotted on nitrocellulose membranes (Amersham Hybond ECL, GE Healthcare) and dried at RT. Membranes were blocked for 1 h in 5% milk/TBST. Subsequently, the primary antibody was incubated with the membrane 1:200 – 1:1,000 o/n at 4°C. The secondary antibody was incubated 1:5,000 for 1 h at RT. Washing steps and signal detection were performed as described above.

2.12. Affinity purification of polyclonal antibodies

Acetylated K49 and methylated R37 peptides were synthesized by Biosyntan Berlin (designed by Anke Samel, AG Ehrenhofer-Murray) and rabbits were immunized against the specific modification peptides on the N-terminus of Cse4. The α-Cse4-K49ac antibody production in rabbit immune serum (animal 2, immunization day 115) was done by Dr. J Pineda Antibody Service; α-Cse4-R37me antibodies were produced in rabbit immune serum (animal 21240 bleeding 06.05.2012) by BioGenes GmbH Berlin.

2.12.1. Peptide-coupling to sulfolink beads

Lyophilized modified and unmodified peptides of the N-terminus of Cse4 (Table 6) were dissolved (1 mg/ml) in binding buffer (50 mM Tris-HCl pH 8.5, 5 mM EDTA-Na). 1 ml Sulfolink beads containing 50% beads in the slurry (Sigma) were washed with 2 column volumes of binding buffer, suspended in 0.5 ml (1:1 ratio) with the dissolved

peptides, and incubated for 1 h at RT rotating on a wheel. Subsequently, both mixtures were washed with 3 column volumes of binding buffer and incubated for 1 h with one column volume of cysteine (50 mM cysteine, 50 mM Tris-HCl pH 8.5, 5 mM EDTA-Na) at RT. Subsequently, the beads were washed, each with 16 column volumes salt buffer (1 M NaCl, TBS, 5mM EDTA-Na, 0.05% NaN_3). Storage of the peptide-bound beads was carried out at 4°C in TBS/5 mM EDTA-Na, 0.05% NaN_3.

Table 6: Peptides used in this study

Peptide sequence of Cse4	***Length/modification***
S I N D R A L S L G G C	(aa 33-41) unmodified
S I N D R**me** A L S L G G C	(aa 33-41) monomethylated on R37
T R A T K N L F P G G C	(aa 45-53) unmodified
T R A T K**ac** N L F P G G C	(aa 45-53) acetylated on K49

2.12.2. Peptide-based affinity purification of polyclonal antibodies

From rabbit immune serum, 5 ml were incubated with a final concentration of 5 mM EDTA for 1 min and clarified by centrifugation at 4000 rpm for 25 min at 4°C. Subsequently, the supernatant was mixed with 125 µl of beads coupled to the modified Cse4 peptide and incubated for 2 h at 4°C while rotating on a wheel. Then the mixture was washed twice with 12 ml TBS/5 mM EDTA and the antibody was eluted twice from the beads with 125 µl 0.1 M glycine, pH 2.5, by incubation for 5 min at RT and two centrifugation steps at 4000 rpm for 15 sec. 3 µl of 1 M Tris, pH 9.5, was added to neutralize the solution, controlled with pH strips. This step was repeated until neutralization was accomplished. The antibody solution was dialyzed o/n against PBS at 4°C. Subsequently, the antibody was incubated with 40 µl of beads coupled to the unmodified peptide for 1 h at RT. Finally, the antibody was cleared by two centrifugation steps at 4000 rpm for 15 sec and 0.05 % NaN_3 was added for storage at 4°C. Specificity of the antibody was analyzed via Dot-blot as described above.

2.13. Analytical purification of Cse4

Cse4 was analytically purified according to the protocol (Waterborg, 2000) from 6,000 OD yeast cells, which were harvested for 10 min at 6,000 rpm. First, histones were extracted using 100 mM butyrate in nuclear isolation buffer (NIB; 20 mM HEPES, 0.25 M sucrose, 10 mM $MgCl_2$, 0.5 mM spermine, 2.5 mM spermidine, 0.1% w/v Trition X-100, 5 mM ß-mercaptoethanol, 1 mM PMSF, pH 7.0). The pellets, each containing 500 OD cells, were suspended in 3 ml NIB using 15 ml falcons. Subsequently, acid washed glass beads were added to the slurry until no supernatant remained. Each sample was homogenized by vortexing for 1-2 min, and the emerging supernatant was again covered with glass beads and vortexed for 1-2 min. Each falcon was supplemented with NIB to the 30 ml mark, shaken carefully and the supernatants were filtrated using Poly-Prep chromatography columns (BIO-RAD). The flow-through was centrifuged for 10 min at 30.000 x g and the supernatant was decanted. The pellet was suspended in 20 ml NIB and the step was repeated. One volume of 100 mM KP_i with 0.1% ß-mercaptoethanol and 40% guanidiumhydrochloride was added to each pellet. The extract was sonified 4 times for 30 sec and 60 sec cooling breaks on ice, and subsequently cleared by centrifugation for 10 min at 30.000 x g. To precipitate the DNA, 0.4 N HCl was added to the suspension and incubated on ice for 30 min, followed by subsequent centrifugation for 30 min at 30.000 x g with the brake function of the centrifuge switched off. The suspension was diluted with 0.1 M KP_i until the refractive index of 5 % guanidiumhydrochlorid was attained, 5 mM ß-mercaptoethanol was added, and the pH was adjusted using 5 N KOH to 6.8. Subsequently, 200 µl settled resin of the cation exchanger BioRex 70 per 10^{10} cells was added for incubation o/n at RT. The resin was washed 3 times with 0.1 M KP_i, 1.3 mM ß-mercaptoethanol and 5% guanidiumhydrochloride. The histone extracts were eluted with 10 column volumes of 0.1 M KP_i, 40% guanidiumhydrochloride and 1.3 mM ß-mercaptoethanol. Subsequently, the eluate was dialyzed twice for 1 h and once again o/n against 2.5% acetic acid with 1 mM ß-mercaptoethanol at 4°C and then filtrated with Amicon Ultra centrifugal filters with molecular weight cutoffs of 10 and 100 kDa to concentrate the eluate to 2 ml. The supernatant was lyophilized for 2 or 3 days and dissolved in 200 µl filtered HPLC buffer (8M urea, 1 M acetic acid, 50 mM NH_4OH, 50 mM DTT). The samples were fractionated for 94 min by reversed-phase HPLC using an Agilent Zorbax 300SB-C3 column performing an acetonitrile gradient between 35 and 53%

(ACN; v/v) in 0.1 % trifluoroacetic acid at a flow rate of 1 ml/min. The fractions were analyzed by dot blot as described above and the Cse4-containing samples were lyophilized and used for Western blot analysis.

2.14. CD spectroscopy

The secondary structure of the N-terminus of Cse4 (aa14-134) was examined by CD spectrometry. Far-UV spectra were recorded using the Jasco J-710 Spectropolarimeter. Purified N-terminal Cse4 (aa 14-134) was diluted to a final concentration of 0.15 mg/ml (in 50 mM KPi and 150 mM NaCl, pH 7.5), and 200 µl of each sample was used for the measurement in 0.1 cm cuvettes (Hellma Analytics, Müllheim). Start and end wavelengths were set to 260 nm and 190 nm, respectively, and the temperature was set to RT. The spectra of purified N-terminal Cse4 (aa14-134), as well as GST as a control were recorded in 25 repeats and averaged for each spectrum. Data processing was performed by separately shifting the blank to zero and subsequent subtraction of the buffer containing blank-spectrum from the protein spectra was carried out. The measurements that were normalized against buffer conditions result in the final Far-UV spectra of GST control protein and Cse4 aa14-134. To estimate the secondary structure content by deconvolution, the CDSSTR algorithm was used (Sreerama and Woody, 2000).

3. Results

3.1. Identification of the histone acetyltransferase (HAT) responsible for the acetylation on K49 of CENP-A^{Cse4}

Two independent research groups detected posttranslational modifications of the N-terminus of CENP-A^{Cse4}, termed Cse4 in the following, by mass spectrometry, such as several phosphorylation sites located in the essential N-terminal domain and in its proximity. Additionally, one methylation on R37 and an acetylation on K49 were detected (Samel et al., 2012; Boeckmann et al., 2013). It was shown that the mutation of R37 to an alanine, which mimics an unmodified state, caused a strong growth defect and an arrest in G2/M phase when combined with the deletion of *CBF1*, which encodes an inner kinetochore component (Samel et al., 2012). Interestingly, when additionally mutating K49 to an arginine to mimic an unacetylated state, the growth defect of *cbf1Δ cse4R37A* was suppressed (A. Samel, unpublished data). This indicates that the acetylation of K49 has an influence on kinetochore establishment or cell cycle progression, but that it acts in a somehow antagonistic function to the R37 methylation. For a thorough understanding of the epigenetic regulation of kinetochore assembly to the centromeric regions of each chromosome during mitosis and meiosis, it is necessary to investigate the function of the posttranslationally modified N-terminal domain of Cse4. Understanding the regulation of accurate kinetochore assembly and chromosome segregation, which likely depends on several specific posttranslational modifications on Cse4, requires the identification of the histone modifying enzymes and the corresponding complexes that are crucial for this process. Accordingly, one part of this study focused on the determination of the HAT responsible for the acetylation on Cse4K49. Furthermore, the question was addressed in which complex this enzyme is engaged during this process.

3.1.1. Purification of polyclonal antibodies against acetylated Cse4K49

To investigate the function of the K49 acetylation via immunoprecipitation and pull-down experiments, a specific polyclonal antibody was raised in rabbits using an acetylated Cse4K49 peptide (amino acid sequence shown in Table 6). To increase the specificity of the α-Cse4-K49ac antibody against the acetylated N-terminal domain of Cse4, the antibody was purified using columns containing modified and unmodified Cse4K49 peptide, and its specificity was tested via dot blot analysis. Decreasing peptide concentrations of acetylated and unacetylated Cse4 peptides were used to define the specificity of the α-Cse4-K49ac antibody.

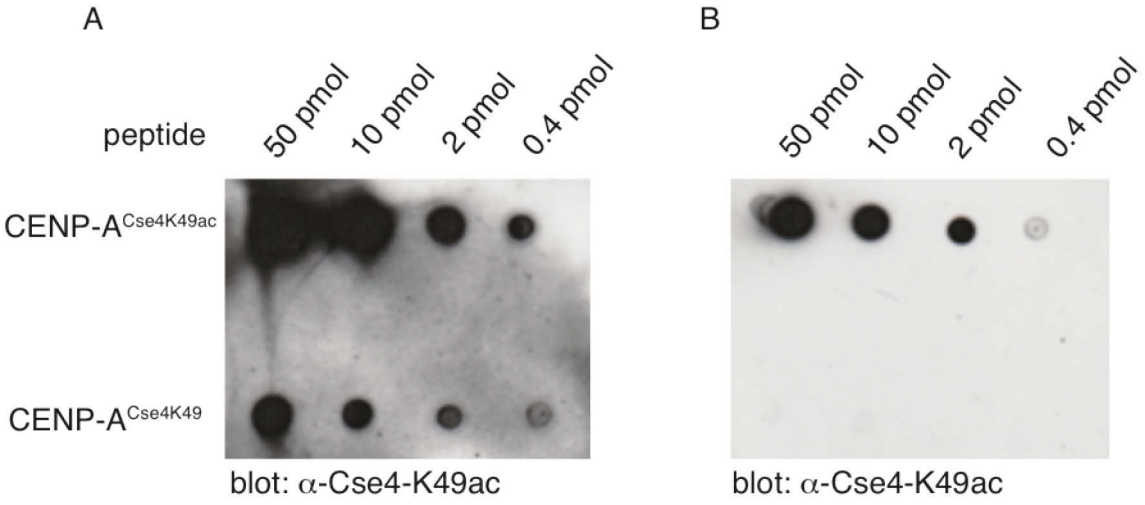

Figure 9: Peptide-based affinity purification of an α-Cse4K49ac specific antibody

Dot blot analyses of the affinity purification of the α-Cse4-K49ac antibody. The indicated amounts of unmodified and modified K49 peptides were spotted on nitrocellulose membranes and probed against the rabbit serum containing α-Cse4-K49ac antibody (1:1000) before clearing the serum solution using unacetylated K49 peptide (A) and after the clearing step of the serum solution (B).

Figure 9 illustrates that the α-Cse4-K49ac antibody is highly specific in distinguishing the acetylated K49 peptide and has a lower affinity for the unmodified K49 peptide. It is, thus, suitable for immunoprecipitation experiments. Furthermore, Figure 9B shows that the limit of detection ranges between 0.4 pmol and 2 pmol.

3.1.2. Cse4K49ac depends on the histone acetyltransferase Gcn5

To investigate the acetylation level on lysine 49 of Cse4, immunoprecipitation experiments using the α-Cse4K49ac rabbit antibody were carried out (see chapter 2.7). For this purpose, the Cse4 acetylation levels in *cse4Δ* strains carrying plasmid-borne 3xHA-*CSE4* or a non-acetylatable mutant allele 3xHA-*cse4K49R* (AEY2960) were compared. Including the internal 3xHA tag, the molecular weight of the entire 3xHA-Cse4 is approximately 32 kDa. For the immunoprecipitation reaction 400 OD yeast cells were used per strain and lysates were produced as described (see chapter 2.4.3.).

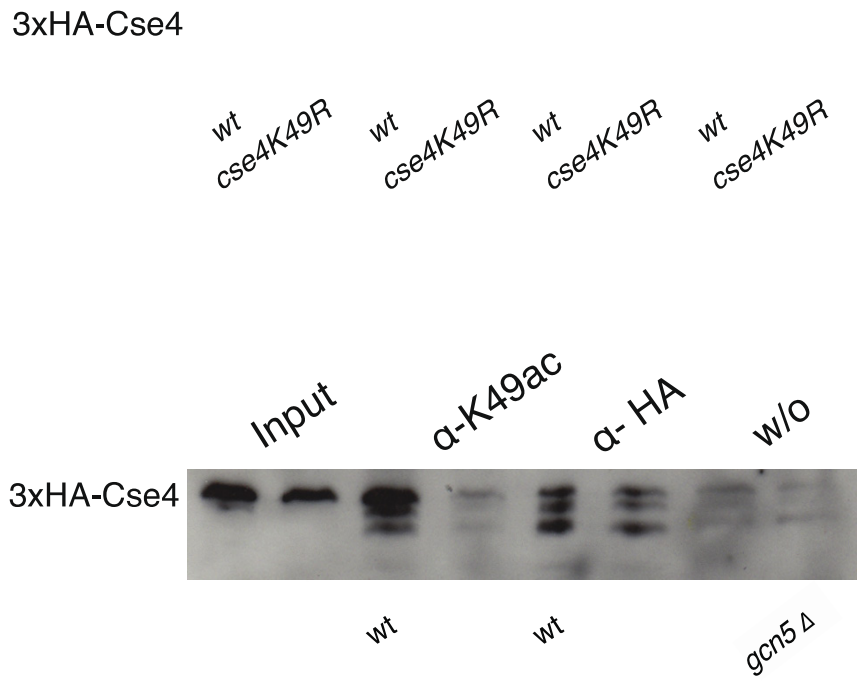

Figure 10: Identification of Gcn5 as the histone acetyltransferase that acetylates Cse4K49
A: Western blotting analysis of immunoprecipitated 3xHA-Cse4K49 acetylation in wild type (AEY2781) and 3xHA-Cse4K49R (AEY2960) showed reduced precipitated Cse4K49 acetylation signal in Cse4K49R **B**: Comparison of wild type (AEY2781) and *gcn5Δ* mutant (AEY5310) showed a significantly reduced acetylation level in the *gcn5Δ* mutant strain in comparison to wild type. Blots were incubated with α-HA antibody 1:1000 and α-mouse HRP 1:1000 antibodies. From left to right: input controls of wild type and mutant; precipitated acetylated Cse4K49 of wild type and mutant; precipitated 3xHA-tagged Cse4; negative controls w/o antibody. Two biological replicates confirmed this result.

As shown in Figure 10 A, the immunoprecipitation of acetylated Cse4 was decreased significantly in the *cse4K49R* mutant compared to wild type *CSE4*, as indicated, whereas the input controls of both strains showed intense 3xHA-Cse4 signals and the α-HA-immunoprecipitated Cse4 or *cse4K49R* controls showed equal protein amounts. However, in the course of the immunoprecipitation procedure, the target proteins were partially degraded, as indicated by comparison of the untreated input controls to antibody-treated lysates. In the gel, 3xHA-Cse4 runs above the calculated size, between 35 and 40 kDa. In a further control, unspecific binding of the target protein to the Protein G Agarose beads was considered, without addition of antibody to the lysates, as indicated, showing that unspecific binding could be excluded. The differences in the immunoprecipitation signals of Cse4 and *cse4K49R* reflect the specificity of the α-Cse4K49ac antibody.

Utilizing the α-Cse4K49ac antibody in further immunoprecipitation experiments, it was then investigated which histone acetyltransferase is responsible for the Cse4K49 acetylation. In a study in yeast, the genetic interaction of a *GCN5* deletion with a *cse41-4* allele demonstrated that the histone acetyltransferase Gcn5 acts at centromeres. Moreover, in *gcn5Δ* cells, G_2-phase as well as sister chromatid separation in anaphase is delayed (Vernarecci et al., 2008). Thus, in an immunoprecipitation experiment, the efficiency of a *gcn5Δ* strain to acetylate K49 on Cse4 was investigated. In Figure 10 B, the western blotting shows that the precipitation of acetylated Cse4K49 decreased significantly in the strain that lacks Gcn5 as compared to wild type. Controls were performed as described above. These results showed that the HAT Gcn5 is required for full acetylation of Cse4K49.

3.1.3. Deletion of other HAT genes did not decrease the acetylation on Cse4K49

The acetylation of Cse4K49 was strongly reduced in the *gcn5Δ* mutant, and it was further investigated if another HAT in *S. cerevisiae* was involved in this acetylation, because it is possible that there is an alternative pathway to acetylate Cse4K49. For example, it was previously shown in this laboratory that Cse4 co-immunoprecipitated with the HAT Sas2, linking Sas2, which is the catalytic subunit of the SAS-I complex, to the centromere (S. Seitz, unpublished data). To test whether auxiliary histone

acetyltransferases are able to acetylate lysine 49 likewise, immunoprecipitation experiments were performed in yeast strains that carry a deletion or a mutant allele of one of the previously identified yeast HATs (Figures 11 and 12).

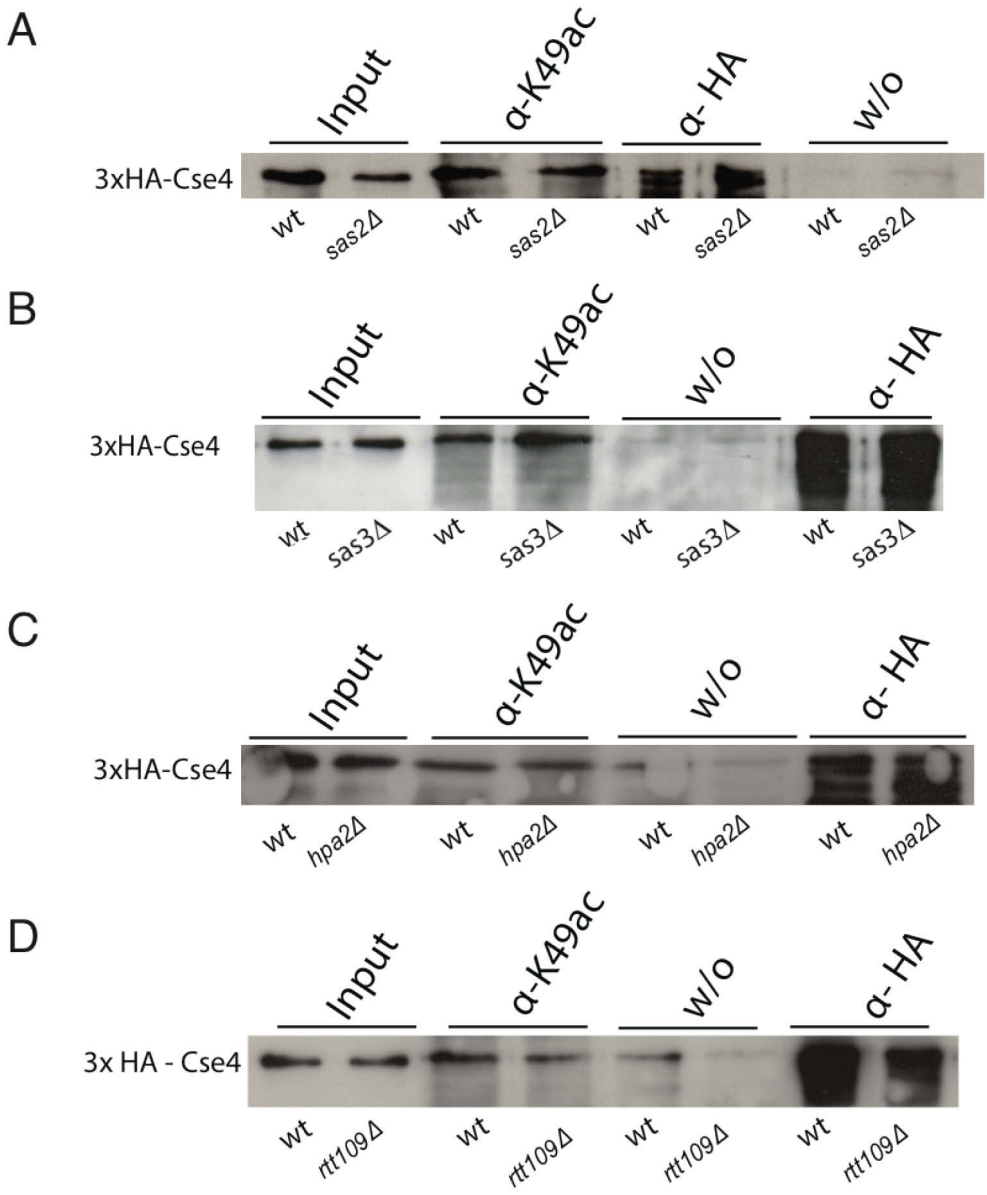

Figure 11: No influence of other histone acetyltransferases on Cse4K49 acetylation.
Western blotting analysis of immunoprecipitated acetylated Cse4K49 in wild type cells (AEY2781) and strains containing mutations in the HAT genes *sas2Δ* (AEY5312), *sas3Δ* (AEY5300), *hpa2Δ* (AEY5308) and *rtt109Δ* (AEY5306). Blots were incubated with α-HA and α-mouse HRP antibodies (1:1000). **A**: *sas2Δ* did not reduce the Cse4K49 acetylation signal detected by immunoprecipitation. The deletion of *sas3Δ* (**B**) *hpa2Δ* (**C**) and *rtt109Δ* (**D**) did not lead to significantly decreased acetylation on Cse4K49.

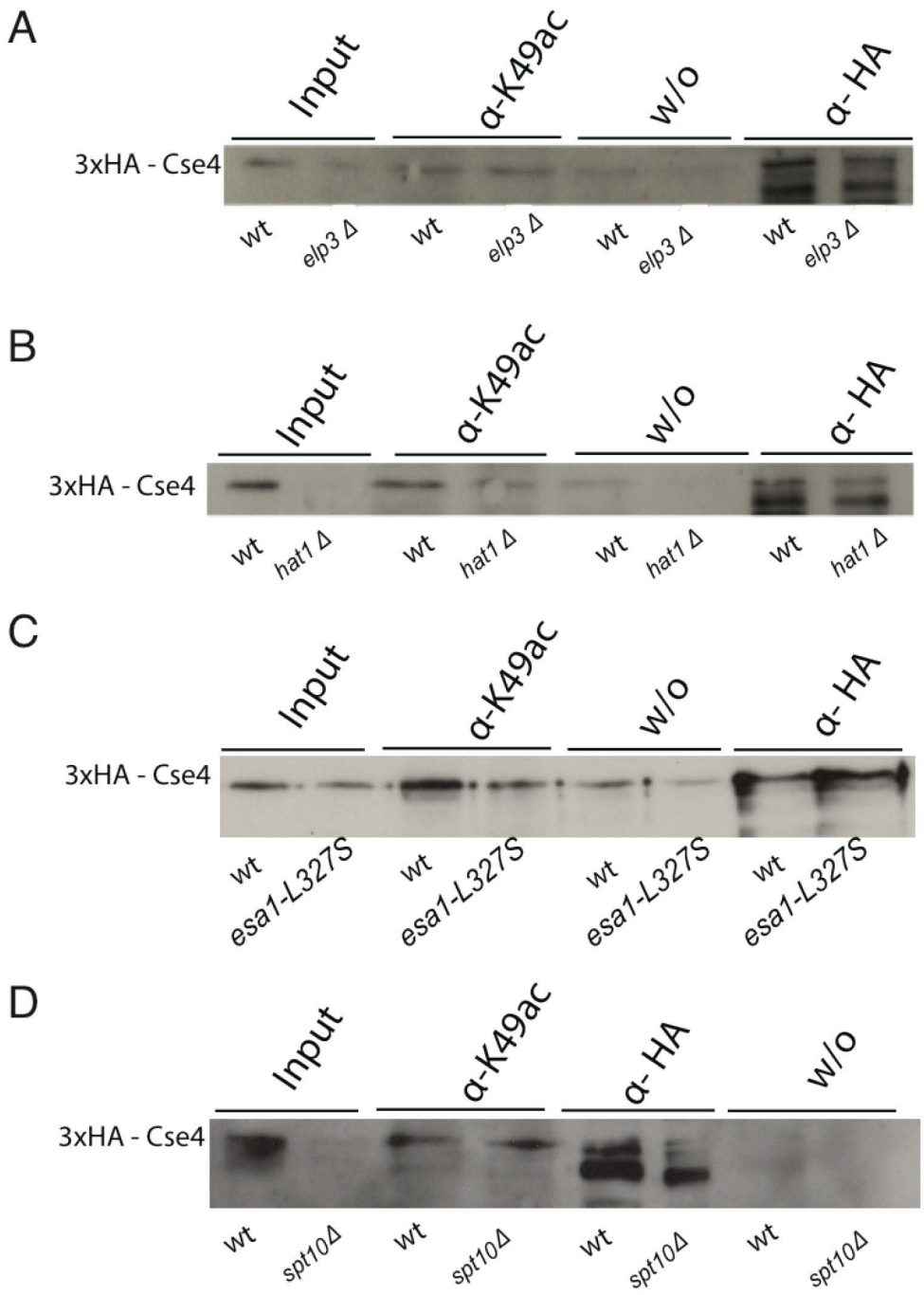

Figure 12: No influence of other histone acetyltransferases on Cse4K49 acetylation.
Western blotting analysis of immunoprecipitated acetylated Cse4K49 in wild type cells (AEY2781) and strains containing mutations in the HAT genes *elp3Δ* (AEY5302), *hat1Δ* (AEY5314), *esa1-L327S* (AEY5316) and *spt10Δ* (AEY5304). **A**: *elp3Δ* did not reduce the Cse4K49 acetylation signal detected by immunoprecipitation. The deletion of *hat1Δ* (**B**) *esa1-L327S* (**C**) and *spt10Δ* (**D**) did not lead to significantly decreased acetylation on Cse4K49. Blots were incubated with α-HA and α-mouse HRP antibodies (1:1000).

According to the western blots shown in Figure 11 A-D, *sas2Δ*, *sas3Δ*, *hpa2Δ* and *rtt109Δ*, showed no decreased immunoprecipitation of acetylated Cse4K49, whereas the input controls of these strains showed intense 3xHA-Cse4 signals and the α-HA-immunoprecipitated Cse4 or *cse4K49R* controls showed equal protein amounts. As in the case of the previously shown immunoprecipitations of *gcn5Δ* and *cse4K49R*, the α-HA-immunoprecipitated Cse4 was partially degraded, indicated by comparison of the untreated input controls to antibody-treated lysates. In a further control, unspecific binding of the target protein to the Protein G Agarose beads was considered without addition of antibody to the lysates, which showed that unspecific binding could be excluded in the case of Cse4 from *sas2Δ* and *sas3Δ*, whereas little unspecific binding was detected in *hpa2Δ* and *rtt109Δ*.

In Figure 12 A-D, the immunoprecipitation of acetylated Cse4K49 in *elp3Δ*, *hat1Δ*, *esa1-L327S* and *spt10Δ* mutants, respectively, is shown. Esa1 is an essential HAT (Clarke et al., 1999). Thus, this mutant was tested by the use of the temperature sensitive allele *esa1-L327S* in an *esa1Δ* mutant background. Here, as found for the HAT defective strains tested before (Figure 11), the acetylation signals in each of the mutants were not decreased compared to wild type signals. The input signals of *hat1Δ* and *spt10Δ* were not detectable, whereas α-HA-immunoprecipitated Cse4 was detected in all of the mutants. Low unspecific signal was detected in *esa1-L327S*.

Taken together, these immunoprecipitation data indicate that the acetylation of Cse4K49 in the essential N-terminal domain was only significantly influenced by the HAT Gcn5, and not by the other known HATs.

3.1.4. Detection of the Cse4K49 acetylation with antibodies in yeast

Immunoprecipitation was shown to be able to detect acetylated Cse4K49. In a further experiment it was investigated whether the Cse4K49 acetylation could be detected directly in histone extracts using the polyclonal α-Cse4K49ac antibody. Therefore, analytical purification of 3xHA-Cse4 from wild type and HAT deleted yeast cells was carried out (Waterborg, 2000; Figure 13 A and B), and it was expected to yield a decreased Cse4K49ac signal in at least one of the HAT mutants compared to equal amounts of wild type Cse4K49ac.

decreased Cse4K49ac signal in at least one of the HAT mutants compared to equal amounts of wild type Cse4K49ac.

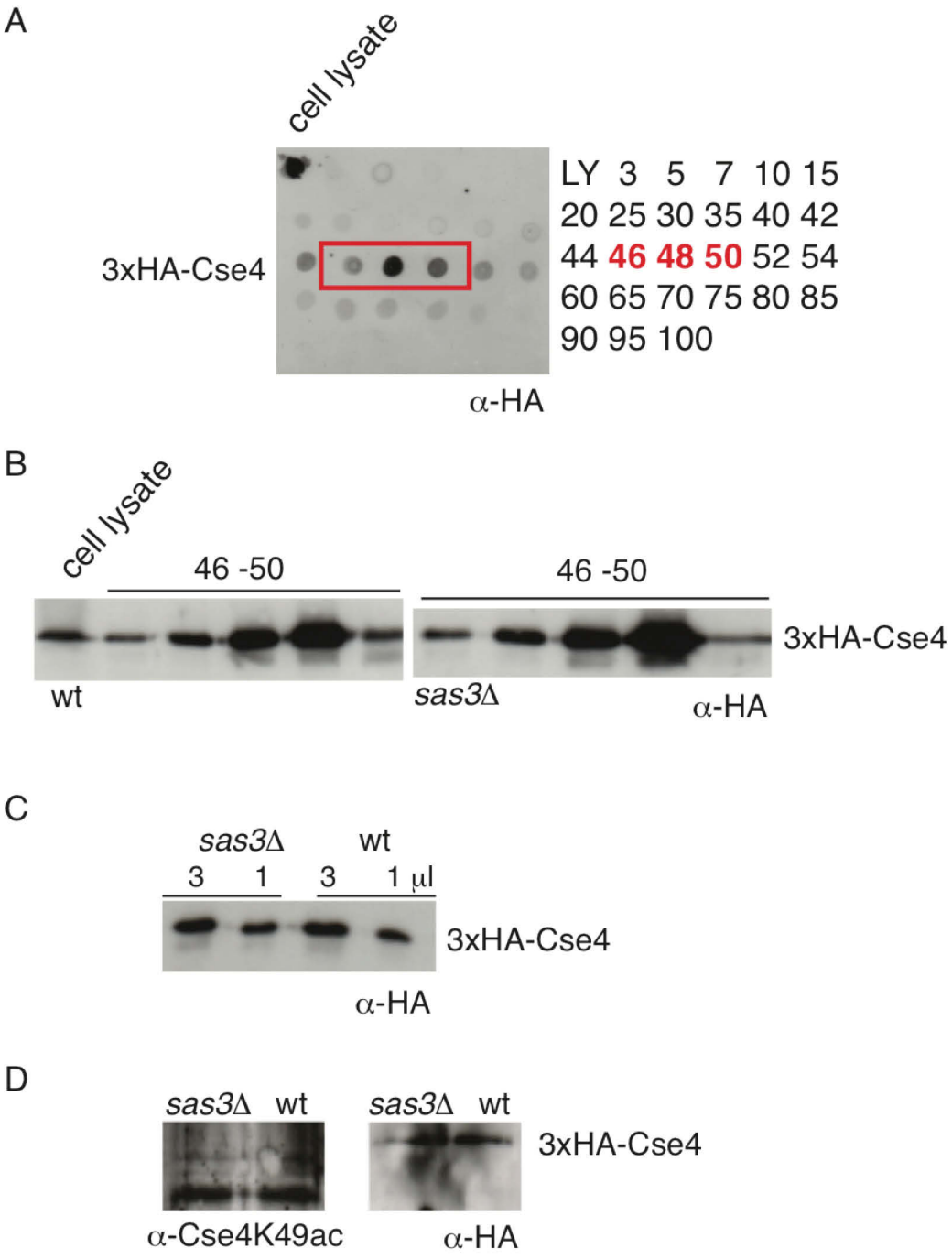

Figure 13: Acetylation on Cse4K49 was not detected in histone extracts

Purification of histone extracts containing 3xHA-Cse4 fractions of wild type and *sas3Δ*. **A**: Dot blot analysis of HPLC-fractions 3-100. Elution of 3xHA-Cse4 mainly occurred in fractions 46-50, as indicated. **B**: Western blots of the corresponding HPLC fractions, extracts were probed with α-HA antibody (1:1000) and α-mouse HRP (1:1000). **C**: Adjustment of protein amounts of wild type and *sas3Δ*. **D**: Histone extracts were probed with α-Cse4K49ac antibody (1:200) and α-rabbit HRP (1:5000).

The result of the western blot against the acetylation on Cse4K49 showed no detectable acetylation signal via the α-Cse4K49ac antibody in the wild type, and in the *sas3Δ* strain that was investigated here. Upon incubation with α-Cse4K49ac antibody, unspecific bands were observed above and below the size where 3xHA tagged Cse4 was expected (Figure 13 D, left). After stripping the blots and subsequent incubation with α-HA antibody the total amount of 3xHA-Cse4 in the samples was detected (Figure 13 D, right). While it was accomplished to purify 3xHA-Cse4 histone extracts from wild type and *sas3Δ* strains, which was verified by detection of the corresponding HA-signals, it was not possible to detect the Cse4K49 acetylation in these partially purified histone extracts.

3.1.5. Definition of the HAT complex, in which Gcn5 acts in the K49 acetylation

It has been shown in *S. cerevisiae*, that three Gcn5 containing protein complexes are active, namely the 1.8 MDa SAGA (Spt-Ada-Gcn5-Acetyltransferase), a derivate of SAGA, SLIK (SAGA-like), and the 0.8 MDa ADA complex (Adaptor) (Eberharter et al., 1999; Grant et al., 1997; Pray-Grant et al., 2002). It was of interest to investigate which of these complexes was responsible for the acetylation of Cse4K49. To examine this, several SAGA/SLIK and ADA specific knock-out mutants were analyzed via immunoprecipitation experiments using the specific α-Cse4K49ac rabbit antibody, and the acetylation levels of Cse4K49 were determined as described in 3.1.2.

The SAGA complex consists of four large protein modules, which serve distinct functions. The architecture module to which the Spt and the Taf subunits belong, are responsible for complex integrity and stability (Lee et al., 2011). The deubiquitination module DUB comprises the Ubp8 and Sgf subunits, of which Ubp8 deubiquitinates H2B K123ub1, which leads to the recruitment of the kinase Ctk1. Subsequent phosphorylation of the C-terminal domain of RNA-polymerase II is responsible for transcriptional elongation (Koutelou et al., 2010). A further module is the acetylation module, containing Gcn5 and Ada subunits. The bromodomain of Gcn5 binds N-terminal tails of acetylated canonical H3 and H4 histones and potentiates cooperative nucleosome acetylation of histone H3 (Baker and Grant, 2007; Brown et al., 2000).

We therefore asked whether the Ada2 subunit, which belongs to all of the HAT complexes, the Ubp8 subunit, which performs the H2B deubiquitination, the Spt7 subunit, which is crucial for the stabilization of the whole SAGA, but not of the ADA complex, and the Ahc1 subunit, which is unique for ADA and responsible for its integrity, also lead to a decreased acetylation signal upon deletion of the corresponding genes. Immunoprecipitation experiments using α-Cse4K49ac antibody were performed in each of the mutant strains as described in 3.1.2. and the precipitated acetylated Cse4K49 levels were compared to wild type acetylation levels (see Figure 14 A-D; respectively). Quantifications of the Western blotting results are shown in the Appendix, Figure 35.

Deletion of the DUB SAGA subunit *UBP8* did not markedly alter the amount of precipitated acetylated Cse4K49 in comparison to the amount that was precipitated from wild type cells (Figure 14 A), although a slight decrease could be observed. In contrast, the loss of the architecture subunit Spt7 of the SAGA complex (Figure 14 B) led to significantly decreased precipitation of acetylated Cse4K49, and the same result was found for the *ada2Δ* mutant, which is part of the acetylation modules of both SAGA and ADA complexes (Figure 14 C). Deletion of *AHC1*, which is a unique subunit of ADA, but not of the SAGA complex, did not influence the amount of precipitated acetylated Cse4K49 (Figure 14 D).

Taken together, our findings show decreased acetylation in *spt7Δ* and *ada2Δ*, but not in *ahc1Δ* cells, indicating the involvement of the SAGA/SLIK, but not of the ADA complex in the K49 acetylation of the centromeric histone variant Cse4. Additionally, the result that the *ubp8Δ* mutant only slightly affected the acetylation level of the Cse4 N-terminus suggests that the DUB module is not directly involved in the acetylation process.

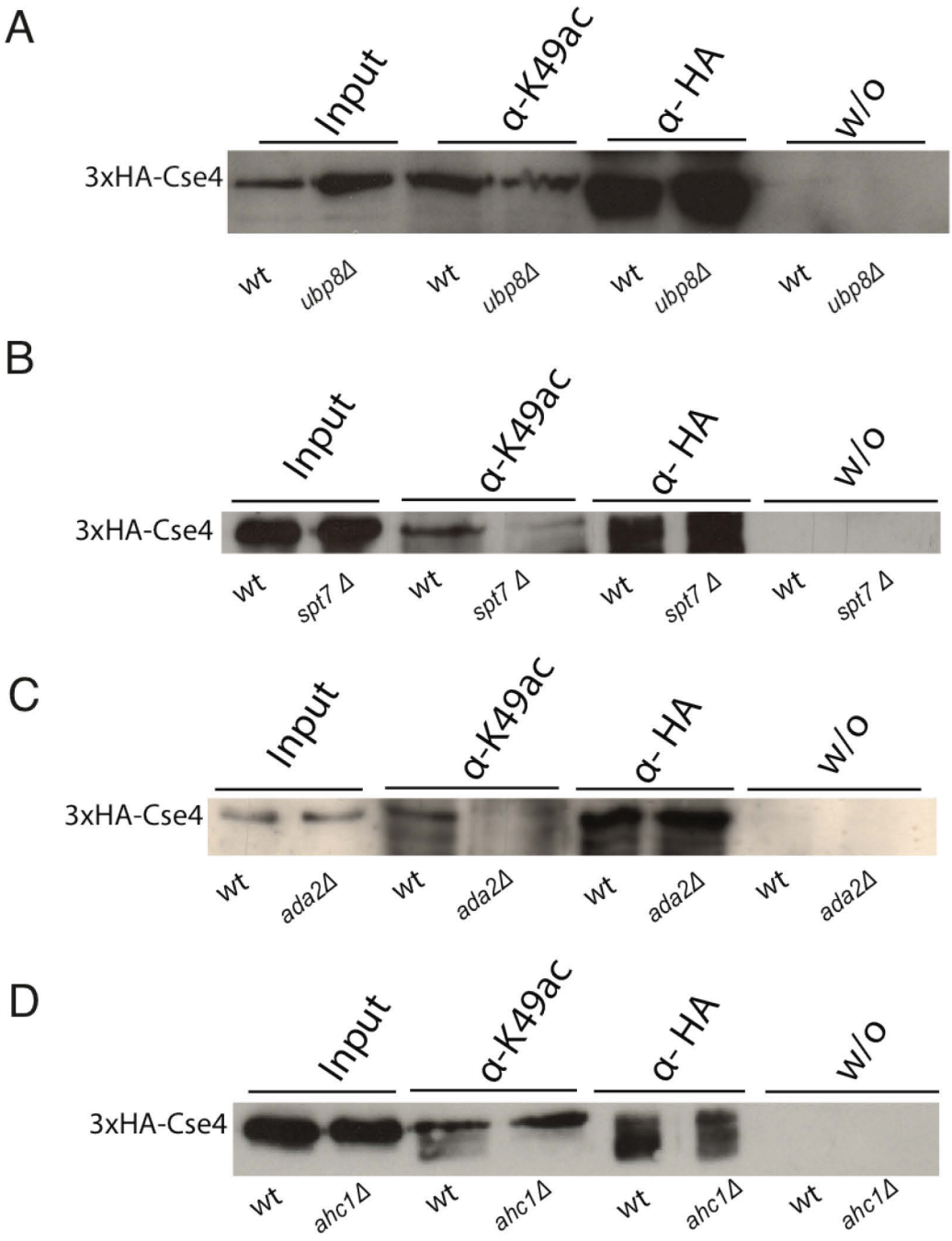

Figure 14: Decreased acetylation of Cse4K49 in SAGA mutants.

Western blotting analysis of immunoprecipitated acetylated Cse4K49 in wild type cells (AEY2781) and SAGA/ADA complex mutants. Blots were incubated with α-HA antibody 1:1000 and α-mouse HRP 1:1000 antibodies. Lanes as described in Figure 10. **A**: Upon deletion of the ubiquitination SAGA subunit *UBP8* (AEY5538), slightly altered Cse4K49 acetylation could be detected. **B**: The deletion of the architecture subunit *SPT7* (AEY5618) led to significantly decreased acetylation of Cse4K49. **C**: The mutation of *ADA2* (AEY5624) led to a complete lack of precipitated acetylated Cse4K49. **D**: The deletion of the ADA subunit *AHC1* (AEY5478) did not alter the amount of precipitated acetylated Cse4K49.

3.1.6. Genetic analysis of SAGA mutants combined with *cbf1Δ* and *cse4R37A*

It has been shown that the additional *cse4K49R* mutation, which mimics an unacetylated state of Cse4K49, suppresses the strong growth defect of *cbf1Δ cse4R37A* (Samel, unpublished data). Since it was found that the Cse4K49 acetylation depends on Gcn5 and acts in the SAGA complex, we asked whether the mutants of the SAGA complex subunits display similar phenotypes in combination with *cbf1Δ cse4R37A*.

It was found in genetic screens in *S. cerevisiae*, that *gcn5Δ cbf1Δ* as well as *ada2Δ cbf1Δ* double mutants showed synthetic lethality (Bandyopadhyay et al., 2010; Costanzo et al., 2010). Consequently, there were no viable triple mutants carrying the genotype *gcn5Δ cbf1Δ cse4R37A* and *ada2Δ cbf1Δ cse4R37A* for further phenotypical tests (data not shown).

The mutant *spt7Δ cbf1Δ cse4R37A* showed a severe growth phenotype as compared to *cbf1Δ cse4R37A* and was marginally able to grow at 30°C (data not shown). Consequently, this triple mutant showed no suppression phenotype of the *cbf1Δ cse4R37A* mutant and was not further characterized phenotypically. To analyze possible genetic interactions of *spt7Δ cbf1Δ* and *spt7Δ cse4R37A*, the growth of both double mutants was compared to the corresponding single mutants (Figure 15).

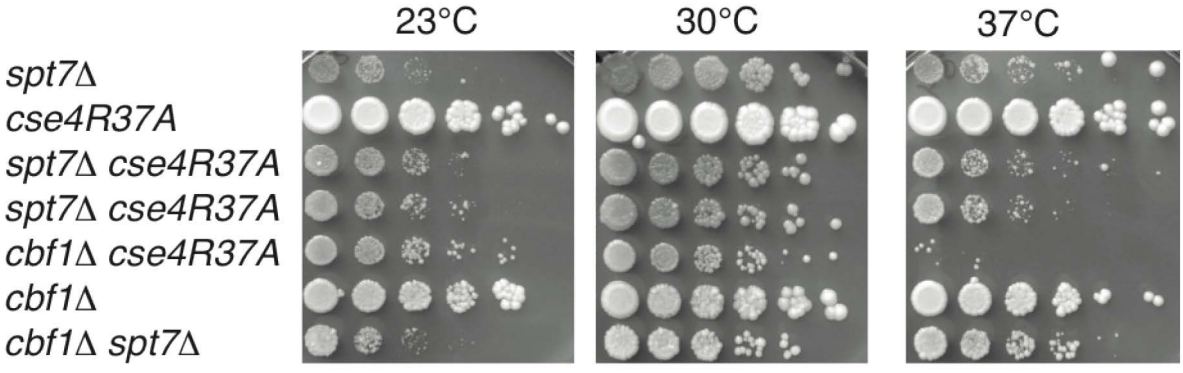

Figure 15: Phenotypical characterization of *spt7Δ* in combination with *cbf1Δ* or the point mutation *cse4R37A* in the essential N-terminal domain.

Serial dilutions of every mutant were made (indicated by the according genotype description on the left side) and spotted on full medium in three equal copies, which were incubated at 23, 30 and 37°C. The single mutant *spt7Δ* (upper row), shows a temperature sensitivity at 37°C and at 23°C.

The growth test at permissive and restrictive temperatures showed that *spt7Δ* had a growth defect at 37 and 23°C, and *spt7Δ cse4R37A* did not show the severe phenotype of *cbf1Δ cse4R37A*. Taken together, the phenotypical analysis of the single SAGA mutants, *gcn5Δ*, *spt7Δ* and *ada2Δ* revealed growth defects in all cases. When these mutants were combined with the centromere-associated component *cbf1Δ* and the non-methyl point mutant *cse4R37A,* no genetic interaction was observed.

3.1.7. Genetic analysis of HAT mutants combined with *cbf1Δ cse4R37A*

A single point mutation in the yeast histone variant Cse4 (*cse4R37A*) shows a strong growth defect, temperature sensitivity and delay in G2/M-phase progression in combination with the inner kinetochore mutant *cbf1Δ*, whereas the single mutations do not lead to such phenotypes, respectively. This genetic interaction hints to an epigenetic regulation of proper kinetochore attachment by this PTM (Samel et al., 2012). Interestingly, a suppression of the growth defect at restrictive temperatures was found, when additionally mutating the acetylation site of K49 to an arginine mimicking an unacetylated state in the *cbf1Δ cse4R37A* mutant. The *cse4K49R* mutant shows no growth phenotype compared to the wild type alone or in combination with *cbf1Δ* (unpublished data). From these findings, it is concluded that the acetylation site on Cse4K49 has an antagonistic function to the methylation site Cse4R37. Further, it is probably involved in the epigenetic regulation of centromere function by mediating the recruitment of kinetochore components, which depends on the yeast specific inner kinetochore component Cbf1.

In parallel to the approach above to identify the HAT for Cse4K49, it was tested, whether it is possible to find genetic interactions using triple mutants with the genotype *cbf1Δ cse4R37A HATΔ*. One could suppose that the *cbf1Δ cse4R37AK49R* suppressor phenotype also emerges in a triple mutant lacking one of the HATs required for the acetylation of Cse4K49. This could give a genetic hint for another HAT acting on Cse4K49 acetylation. Serial dilutions of the triple mutants and the control strains were made, spotted on full medium and the growth was compared to

the single and double mutants as well as to the *cbf1Δ cse4R37AK49R* (Figures 16 and 17).

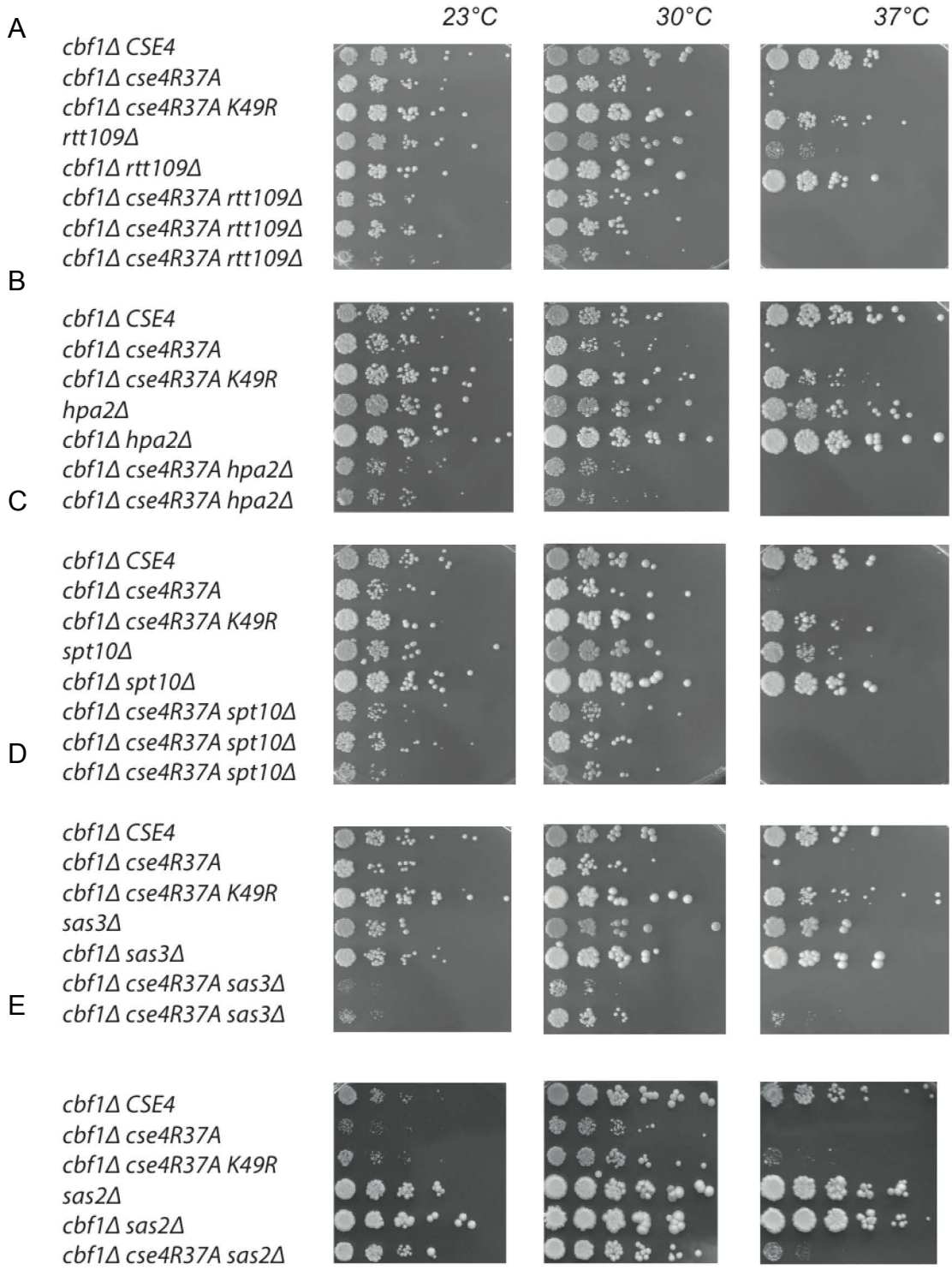

Figure 16: Genetic analysis of HAT mutants in combination with *cbf1Δ* and the point mutation in the essential N-terminal domain of Cse4 (*cse4R37A*).

Serial dilutions of every mutant (indicated by the according genotype description on the left side) were made and spotted on full medium in three equal copies, which were incubated at 23, 30 and 37°C. The single HAT knock-outs *rtt109Δ, hpa2Δ, spt10Δ, sas3Δ, sas2Δ* as shown in A-E in the fourth

panels, respectively, showed no or a weak growth phenotype. None of these HAT mutants could rescue the *cbf1Δ cse4R37A* phenotype (lower panels of A-E) as compared to *cbf1Δ cse4R37AK49R* triple mutant suppressor phenotype (third panels A-E).

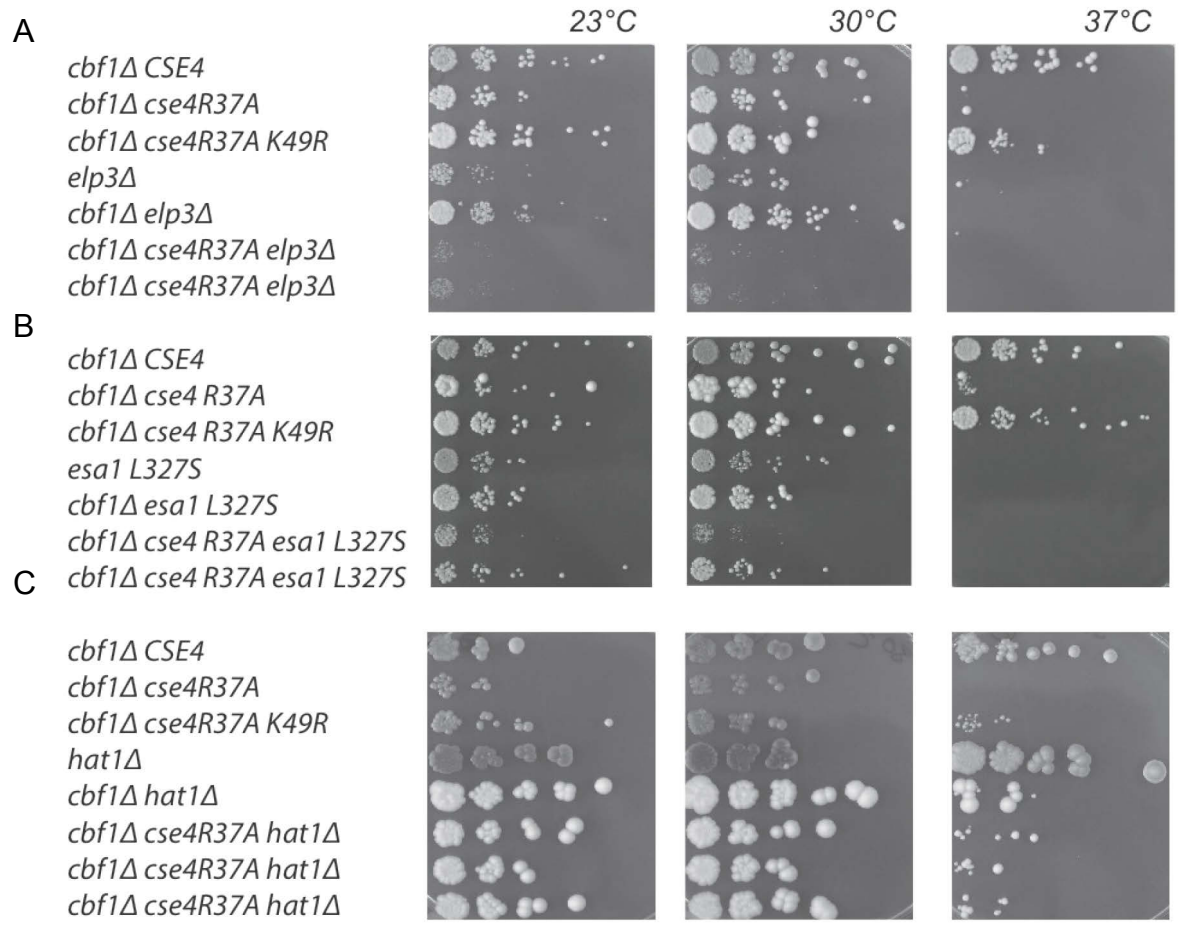

Figure 17: Genetic analysis of HAT mutants in combination with *cbf1Δ* and the point mutation in the essential N-terminal domain of Cse4 (*cse4R37A*).

Serial dilutions of every mutant were made and spotted on full medium in three equal copies, which were incubated at 23, 30 and 37°C. The single HAT mutants *elp3Δ*, *esa1L327S* and *elp3Δ* are shown in A and B and C in the fourth panels, respectively. None of these HAT mutants could rescue the *cbf1Δ cse4R37A* phenotype.

All tested HAT deletion mutants showed no suppression phenotype of the *cbf1Δ cse4R37A* mutant at 37°C. Either the single HAT mutations caused a strong growth defect (*elp3Δ* and *esa1L327S*; Figure 17 A and B), or the *cbf1Δ cse4R37A HATΔ* triple mutants were unable to grow at restrictive temperatures (*rtt109Δ*, *hpa2Δ*, *spt10Δ*, *sas3Δ*, *sas2Δ*, Figure 16 A-E), possibly caused by the increasing sickness of the multiple mutations of these strains. The *hat1Δ* mutant showed no temperature

sensitivity, but the double mutant *cbf1Δ hat1Δ* was barely able to grow at restrictive temperatures (Figure 17 C).

All of the *cbf1Δ cse4R37A HATΔ* triple mutants were viable at permissive temperature, except *cbf1Δ cse4R37A gcn5Δ*. Taken together, these results indicate that none of the tested HAT triple mutants could suppress the growth phenotype of the *cbf1Δ cse4R37A* double mutant, and thus gave no genetic indication for a redundant mechanism in Cse4K49 acetylation.

3.1.8. Effect of *SAS2* overexpression on the acetylation status of Cse4K49

We further sought to investigate if the MYST histone acetyltransferase Sas2 influences the acetylation level on Cse4K49, as previous work from our lab showed a physical interaction of Sas2 and Cse4. While the main target of Sas2 is H4K16 *in vivo*, it has been shown *in vitro* that Sas2 also acetylates H3K14, though to a lesser extent (Sutton et al., 2003). Sas2 has a role on centromeres, though its precise function on centromeres has not been defined. Genetic interactions and synthetic dosage lethality (SLD) were demonstrated in strains, containing SAS-I complex (*SAS2*, *SAS4* or *SAS5*) overexpression plasmids. These strains were combined with *CSE4* alleles and kinetochore mutants and showed temperature sensitivity or lethality. Additionally, *SAS2* overexpression has been shown by chromosome loss assay to affect chromosome segregation (Choy et al., 2011).

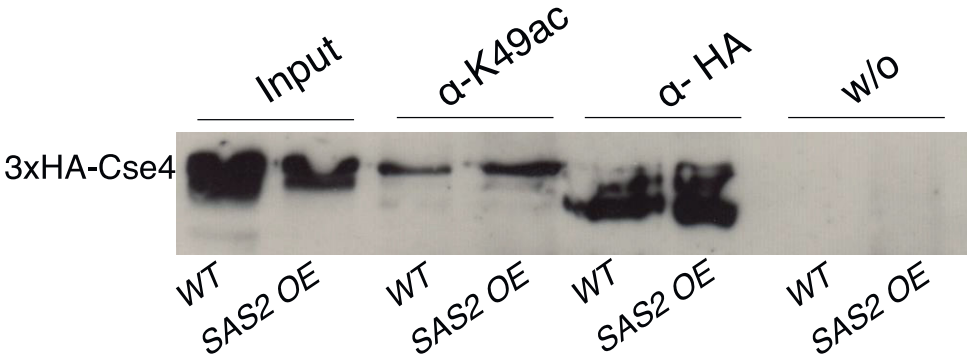

Figure 18: Influence of Sas2 overexpression on Cse4.

Depicted is a western blotting analysis of the immunoprecipitation of acetylated Cse4K49 in a strain that overexpressed the MYST HAT Sas2 (*SAS2* OE) in comparison to a wild type strain. No significant

differences in the precipitated acetylated Cse4K49 were detected. Blots were incubated with α-HA and α-mouse HRP antibodies (1:1000). Lanes as described in Figure 10.

If overexpression of *SAS2* affects centromere function, it is possible that it also leads to either a direct effect on Cse4, maybe by an increased acetylation of Cse4K49, or it affects the acetylation status indirectly. Therefore, the hypothesis that this HAT has an influence, direct or indirect, on the acetylation status of Cse4K49, was tested. A strain was constructed, which carried 3xHA-Cse4 on a plasmid (AEY2781) and an overexpression plasmid carrying the *SAS2* gene (pAE240). The immunoprecipitation experiment was performed as described. As Figure 18 shows, no significant alteration of the acetylated Cse4K49 could be detected in the overexpression mutant compared to wild type acetylation signal, which indicates that Sas2 mediated acetylation is not involved in the acetylation of the N-terminal domain of the centromeric histone variant Cse4.

3.2. Cell-cycle dependence of posttranslational modifications on Cse4

There is evidence that the PTMs on Cse4 have an impact on centromere function. It was of interest to see whether the PTMs on the N-terminus of the centromeric histone variant are cell cycle dependent. The notion that the methylation on R37 as well as the acetylation on K49 seem to be involved in the recruitment of the kinetochore could lead to the assumption that the marking of the histone variant is coupled to a specific cell-cycle phase. Correspondingly, it was shown before, that the R37 methylation increases in S-phase (A. Samel, unpublished data).

3.2.1. Cell-cycle study of the suppressor triple mutant *cbf1Δ cse4R37AK49R*

In a former study, our group showed that the *cbf1Δ cse4R37A* mutant exhibits a strong growth defect, temperature sensitivity and a delay in G2/M-phase. These findings were confirmed by FACS analysis, which showed a cell-cycle phenotype of this double mutant in comparison to the wild type. All in all, the cells exhibited a cell-

cycle progression defect and remained longer in G2/M-phase (Samel et al., 2012). To test whether *cbf1Δ cse4R37AK49R* is phenotypically and functionally restored, wild type and mutant cells were grown to early logarithmic phase at 23 °C, shifted to 37 °C and incubated for 5 h. Subsequently, the DNA content was measured by FACS to determine cell-cycle progression, revealing that the cell cycle of the triple mutant is functionally restored in its cell cycle, compared to wild type cell cycle (Figure 19).

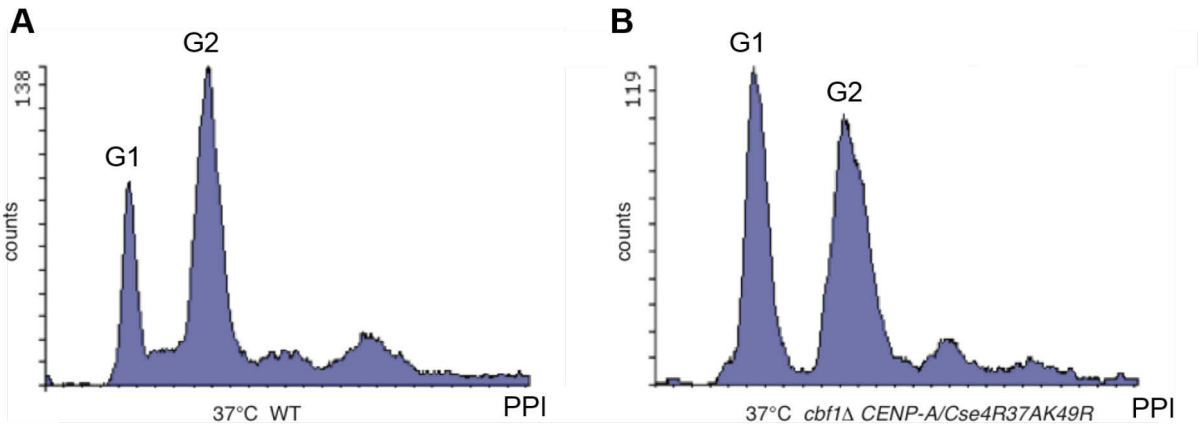

Figure 19: *cse4K49R* suppresses the G2/M-phase delay in *cbf1Δ cse4R37A*

A: Whereas *Cse4R37A* is required for proper cell cycle progression, an additional mutation in K49 to an arginine could suppress the growth phenotype in the inner kinetochore mutant background *cbf1Δ*. **B**: Using FACS analysis, it was shown, that the arrest of *cbf1Δ cse4R37A* (Samel et al., 2012) in G2/M phase at restrictive temperature was restored in the triple mutant. Wild type cells and *cbf1Δ cse4R37AK49R* triple mutant cells were grown to early logarithmic phase, shifted to 37°C and incubated for 5h. PPI: Cells were stained with propidium iodide (PPI).

3.2.2. Study of the cell-cycle dependence of Cse4K49 acetylation

In order to investigate a potential cell-cycle dependent appearance of Cse4K49 acetylation, cells expressing 3xHA-Cse4 from plasmid (AEY2781) were arrested in several cell-cycle stages to follow the modification state throughout the cell cycle (as described in 2.8.1.). The amount of immunoprecipitated Cse4K49 acetylation in every cell-cycle phase was compared to asynchronous cells (see chapter 2.8). As control, α-HA immunoprecipitated 3xHA-Cse4 and samples without antibody incubation were used.

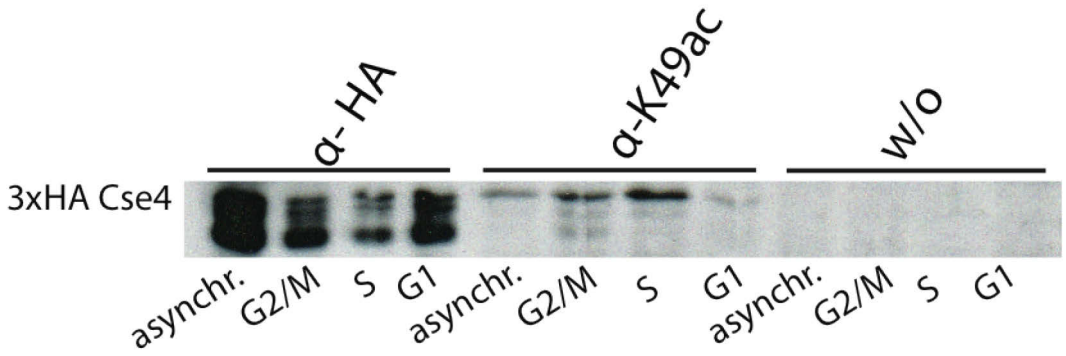

Figure 20: Cell-cycle dependence of Cse4K49 acetylation.

Yeast cells, which carry 3xHA-Cse4 on a plasmid in a *cse4Δ* background (AEY2781), were arrested in cell-cycle phases G1, S and G2/M, respectively, and acetylated Cse4K49 was immunoprecipitated (middle four lanes). Acetylation on K49 of Cse4 increased in S-phase as compared to G2/M phase, G1 phase or asynchronous cells. As controls, equal amounts of lysates were used, and Cse4 was immunoprecipitated by the use of α-HA antibody (left four lanes). The second control was made without antibody incubation (right four lanes). A second biological replicate confirmed this result.

Figure 20 shows that the acetylation of Cse4K49 was increased in cells arrested in S-phase, whereas G2/M-arrested and asynchronous cells showed weaker acetylation, and in G1-phase the acetylation was lowest. The control samples showed no unspecific binding of unacetylated Cse4. These results support the assumption that the acetylation of Cse4K49 is coupled to the cell cycle. It increased in S-phase, and decreased in G2/M- and G1-phases (the corresponding FACS profiles and western blot quantifications are shown in the appendix).

3.3. Investigation of R37 methylation and K49 acetylation on Cse4 during the cell cycle

To investigate the role of the acetylation on Cse4K49 and the methylation on Cse4R37, yeast cells carrying a *cse4Δ* and plasmid born 3xHA-*CSE4* (AEY 5689) were arrested in G1-phase and subsequently released into S-phase. FACS samples of early-, mid- and late S-phase were taken, and as controls, samples were taken from G1-arrested and asynchronous cells. Following S-phase progression, it was possible to determine Cse4K49 acetylation and Cse4R37 methylation levels by immunoprecipitation using specific modification antibodies, shown in Figure 22.

3.3.1. Immunoprecipitation of methylated Cse4R37

To investigate the methylation level on Cse4R37 via immunoprecipitation experiments using the α-Cse4R37me rabbit antibody (see chapter 2.7), Cse4R37me levels in *cse4Δ* strains carrying plasmid borne 3xHA-*CSE4* (AEY 2781) or a non-methyl mutant 3xHA-*cse4R37A* (AEY 5040) were compared (Figure 21).

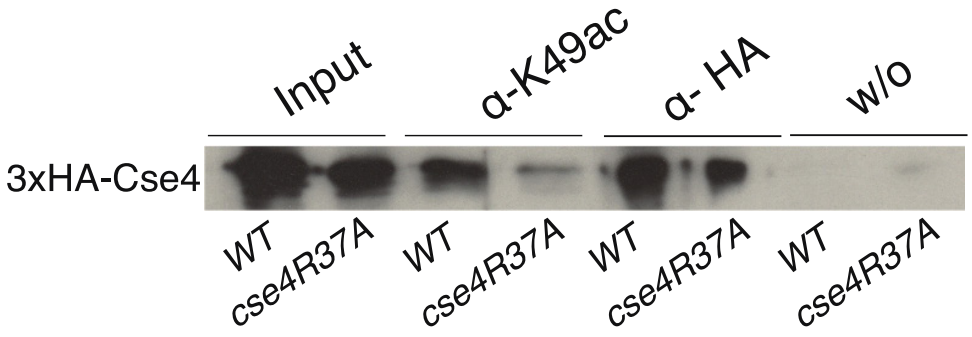

Figure 21: Immunoprecipitation of methylated Cse4R37
A wild type Cse4 strain (AEY 2781) and a mutant *cse4R37A* strain (AEY 5040) were used for the immunoprecipitation experiment. The *cse4R37A* mutant showed a significantly decreased methylation signal in comparison to the wild type condition. Blots were incubated with α-HA and α-mouse HRP antibodies (1:1000). Lanes as described in Figure 10.

The comparison of the methylation levels of Cse4R37 and *cse4R37A* revealed as expected that the methylation level was decreased in *cse4R37A.* As controls α-HA antibody was used to precipitate 3xHA-Cse4, and w/o antibody control. Although a weak unspecific binding was detectable in Cse4R37A, the α-Cse4R37me antibody distinguished the methylated Cse4R37 and Cse4R37A and recognized the unmethylated R37 to a much less extend (Figure 21).

3.3.2. Fluctuation of K49 acetylation and R37 methylation on Cse4 during S-phase

To investigate possible differences in the K49 acetylation and R37 methylation in the N-terminal part of Cse4, an immunoprecipitation experiment of S-phase released cells was performed. For this purpose, wild type cells were arrested in G1-phase and subsequently released into S-phase. At time points 20, 40 and 60 min after S-release, samples for immunoprecipitation were taken. Moreover, S-phase

progression was monitored by FACS analysis. As controls, samples were taken from G1-arrested and asynchronous cells, respectively. Additionally, a control without antibody was used to determine whether unspecific binding of lysate proteins to the beads occurred.

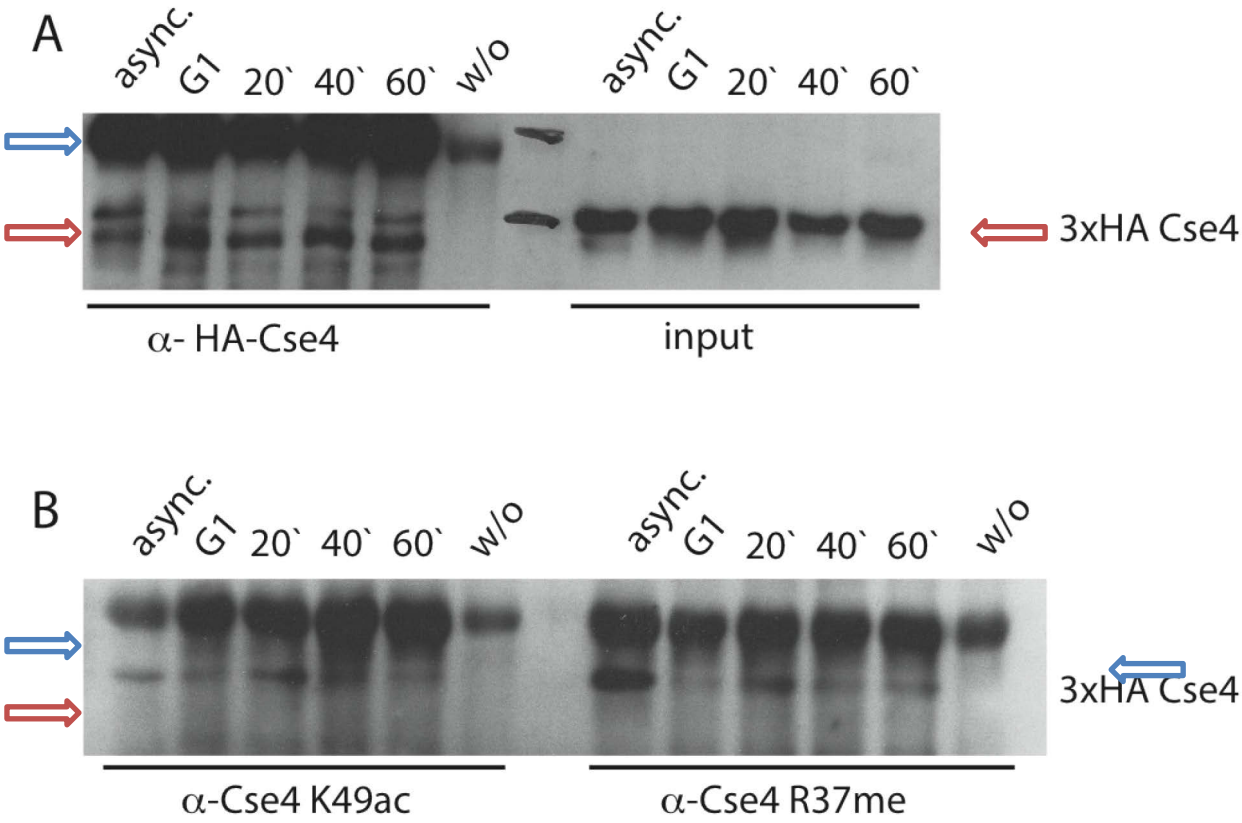

Figure 22: Acetylation of Cse4K49 was decreased whereas methylation of Cse4R37 remained at a constant level at the end of S-phase

A: Illustrated is the α-HA western blot of the immunoprecipitated 3xHA-Cse4 of cells (AEY5689) (shown in A left) and input controls (shown in A right). **B:** Immunoprecipitated Cse4 of S-phase released cells, using the α-Cse4K49ac antibody (shown in **B** left) and the α-Cse4R37me antibody (shown in **B** right) is depicted with red arrows. Heavy antibody chains are indicated with blue arrows. 3xHA-Cse4 runs between light (25 kDa, not shown) and heavy (55 kDa) antibody chains in the gel (see full blot in the Appendix). The modification status was monitored throughout S-phase. Time points for early, mid and late S-phase are indicated (20, 40 and 60 min, respectively) as well as G1-arrested and asynchronous samples. Blots were incubated with α-HA and α-mouse HRP antibodies (1:1000).

As shown in Figure 22 B, the levels of immunoprecipitated acetylated Cse4K49 increased early and decreased during the progression of S-phase, whereas the immunoprecipitated methylated Cse4R37 increased in early S-phase about 2-fold and stayed high throughout S-phase progression. As controls, immunoprecipitated 3xHA-Cse4 was used and input controls as described above, shown in Figure 22 A.

Heavy chains of the precipitation antibodies and/or the beads antibodies run above the 3xHA-Cse4. The α-HA precipitations as well as the α-Cse4K49ac and α-Cse4R37me precipitations were used for quantification. In case of the Cse4K49 acetylation, a decrease of the immunoprecipitation of one third at the end of the S-phase was calculated (Figure 23).

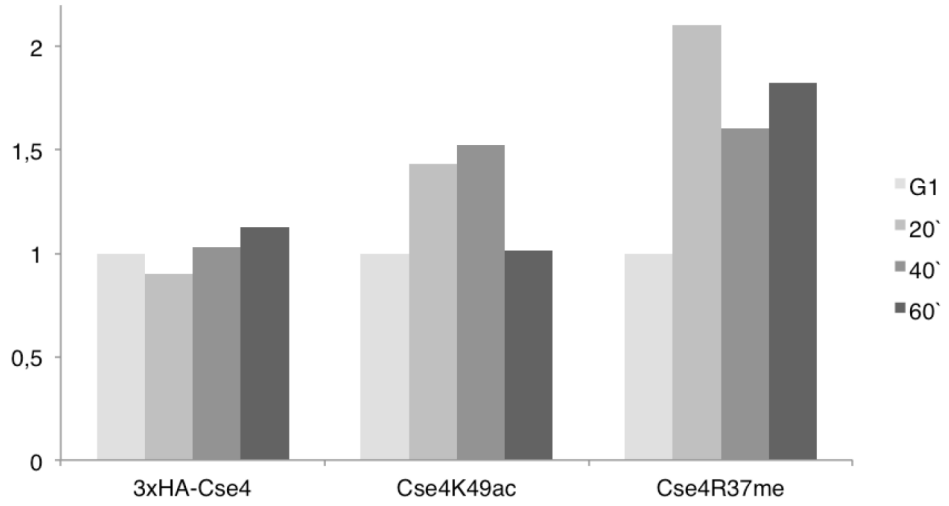

Figure 23: Quantification of alterations of the posttranslational modifications Cse4K49 acetylation and Cse4R37 methylation in S-phase progression

Western blot quantification of Cse4K49 acetylation and Cse4R37 methylation in S-phase released wild type yeast cells. G1-phase levels of 3xHA-Cse4, Cse4K49 acetylation and Cse4R37 methylation were set to 1, and the alterations of each of the PTMs in comparison to 3HA-Cse4 levels were followed through S-phase, indicating that both PTMs increase in early S-phase. The increase of Cse4R37 methylation was about 2-fold and stayed high throughout S-phase progression. Cse4K49 acetylation decreased at the end of S-phase. This result was confirmed by a second biological replicate.

3.4. Protein-protein interaction studies of Cse4 with COMA kinetochore components

The histone variant CENP-A^{Cse4} consists of two domains: first, the C-terminal, “classical” histone fold domain (aa 135-229), which shows 64% sequence homology to the canonical histone H3 (Stoler et al., 1995; Wells and McBride, 1989), and second, the N-terminal domain (aa 1-134) building a large tail of CENP-A^{Cse4}, which is specific in its amino acid sequence and comprises the essential N-terminal domain (END) (Keith et al., 1999; Stoler et al., 1995). It has been previously demonstrated

that this END domain of the Cse4 N-terminus is responsible for the recruitment of linker layer kinetochore components, such as subunits of the CTF19 and the Mtw1/MIND complexes, and that the recruitment is epigenetically regulated, depending on the methylation of R37 of this Cse4 histone tail (Samel et al., 2012). In case of the subunits Ctf19, Mcm21, Ame1 and Okp1 of the CTF19 subcomplex COMA, this was demonstrated via analysis of genetic crosses. While the mutation of *cse4R37* to alanine caused synthetic lethality when combined with mutations in the genes for Ctf19 or Mcm21 and Ame1, it showed a strong growth defect in combination with Okp1, and a slight growth defect was shown with the MIND component Mtw1. These genetic interactions indicate an essential role of this PTM for full kinetochore function. Further, it was shown that the double mutant of the centromere binding factor *cbf1Δ* in combination with *cse4R37A* leads to a growth defect and G2/M-phase delay. Moreover, by chromatin immunoprecipitation, it could be found that the recruitment of Ame1 and Mtw1 to CEN4 (*S. cerevisiae* centromere 4) was significantly reduced in a *cbf1Δ cse4R37A* background at restrictive temperatures (Samel et al., 2012). These data demonstrate that the methylation of Cse4R37 is responsible for the recruitment of linker kinetochore components to the centromere.

Analysis of a genetic cross of the non-acetylateble point mutant *cse4K49R* and the *cbf1Δ cse4R37A* showed that the K49 acetylation on Cse4 acts in an antagonistic way to the R37 methylation. This was indicated by a suppression phenotype, which was found in a *cbf1Δ cse4R37A K49R* triple mutant, suggesting that the role of this acetylation is also linked to proper kinetochore assembly (unpublished data). The counteracting function of the K49 acetylation to Ctf19 and Okp1 was investigated here by using acetylated and unacetylated K49 peptides in peptide pull-down experiments. The question of whether the recruitment of these kinetochore subunits depends on the acetylation of K49 was addressed. Further, one aim of this study was to gain insights into the protein-protein interactions of the N-terminal domain of Cse4 with Ctf19 by *in vitro* pull-down experiments.

3.4.1. Purification of the N-terminal domain of Cse4

For biochemical studies of the N-terminal domain of Cse4, this domain was recombinantly expressed and purified (see Material and Methods, Chapter 2.6.). GST-tagged N-terminal regions of Cse4 were cloned and four different N-terminal *CSE4* fragments were used, one fragment spanning almost the whole N-terminal tail (aa 1-134) and three shorter fragments (aa 1-100, 14-134 and 33-132), with all four containing the essential N-terminal domain encompassing aa 28-60 (Keith et a., 1999). These constructs were tested for heterologous expression levels and solubility in *E. coli* (data not shown). The construct GST-CENP-A$^{Cse4 14-134}$ was used for preparative protein purification and further biochemical studies. The calculated size of GST-Cse4$^{14-134}$ is 41 kDa, with the GST tag being 26 kDa and the N-terminus of CENP-A^{Cse4} being 14.3 kDa in size. Figure 24 shows the Coomassie blue staining of the affinity purification steps. GST-Cse4$^{14-134}$ could be purified in substantially amounts and was used as `bait` protein in a pull down assay (see chapter 3.3.3.).

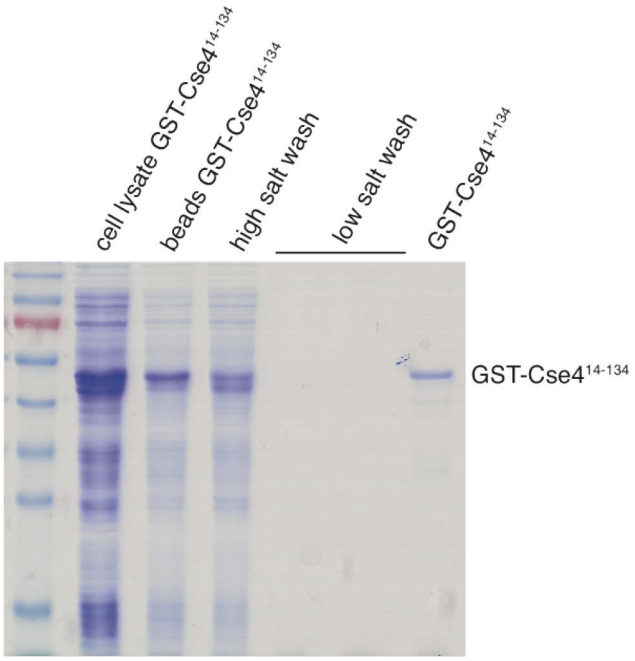

Figure 24: Affinity purification of the fusion protein GST-Cse4$^{14-134}$.
SDS-PAGE and Coomassie blue staining of affinity purified GST-Cse4$^{14-134}$. Recombinant GST-Cse4$^{14-134}$ containing lysate was bound to Glutathione agarose matrix and could be purified using thorough low salt (0.15 M NaCl) and high salt (0.5 M NaCl) washing steps. 2 µl of the lysate, the beads and the washing steps were analyzed in this SDS-PAGE. The calculated size of 41 kDa of GST-Cse4$^{14-134}$ correlates with the SDS-PAGE analysis. The protein marker is shown left.

3.4.2. Affinity purification and elution of 6x His-Ctf19$^{35-363}$

For purification of the kinetochore subunit Ctf19, which belongs to the COMA subcomplex, the co-expression vector system pETDuet was used, as described in chapter 2.5. This system was used based on the assumed insolubility of the *Kluyveromyces lactis* Ctf19 when this protein is expressed without its interaction partner Mcm21 (Schmitzberger and Harrison, 2012). It was expected that the yeast homologue Ctf19 was insoluble as well when expressed separately, but in case of Ctf19$^{35-363}$, which was used in this study, this protein was soluble when expressed alone at low temperatures, as shown in Figure 25. The approximate size of the protein was 40 kDa, including the N-terminal 6xHis-tag. For affinity purification, 50 ml of the lysate was incubated with 2 ml Ni^{2+}-NTA matrix and washed thoroughly to eliminate unspecific protein binding. Affinity purification of 6xHis-Ctf19$^{35-363}$ was carried out as described in 2.6.4 and analyzed by SDS-PAGE and Coomassie blue staining (Figure 25). Purification steps are indicated, showing that the Ni^{2+}-NTA matrix bound 6xHis-Ctf19$^{35-363}$, but some unspecific binding proteins were also detected.

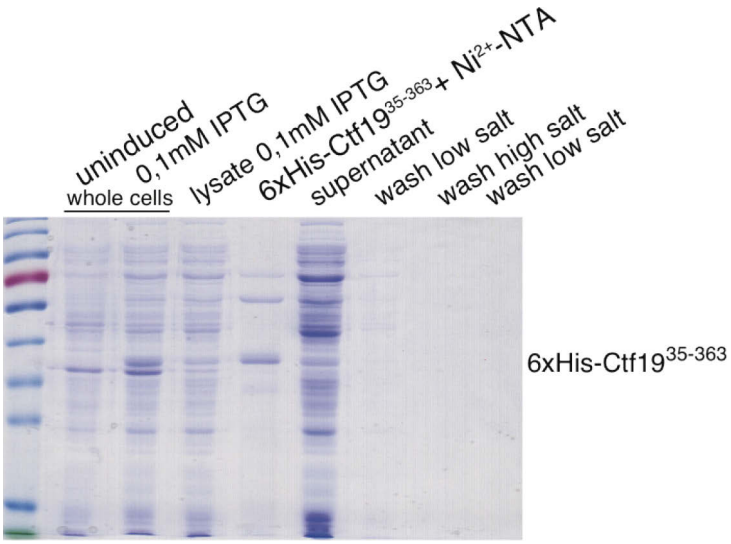

Figure 25: Expression and affinity purification of 6xHis-Ctf19$^{35-363}$.
SDS-PAGE and Coomassie blue staining of expression and affinity purification of 6xHis-Ctf19$^{35-363}$. Induction with 0.1 mM IPTG resulted in 6xHis- Ctf19$^{35-363}$ expression, 1 µl of the whole cells and the lysates were analyzed in the SDS-PAGE. Recombinant 6xHis-Ctf19$^{35-363}$ was bound to Ni^{2+}-NTA agarose and could be partially purified as indicated using low salt (0.15 M NaCl) and high salt (0.5 M NaCl) washing steps. 2 µl of the washing steps were analyzed. The calculated size of 40 kDa of 6xHis-Ctf19$^{35-363}$ correlates with the SDS-PAGE analysis.

Furthermore, 6xHis-Ctf19$^{35-363}$ was eluted from the Poly-Prep chromatography columns (BIO-RAD) Ni^{2+}-NTA matrix, using 150 mM imidazole buffer. Figure 26 shows that 6xHis-Ctf19$^{35-363}$ was finally eluted using 150 mM imidazole and further used for pull-down experiments. The protein was concentrated in pull-down buffer to a final volume of 2 ml.

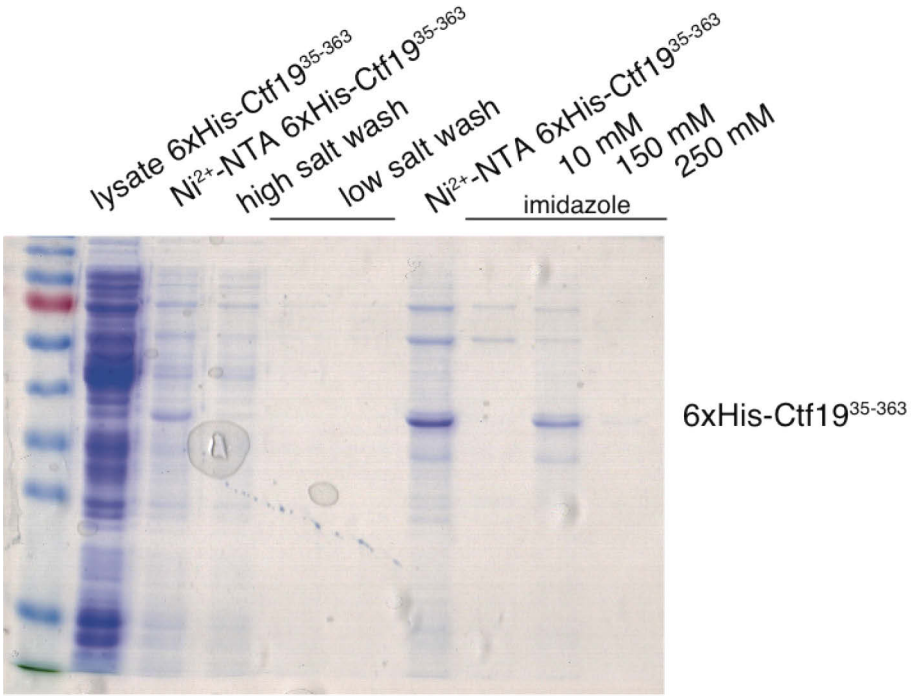

Figure 26: Elution steps of 6xHis-Ctf19$^{35-363}$.
SDS-PAGE and Coomassie blue staining of affinity purified and eluted 6xHis-Ctf19$^{35-363}$. Affinity purification steps were applied as indicated. The matrix bound 6xHis-Ctf19$^{35-363}$ served as control. Elution steps using 10, 150 and 250 mM imidazole buffer are depicted indicating that recombinant 6xHis-Ctf19$^{35-363}$ was eluted with 150 mM imidazole.

3.4.3. Interaction of 6x His-Ctf19$^{35-363}$ and GST-Cse4$^{14-134}$

In order to investigate direct protein interactions of the linker kinetochore subunit Ctf19 and the N-terminal domain of the centromeric histone variant CENP-A^{Cse4}, an *in vitro* pull-down assay of the matrix bound bait protein GST- Cse4$^{14-134}$ and the target protein 6xHis-Ctf19$^{35-363}$ was performed. 6x His-Ctf19 was eluted from the Ni^{2+}-NTA resin using 150 mM imidazole and concentrated in pull-down buffer containing 0,5% NP 40 to eliminate unspecific protein interactions. Matrix-bound GST- Cse4$^{14-134}$ was not eluted and functioned as “immobilized bait“. As control, 6xHis-Ctf19$^{35-363}$ was incubated with the equilibrated matrix in the absence of GST- Cse4$^{14-134}$. SDS-

PAGE analysis followed by Coomassie blue staining was performed to assess protein-protein interactions (Figure 27). During the pull-down procedure, GST-Cse4$^{14-134}$ was partially degraded, as indicated by the occurrence of an additional gel bands below the GST-Cse4$^{14-134}$. As controls, the bait and the prey proteins were analyzed in the same SDS-PAGE. Strikingly, 6xHis-Ctf19$^{35-363}$ bound specifically to GST-Cse4$^{14-134}$, as indicated, but did not bind unspecifically to the glutathione agarose beads.

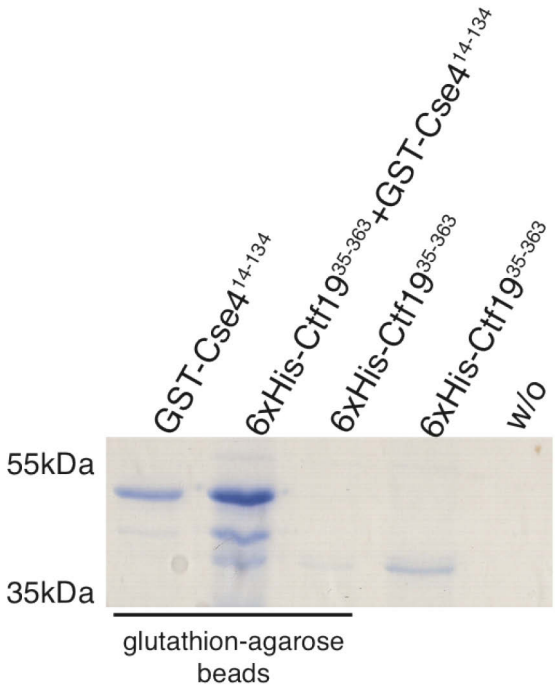

Figure 27: Interaction of 6xHis-Ctf19$^{35-363}$ and GST-Cse4$^{14-134}$ in pull-down assay

SDS-PAGE and Coomassie blue staining of pull-down analysis of GST-Cse4$^{14-134}$ and 6xHis-Ctf19$^{35-363}$. Binding of 6xHis-Ctf19$^{35-363}$ to GST-Cse4$^{14-134}$ is indicated. No unspecific binding to glutathione agarose beads. 10 µl of the suspension applied to the gel. In lanes 1 and 4, the single bait and prey proteins are shown as indicated. As control, 6xHis-Ctf19$^{35-363}$ was incubated with the equilibrated matrix in the absence of GST- Cse4$^{14-134}$ (Lane 3). Lane 5 shows a control with beads and buffer. 5 µl were subjected to SDS-PAGE, respectively.

3.4.4. Peptide pull-down of 6xHis-Ctf19$^{35-363}$

It was previously shown that a deletion of *CTF19* shows synthetic lethality when combined with the *cse4R37A* allele, indicating an essential function of this modification in the assembly of the kinetochore (Samel et al., 2012). To investigate the differential binding of 6xHis-Ctf19$^{35-363}$ to acetylated and unacetylated Cse4K49

peptides (for peptide amino acid sequences see table 6), a peptide pull-down assay was carried out as described in 2.8.1. For this purpose, 6xHis-Ctf19$^{35-363}$ of induced and non-induced cell lysates was compared to the peptide pull-downs on the same blot (Figure 28 A).

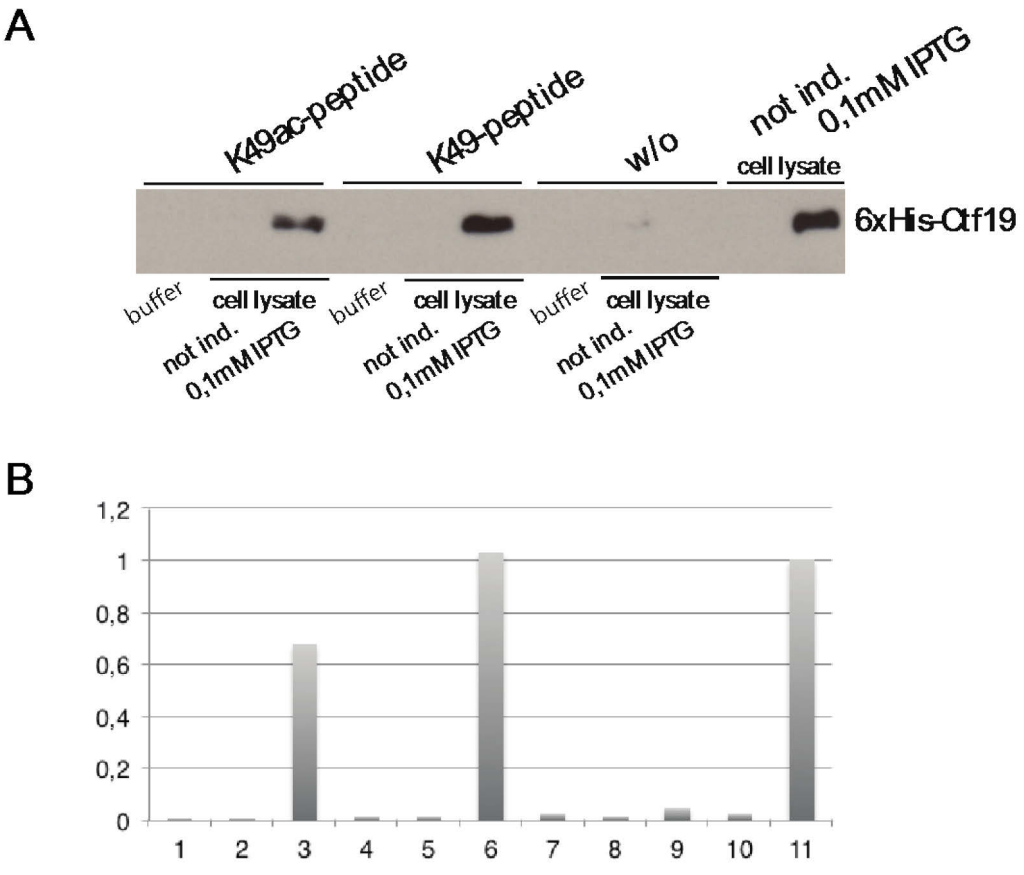

Figure 28: Ctf19 binding to Cse4K49ac and Cse4K49 peptides

A: Western blotting analysis of a peptide pull-down experiment using acetylated and unacetylated Cse4K49 peptides immobilized on sulfolink beads and 6xHis-Ctf19$^{35-363}$ containing cell lysate as prey proteins. As indicated, 6xHis-Ctf19$^{35-363}$ was pulled specifically by both peptides. 6xHis-Ctf19$^{35-363}$ was preferentially pulled by the unacetylated K49 peptide. 6xHis-Ctf19$^{35-363}$ did not bind to sulfolink beads unspecifically. As controls, untreated cell lysates of non-induced and induced (0.1mM IPTG) 6xHis-Ctf19$^{35-363}$ are shown in lanes 10 and 11, respectively. The blot was incubated with α-His (1:5000) and α-mouse HRP antibodies (1:1000). **B**: Quantification of western blotting analysis. Signals were normalized against input, lane 11. Controls with buffer conditions as indicated (lanes 1,4,7) as well as non-induced controls (lanes 2, 5, 8). As shown in lanes 3 and 6, 6xHis-Ctf19$^{35-363}$ was pulled preferentially by the unacetylated K49 peptide. This experiment was done in two independent biological replicates.

The Western blotting analysis showed that 6xHis-Ctf19$^{35-363}$ bound specifically to Cse4K49 peptide-coupled sulfolink beads, but not to the beads alone. The amount of

6xHis-Ctf19$^{35-363}$ increased upon binding to the unacetylated peptide, compared to the binding to the acetylated K49 peptide, indicated by quantification (Figure 28 B). From this it can be concluded that the recombinant Ctf19 construct binds to the N-terminal peptide of Cse4, with a preference to unacetylated K49 on Cse4.

3.4.5. Peptide pull-down of Okp1 and Okp1^{R164C}

The recruitment of linker kinetochore subunits such as Okp1 depends on the methylation of R37 of the Cse4 histone tail (Samel et al., 2012). Furthermore, our lab found that the point mutation *okp1R164C* suppresses the growth phenotype of the *cbf1Δ cse4R37A* double mutant (unpublished data). These genetic findings lead to the question whether Okp1 also interacts physically with the N-terminus of Cse4. Therefore, biochemical peptide pull-down experiments using N-terminally acetylated and unacetylated Cse4K49 peptides (Table 6) were used here to assess the binding of Cse4 to the kinetochore linker layer components Okp1. The peptide pull-down experiment was carried out as described above. Lysates of Okp1 wild type and GST-Okp1^{R164C} cells were used, shown in Figure 29 (cell lysate). Because of the GST tag of Okp1, unspecific peptide binding to GST had to be ruled out. The controls showed the absence of binding of GST alone to acetylated and unacetylated K49-peptides. A further control showed that neither GST-Okp1, nor GST-Okp1^{R146C} bound unspecifically to the sulfolink beads (Figure 29, “w/o”).

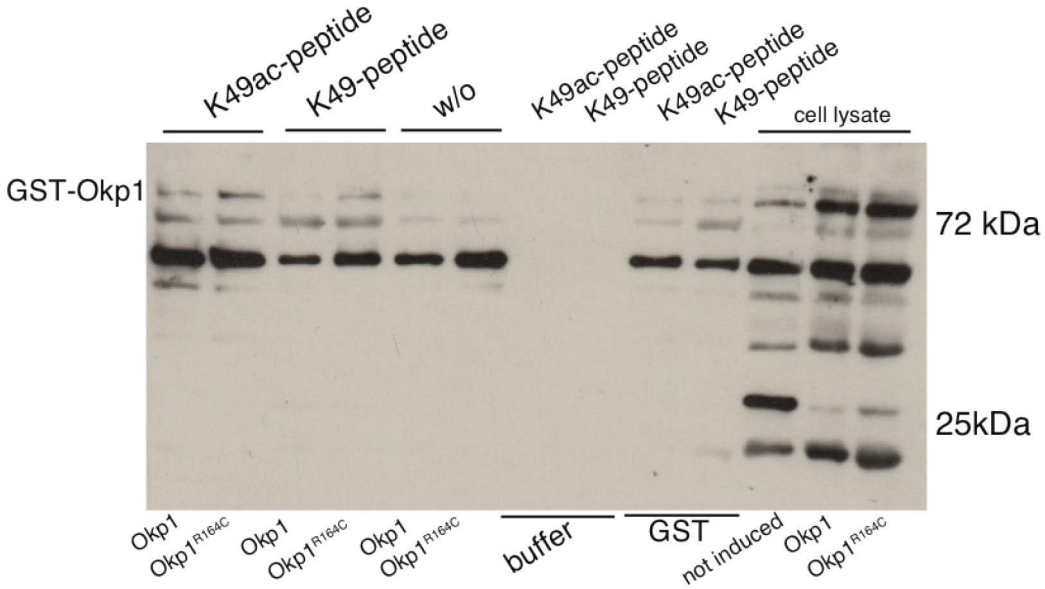

Figure 29: Peptide pull-down of Okp1 and Okp1^{R164C}.
Western blotting analysis of a peptide pull-down experiment using acetylated and unacetylated CENP-A^{Cse4K49} peptides immobilized on sulfolink beads and Okp1 and Okp1^{R164C} containing cell lysates as prey proteins. As shown in lanes 1 and 2, GST-Okp1 and GST-Okp1^{R146C} were pulled by the K49ac-peptides slightly. Lane 3 shows no binding of GST-Okp1 to K49-peptides, lane 4 indicates a weak binding of K49-peptides and GST-Okp1^{R146C}. Controls are indicated in lanes 5-10, cell lysates in lanes 11-13. The blot was incubated with α-GST (1:1000) and α-mouse HRP antibodies (1:1000).

GST-Okp1 as well as GST-Okp1^{R146C} bound weakly to the acetylated K49-peptide, whereas the unacetylated K49-peptide was not bound by GST-Okp1 and showed a weak binding of GST-Okp1^{R146C}. Different replicates of this experiment revealed inconsistent results with regard to the interpretation of the final western blots of each experiment. Discontinuity in the occurring binding properties of Okp1, Okp1^{R146C} to unmodified and acetylated K49 peptides do not exclude the possibility of a biochemical interaction of GST-Okp1 and N-terminal Cse4 peptide species, or Cse4K49 *in vivo*. These data have to be regarded with caution and could not lead to a conclusion as to whether Okp1 prefers acetylated or unacetylated K49 on Cse4.

3.5. CD-spectroscopy of GST-Cse4$^{14-134}$

The N-terminal regions of canonical histones are commonly described as unstructured tails, which protrude from the core domains of the nucleosomes and represent target regions of histone modifying enzymes (Luger, 2001; Jenuwein and Allis, 2001; Kouzarides, 2007). In comparison to canonical histone tails, the N-terminus of Cse4 is exceptionally long, raising the question of a specific function of this domain (Stoler et al., 1995; Meluh et al., 1998). An initial structural approach was used here to investigate the biochemical properties of this domain. Therefore, the N-terminus was purified recombinantly from *E. coli* and characterized biochemically. Purification of the N-terminal domain of Cse4 allowed the characterization of its secondary structure by circular dichroism (CD) spectroscopy.

For this purpose, the GST-Cse4$^{14-134}$ target protein was affinity-purified using glutathione-containing buffer. The GST-tag was specifically cleaved off using the PreScission Protease, followed by size exclusion chromatography to separate

Cse4$^{14-134}$ from free GST and the PreScission Protease. Each of the detected peaks was concentrated using Amicon Ultra centrifugal filters, and the three remaining fractions were further analyzed by SDS-PAGE and Coomassie blue staining (Figure 30). The SDS gel shows that the N-terminal domain of Cse4 could be purified via size exclusion chromatography (Figure 30, lane 4). The first fraction contained the remaining uncut fusion protein GST-Cse4$^{14-134}$ as well as free GST to a lesser extent (lane 2). In the second fraction, the main protein was free GST and to a lesser extent GST-Cse4$^{14-134}$ (lane 3). The third fraction contained mainly Cse4$^{14-134}$ (lane 4). The purified and untagged N-terminal domain of Cse4 was used to investigate the secondary structural elements by CD spectroscopy.

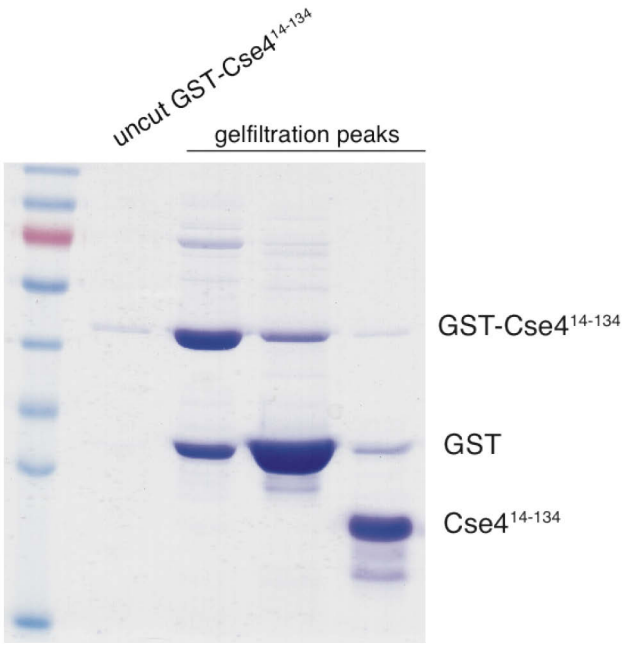

Figure 30: Size exclusion chromatography of Cse4$^{14-134}$.
SDS-PAGE and Coomassie staining of chromatographically purified Cse4$^{14-134}$. Recombinant GST-Cse4$^{14-134}$ was incubated with PreScission Protease and further separated by analytical gel filtration (second - fourth lanes). As control, 1 µl of the GST-Cse414-134 eluate was used (first lane).

The secondary structure of the N-terminus of Cse4$^{14-13}$ was examined by CD spectrometry. The spectrum of purified Cse4$^{14-134}$, as well as GST as a control was recorded in 25 repeats at RT and averaged for each spectrum. Subsequent subtraction of the buffer containing blank-spectrum of the protein spectra was carried out, resulting in the final CD spectra shown in Figure 31. Generally, proteins that

predominantly contain α-helices show two characteristic peaks in a spectrum range of about 205-220 nm. Unstructured, random coiled proteins appear to have one characteristic negative peak, and this peak appears at 190 nm. Proteins that contain both structural elements show a combination of both of the extreme CD-spectra. GST is a very well structured protein, mostly consisting of α-helices and a few β-strands (Lim et al., 1994). A spectrum of purified GST was recorded as control protein and displayed an α-helical structure, indicated by two specific negative peaks at 205 and 220 nm (shown in Figure 31 A). The spectrum of Cse4$^{14-134}$ shows one negative peak at 200 nm, indicating a domain of the protein that is less structured with helices and consisting of large regions of random coils and small α-helices (Figure 31 B). The shape of the spectrum indicates a protein domain that is flexible and partially structured with helices. Secondary structure deconvolution of the CDSSTR algorithm (Sreerama and Woody, 2000) confirmed 26 % helix, 9 % sheet and 26 % turns and 39 % coiled regions (Figure 31 C).

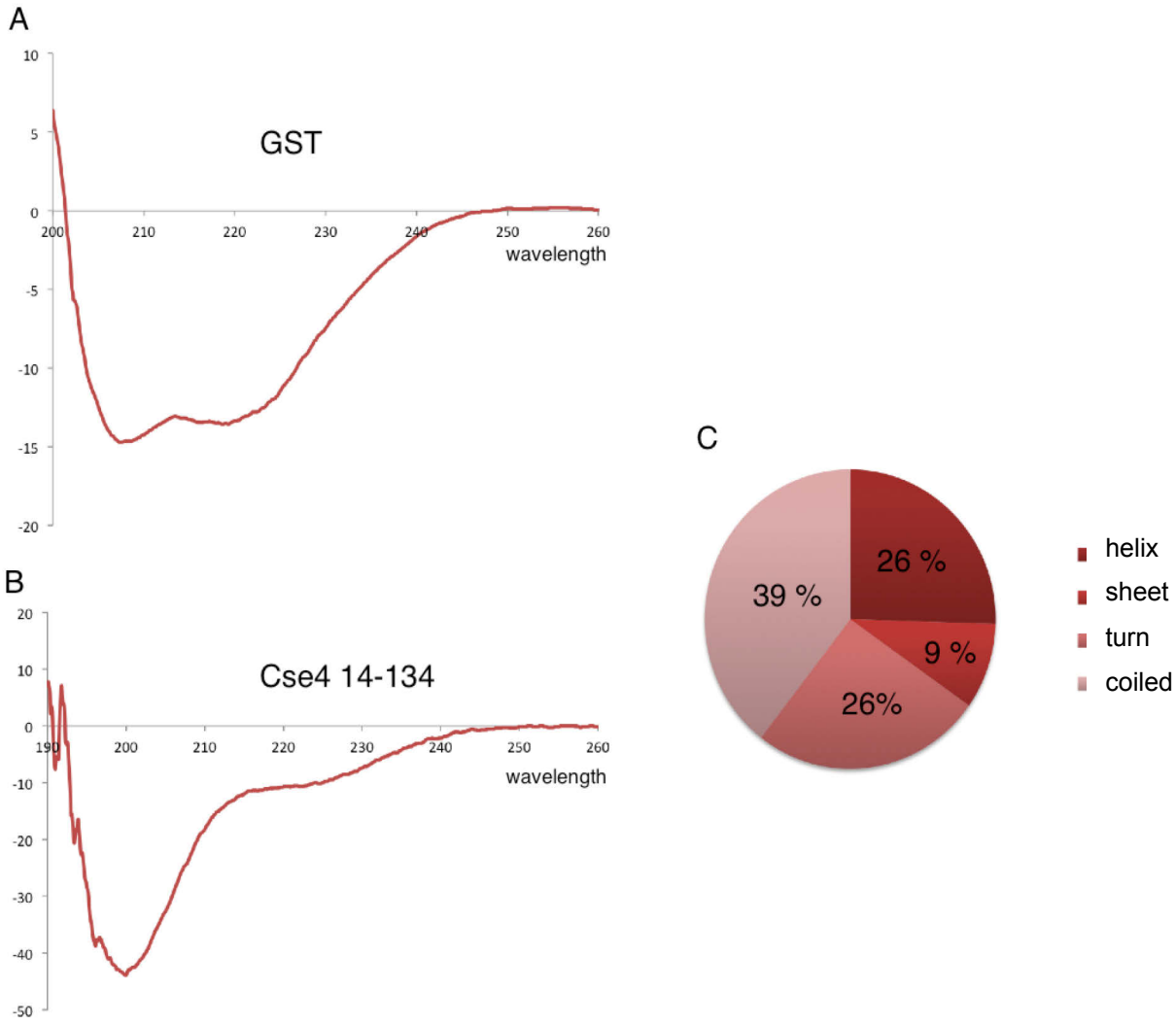

Figure 31: Far-UV spectra of Cse4$^{14-134}$ and GST

Depicted are the CD spectra of the purified N-terminal domain Cse4$^{14-134}$ (B) in comparison to the well-structured control protein GST (A), demonstrating a highly flexible structure for Cse4$^{14-134}$. The peaks of each of the spectra were at 205 and 220 nm in case of GST, and 200 nm in case of Cse4$^{14-134}$. Secondary structure deconvolution of the CD spectrum using CDSSTR algorithm confirmed 26% helix, 9% sheet, 26% turn and 39% random coil elements, indicated by the corresponding colors (C).

Finally, CD-spectroscopy of Cse4$^{14-134}$ showed that this protein domain displays a flexible structured tail. The structured portion of this domain including α-helixes, β-sheets and turns is about 60%, and it would be interesting to investigate the tertiary structure properties of this domain and whether the essential N-terminal domain or the single modification sites R37 and K49 (or the multiple phosphorylation sites) are located in a structured or an unstructured part of the N-terminus. It is likely, that this flexible domain folds upon binding, which increases physical interaction to other, non-histone proteins like histone modifying enzymes and kinetochore subunits.

3.6. Interactions of Cse4 N-termini with each other

It is likely that the point centromeric Cse4 is part of a centromeric nucleosome, which comprises an octameric core and in which two Cse4 molecules replace canonical H3. Possibly, the tails of these Cse4 molecules interact with each other in the centromeric nucleosome. To investigate interactions of the N-terminal Cse4 domain, a yeast-two-hybrid assay was performed with strains expressing full-length Cse4, an N-terminal Cse4$^{11-139}$ fragment, or as control Ctf19 (Figure 29). The yeast-two-hybrid reporter strain used here contained two reporters under the control of a *GAL4* regulated promoter, the *HIS3* gene and a *lacZ* reporter. The activation of the *lacZ* reporter was analyzed by incubating the strains on a nitrocellulose membrane, which was frozen in liquid nitrogen and incubated with buffer Z containing 0.1% X-Gal to induce the color reaction. The appearance of blue color indicated the activation of the *lacZ* gene in the Cse4 full length and Ctf19 clones, but not in the Cse4 N-terminal clones (Figure 29 C). Activation of the *HIS3* reporter gene was tested by incubating the strains on plates lacking histidine for three days at 30°C, indicated an interaction of Ctf19 and full length Cse4 (Figure 29 B, e). The further results indicated no protein-protein interaction of Cse4 N-terminal domains with each other.

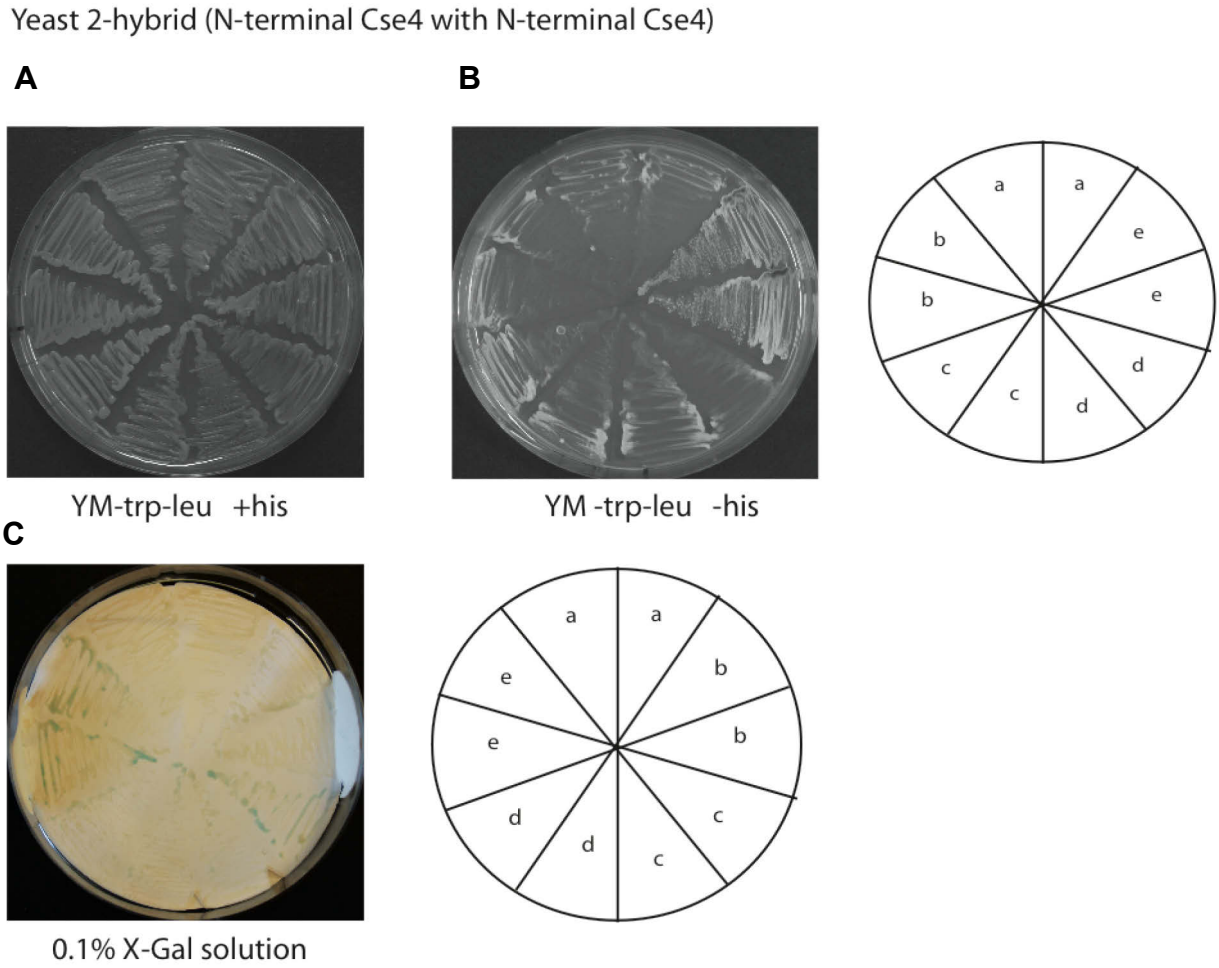

Figure 32: Yeast-two-hybrid assay of N-terminal CENP-A^{Cse4}

Yeast-two-hybrid transformants were plated on YM medium and stamped on a nitrocellulose membrane (C). Interaction was analyzed by β -galactosidase filter assay and confirmed by blue stained colonies after incubation at 30°C. Growth control was performed on YM medium +his (A). *HIS3* reporter activation of Ctf19 and CENP-A^{Cse4} full length (B) and empty vector controls are indicated.

4. Discussion

In budding yeast, a single nucleosome defines the centromeric region and therefore constitutes a so-called point centromere, in which the centromeric histone H3 variant Cse4 replaces H3. Cse4 is crucial for the centromere targeting, the establishment of a functional kinetochore and proper chromosome segregation (Morey et al., 2004). The histone-fold domain of Cse4 shares high sequence homology to histone H3, but the large N-terminal domain, which is approximately 135 amino acids in length, most likely constitutes a separate domain and is not conserved in higher eukaryotes. It has been shown that it contains an essential region spanning amino acids 28-66 (Chen et al., 2000).

Interestingly, in this region, at R37, a methylation site was found by mass spectrometric analysis. Further it has been shown that this modification functions as an epigenetic regulator in kinetochore recruitment and proper chromosome segregation, as indicated by negative genetic interactions of the point mutation *cse4-R37A* with subunits of the inner and the linker kinetochore regions (Samel et al., 2012). Additionally, an acetylation on Cse4K49 was defined, but the significance and enzymatic basis of this modification remained to be determined (Boeckmann et al., 2013). Unpublished data of a genetic study from our group revealed that this acetylation acts in an antagonistic way to the R37 methylation, as indicated by a suppression of the mentioned negative genetic interactions of *cse4-R37A* by a mutation of K49.

It was shown here that the acetylation on Cse4K49 is dependent on the histone acetyltransferase Gcn5. We further found that the disruption of the SAGA/SLIK, but not of the ADA complex led to decreased acetylation on Cse4K49. Furthermore, a potential cell-cycle dependence of this modification was addressed, and an increase in early S-phase and a decrease in late S-phase was observed, whereas the R37 methylation was shown to persist throughout the entire S-phase. Furthermore, we sought to investigate direct protein-protein interactions of Cse4 with kinetochore COMA subunits, and found that Ctf19 binds acetylated and unacetylated Cse4K49 with a preference for unacetylated Cse4.

4.1. The acetylation of Cse4K49 depends on Gcn5

To obtain insight into the epigenetic regulation of the process of chromosome segregation, it is necessary to define the CENP-A modifying enzymes. For example, the Aurora B homolog Ipl1, a kinase in yeast, was demonstrated to phosphorylate and dynamically regulate several kinetochore subunits, for example Ndc80 and Dam1, which links this kinase to centromere function and the establishment of a functional kinetochore (Cheeseman et al., 2002), which is essential for proper chromosome segregation during mitosis. It has recently been shown that the phosphorylation of the Cse4 N-terminus likewise depends on Ipl1, suggesting multiple targeting functions as a histone-modifying enzyme, and an epigenetic regulatory function in chromosome segregation (Boeckmann et al., 2013).

This study was aimed at gaining insight into the regulation and biochemical basis of the newly identified Cse4K49 acetylation site. We sought to identify the corresponding HAT and the complex in which this enzyme is active. Immunoprecipitation experiments using the α-Cse4K49ac antibodies showed that the acetylation of Cse4K49 depends on Gcn5 (Figure10). Particular lysine residues can be acetylated by more than one HAT. For example, the acetylation of H3K14 in yeast is mediated by Gcn5 as well as its distant relative GNAT family member Hpa2. The MYST Sas2 can also acetylate H3K14 next to H4K16 (Kuo et al., 1996; Sterner and Berger, 2000). Furthermore, the MYST HAT Sas3 has also been shown to be involved in acetylation of H3K14 *in vivo*, whereas the catalytic subunit of NuA4, Esa1, can acetylate this residue *in vitro* (Berndsen and Denu, 2008; Sterner and Berger, 2000). It was therefore conceivable that Cse4K49 acetylation depends on more than one HAT. By means of immunoprecipitation experiments using the HAT mutants *sas2Δ*, *sas3Δ*, *hpa2Δ*, *rtt109Δ*, *elp3Δ*, *hat1Δ*, *esa1-L327S* and *spt10Δ*, it was found that these yeast HATs do not appear to participate in Cse4K49 acetylation. This makes redundancy in the HATs responsible for Cse4K49 unlikely.

It has been shown that Sas2 and full-length Cse4 interact, as indicated by immunoprecipitation experiments and Yeast-2-Hybrid interaction (Seitz, 2004). As it was shown that acetylation on H4K16, the main target of Sas2, is decreased at centromeric $(H4\text{-}Cse4)_2$ containing nucleosomes (Choy et al., 2012; Choy et al., 2011), it is conceivable that Sas2 has another target at centromeric sites. However,

the exact role of Sas2 in this process has not been resolved. Neither in *sas2Δ* nor in a *SAS2* overexpression strains, an influence on the levels of Cse4K49 acetylation could not be detected. In agreement with this, upon *SAS2* overexpression, cells showed temperature sensitivity or synthetic lethality when combined with *CSE4* alleles containing mutations in the HFD, but not in the N-terminal domain (Choy et al., 2011). A putative role of Sas2 is based on the idea that it might regulate centromere function by acetylating non-histone targets. For example, it has been shown that the human MYST HAT MOF (Males absent on the first) not only acetylates histone lysines, but also displays auto-acetylation activity and acetylates the non-histone substrate p53K120 (Li et al., 2009; Sykes et al., 2006; Tang et al., 2006), which supports the assumption that Sas2 may be recruited to the centromere to catalyze the acetylation of non-histone proteins.

The data presented here are based on immunoprecipitation experiments using mutant yeast strains. While these approaches provide valuable information on the role of Gcn5 in the process of Cse4K49 acetylation *in vivo*, direct biochemical evidence is required to confirm the catalytic acetyltransferase activity of Gcn5 towards this specific residue of Cse4. This in principle can be done with mass-spectrometry analysis of Cse4 peptides from a *gcn5Δ* strain. In such a strain, the acetylation on K49 of Cse4 should not be detectable if only Gcn5 mediates the acetylation at this particular lysine. Furthermore, this can be done with a conventional HAT assay (Berndsen and Denu, 2005), using radiolabeled acetyl-CoA to detect the acetylation of Cse4 peptides or the purified N-terminal domain of Cse4 by recombinantly expressed and purified Gcn5. Ideally, the presumed non-redundancy of Cse4K49 acetylation should also be addressed by similar means, using established HAT assays and a number of putative HATs *in vitro.* If necessary, their native complexes would be purified in order to allow for the respective HAT to be catalytically active (Brownell and Allis, 1995). This would underscore the direct influence of Gcn5 and could help to rule out the possible role of other HATs in establishing this epigenetic mark. Furthermore, such an approach could be the starting point of detailed mechanistic analyses of the establishment of Cse4 modifications that are crucial for its function within the cell.

4.1.1. Which complex containing Gcn5 participates in Cse4K49 acetylation?

The histone acetyltransferase Gcn5 is a highly conserved enzyme, and homologues have been identified in numerous organisms, including humans, *D. melanogaster* and *A. thaliana* (Candau et al., 1996; Pandey et al., 2002; Smith et al., 1998). This points at a potential functional conservation in the processes in which Gcn5 is involved, like transcription activation of specific genes in the course of stress response. Recombinant Gcn5 is able to acetylate lysine residues on free histone tails, but is unable to acetylate histones in the nucleosomal context (Grant et al., 1997; Kuo et al., 1996). However, the incorporation of Gcn5 into native multisubunit HAT complexes more closely resembles the physiological environment of Gcn5 activity and, consequently, leads to an increase of Gcn5 HAT activity. These complexes are SAGA/SLIK and ADA in yeast. Generally, they are involved in transcription activation and elongation with partially overlapping function. The modification pattern of both complexes also overlaps; ADA has been shown to acetylate H3K14 and K18, SAGA acetylates H3K9, K14, K18 and K23 (Eberharter et al., 1998; Grant et al., 1999). Mutant analyses have revealed that SAGA activates transcription of a subset of genes, such as *HIS3*, *TRP3* and *GAL1* (Belotserkovskaya et al., 2000; Dudley et al., 1999). The SAGA derivate SLIK has also been shown to stimulate transcription, but additionally in a subset of genes that are activated in the retrograde response pathway, when mitochondrial dysfunction leads to a decreased mitochondrial membrane potential (Jazwinski, 2013; Pray-Grant et al., 2002). Interestingly, the biological function of ADA has not been determined yet, but it does not seem to participate in transcription activation. In contrast to SAGA, ADA did not interact with acidic activation domains *in vitro* (Utley et al., 1998), and thus seems to have a distinct biological function. It was therefore interesting to see whether ADA has a function on centromeres and to experimentally address the involvement of ADA in Cse4K49 acetylation.

The yeast protein Ada2 is the common component of the complexes ADA and SAGA and belongs to the acetylation/adapter module. It has been shown that Ada2 forms a catalytic core with Gcn5 (together with Ada3) and thereby potentiates the catalytic HAT activity of Gcn5 (Balasubramanian et al., 2002). The immunoprecipitation experiments shown here reveal that the deletion of the *ADA2* gene led to a

its absence is known to lead to the destabilization of the SAGA, but not the ADA complex. Upon deletion of the *SPT7* gene, a decreased Cse4K49 acetylation signal was observed, whereas no such effect was detected upon the deletion of the *UBP8* gene coding for the deubiquitination subunit Ubp8. The Ahc1 subunit is crucial for the structural integrity of the ADA complex, but is not a part of the SAGA complex. It was found that yeast extracts from *ahc1Δ* cells exclusively lacked the ADA, but not the SAGA complex. Consequently, an *ahc1* null mutant leads to the destabilization of the whole ADA complex (Eberharter et al., 1999). However, there was no detectable decrease in Cse4K49 acetylation upon disruption of the ADA complex by *ahc1Δ* in this study (Figure 14).

In summary, the absence of each of the two subunits Ada2 and Spt7 led to decreased precipitated acetylated Cse4K49. From these findings, it can be concluded that the Cse4K49 acetylation depends on SAGA (SLIK), and that ADA does not contribute to this specific acetylation. Furthermore, ADA was not able to compensate for the acetylation function of SAGA at these chromatin sites. The SAGA complex seems to have various subunit compositions when acting on sites different from actively transcribed genes, as indicated by the derivate of SAGA, SLIK. Therefore, it is conceivable that the subunit composition at centromeres represents a distinct complex performing this specific task. For example, it is unlikely that the TATA-binding protein associated factors are required at these sites. In conclusion, it would be interesting to find out whether more, less or different subunits are located within the SAGA complex, and whether this represents a centromere specific SAGA. A possible approach would be chromatin immunoprecipitation (ChIP) of different subunits of the SAGA complex focusing on the residence of these subunits at centromeric sites in the genome of *S. cerevisiae*.

In this study, a novel *in vivo* histone lysine acetyl transferase complex SAGA (SLIK) was defined and, therefore a novel function for the complex is proposed. While it was formerly described to function in transcriptional activation, it also seems to be involved in centromere biology with a distinct function in acetylating Cse4K49, which is in turn involved in the recruitment of kinetochore subunits of the COMA complex depending on its PTMs. This links SAGA function to the complex epigenetic regulation of kinetochore assembly and chromosome segregation during mitosis, which are yet to be understood. Many questions remain to be addressed in this context. Besides the

which are yet to be understood. Many questions remain to be addressed in this context. Besides the investigation of the subunit composition of SAGA at the centromeres, it would be interesting to elucidate the mechanism required to recruit SAGA to the centromeric regions, and how this process is regulated. Moreover, the question arises as to how the catalytic activity is regulated. It would be interesting to examine if it depends on specific residues in the N-terminal domain of Cse4 and, in particular, their modification status.

4.2. Phenotypical characterization of HAT and SAGA mutants

With respect to the strong synthetic growth phenotype, which has been shown in *cbf1Δ cse4R37A* cells and the suppression of this phenotype by an additional point mutation of *cse4K49R* (Samel, unpublished data), we asked whether this phenotype could also be suppressed with deletions in genes that code for HATs. The rationale was that the absence of the HAT that is responsible for the acetylation on Cse4K49 showed a similar phenotypical suppression as it was found for the *cbf1Δ cse4R37A K49R* triple mutant. Therefore, potential genetic interactions of different HAT mutants to complement the characterization of the acetylation of Cse4K49 were addressed, and it was investigated whether synthetic phenotypes can be discovered in double or triple mutants of HAT mutants, mutations of the inner kinetochore component *CBF1* and the point mutant *cse4R37A*.

4.2.1. Deletion of HAT genes did not suppress the phenotype of *cbf1Δ cse4R37A*

We asked whether another HAT might be involved in the acetylation of Cse4K49. The immunoprecipitation experiments did not point at the involvement of other HATs in this process, so the phenotypes of *HATΔ cbf1Δ cse4R37A* mutants were assessed as a complementary approach. The HAT mutants tested here were *esa1-L327S*, *sas2Δ*, *sas3Δ*, *hpa2Δ*, *rtt109Δ*, *elp3Δ*, *hat1Δ* and *spt10Δ*. It was hypothesized that the growth defect of the *cse4R37A* allele in the *cbf1Δ* background might be suppressed upon additional mutation of HATs, analogous to the restored growth observed in *cbf1Δ cse4R37A K49R* cells. A suppression caused by one of these HATs would

demonstrate a genetic interaction. However, no such suppression phenotype was detected in any of the tested triple mutants. Consequently, it is possible that none of the HATs has an impact on the acetylation on Cse4K49. Moreover, the mutation of a HAT often results in altered modification patterns of many histone or non-histone targets and thus impairs cellular function by interfering with a plethora of cellular processes. In yeast, for example, the essential HAT Esa1 is responsible for cell-cycle progression, acetylates H4 and acts in the NuA4 complex, which is involved in transcriptional activation (Allard et al., 1999; Clarke et al., 1999). Further, it regulates autophagy via acetylation of the signaling component Atg3 (Yi et al., 2012) and affects transcriptional silencing at telomeres (Clarke et al., 2006). This exemplifies the complexity of functions of a single HAT. In this context, the outcome of HAT phenotypes in combination with *cbf1Δ cse4R37A* was possibly affected by the increased sickness of the respective strains caused by the multiple mutations.

4.2.2. Deletion of *GCN5*, *ADA2* and *SPT7* did not suppress the phenotype of *cbf1Δ cse4R37A*

To investigate the *gcn5Δ*, *spt7Δ* or *ada2Δ* phenotypes corresponding to centromere function, strains carrying *gcn5Δ*, *spt7Δ* or *ada2Δ* were crossed with *cbf1Δ cse4R37A* and the segregants of the tetrad dissections were analyzed. It was found that *gcn5Δ cbf1Δ* as well as *ada2Δ cbf1Δ* double mutants showed synthetic lethality, as described earlier (Costanzo et al., 2010; Bandyopadhyay et al., 2010) and no viable triple mutants carrying the genotypes *gcn5Δ cbf1Δ cse4R37A* or *ada2Δ cbf1Δ cse4R37A* were observed.

As the acetylation of K49 should be abolished upon the deletion of *SPT7,* the triple mutant *spt7Δ cbf1Δ cse4R37A* was expected to show a suppression of the strong growth defect observed in the double mutant *cbf1Δ cse4R37A*, comparable to the triple mutant *cbf1Δ cse4R37A K49R*. It was found that the *spt7Δ cbf1Δ cse4R37A* strain was viable at permissive temperatures, but showed strongly impaired growth, indicating that there is no genetic interaction of *spt7Δ* with *cbf1Δ* and *cse4R37A*. It was further found that the double mutants of *spt7Δ cbf1Δ and spt7Δ cse4R37A* both did not exhibit a more severe phenotype than the single mutation of *spt7Δ*.

Mutations or deletions in genes that code for single subunits of transcription co-activator complexes can result in severe growth phenotypes in yeast, as shown for *GCN5*, *ADA2* or *SPT7*, respectively. In higher organisms, these subunits perform important roles during development. In mice, Gcn5 null mutants did not develop mesodermal tissue and died during embryogenesis (Xu et al., 2000). Additionally, Gcn5 plays a role in cancer development, where it regulates the oncogenic activity of c-Myc and the tumor suppressor p53 (McMahon et al., 2000). In yeast, it has been demonstrated that Ada2, an integral subunit of SAGA and ADA, functions as a transcriptional adaptor and potentiates the catalytic activity of Gcn5 (Eberharter et al., 1999; Marcus et al., 1994). Consequently, disruption of one of these two genes results in similarly strong phenotypes. The cells show phenotypes that correlate with the large-scale changes in transcription, depending on acidic activators like Gcn4. It was shown that null mutants of both *ada2* and *gcn5* display slow growth, temperature sensitivity and abnormal bud morphology, which indicate a function in cell-cycle progression (Berger et al., 1992; Watanabe, 2009). Taken together, the severe growth defects of SAGA/SLIK or ADA mutants, resulting from the multiple roles of SAGA (SLIK), were probably the reason why the mutants tested here could not be combined with *cbf1Δ* and the *cse4R37A* point mutant. In conclusion, this approach could not be used to experimentally substantiate the functional significance of the identified role of Gcn5 and the SAGA complex in Cse4K49 acetylation.

4.3. The dynamics of Cse4K49 acetylation levels in the cell cycle

The PTMs on the N-terminal tail of Cse4 may serve several functions. First, they might directly cause structural alterations in the nucleosome, forming a basis of the PTM-dependent recruitment of kinetochore proteins during cell division. A second role of PTMs on the centromeric histone variant might to serve as a signal for interactions with other proteins.

Severe groups have linked histone acetylation to transcriptional activation in many different eukaryotic organisms. HATs have been shown to acetylate specific residues on histone tails and transcription factors *in vivo*, which affect the activation of genes (Berger et al., 1999). Acetylation neutralizes the positively charged lysine residues of those tails, which leads to a reduction in the affinity of the histones to the negatively

charged DNA backbone, which in turn leads to a less compact chromatin conformation and increased access of transcription factors to the chromatin template (Cheung et al., 2000). Also, higher order chromatin structures depend in part on the N-termini of histones (Bailey et al., 2013). These structural changes are not only found at transcriptionally activated chromatin regions. It has been shown that PTMs of the N-terminal domain of CENP-A influence the conformation of centromeric chromatin directly. In the respective study, the N-terminal glycine 1 of human CENP-A was shown to be trimethylated and the serines 16 and 18 are phosphorylated, and it was reported that these PTMs affect the secondary structure and alter the centromeric chromatin fiber. The phosphorylations act in a patch and decrease via secondary structure alterations the oligomeric state of the CENP-A arrays (Bailey et al., 2013). Furthermore, it was demonstrated on human CENP-A that the centromeric nucleosomes of humans are transient in their structure during the cell cycle, oscillating between a tetrameric and an octameric state, and that this oscillation is dependent on PTMs within the HFDs of CENP-A and H4, which occur at the key transition point from G1 to S-phase (Bui et al., 2012). Recent studies based on AFM data suggested that CENP-A nucleosomes are octameric, but more dynamic than H3 nucleosomes (Miell et al., 2014). In yeast, it has been demonstrated that the centromeric nucleosome is replaced at the transition of G1- to S-phase (Wisniewski et al., 2014). Due to these data, it is likely that yeast centromere structures are highly dynamic, and it is possible that Cse4K49 acetylation plays a role in regulating these structural changes at the specific centromeric chromatin locus. Eventually, the point centromere needs to be made accessible for the binding of factors involved in centromere formation and kinetochore assembly in early S-phase.

The data presented here show an increase of the Cse4K49 acetylation in early S-phase (Figure 22), and it is possible that this lysine acetylation functions in dynamic kinetochore formation. Acting together with the numerous phosphorylation sites of the N-terminus, these PTMs alter the net charge of the histone tail, and therefore could directly lead to a more loose conformation of the point centromere.

Second, apart from their biophysical function, the PTMs of the N-terminus that were targets of investigations so far, have all been linked to chromosome segregation or kinetochore attachment. This was shown for the methylation on Cse4R37 (Samel et al., 2012) and for the phosphorylation of S22, S33, S40, and S105 of Cse4

(Boeckmann et al., 2013). Unpublished data from our group indicated that the acetylation on Cse4K49 is also linked to centromere function. This was shown by a genetic interaction of the R37 methylation and the K49 acetylation indicating an antagonistic function of both. Because the methylation on Cse4R37 functions in the epigenetic regulation of kinetochore recruitment (Samel et al., 2012), a function of acetylation on Cse4K49 in kinetochore recruitment was also assumed. The function of PTMs on histone tails is at least in part based on their ability to promote or prevent direct protein interactions. Histone acetyl moieties can function as signals for interaction with other regulatory proteins, which was shown in many cases (Berger 1999). These findings are in agreement with the experimental data presented here which show an increase of the Cse4K49 acetylation and the R37 methylation in S-phase (Figure 22). It is likely that newly synthesized Cse4 assembles into centromeric nucleosomes in early S-phase, and subsequently is acetylated and methylated. It was shown here that the acetylation is dependent on Gcn5, and SAGA associated Gcn5 is known to be able to acetylate nucleosome-bound histones (Grant et al., 1997). The results suggest that SAGA might be recruited to centromeres at late G1/early S-phase and specifically acetylates K49 after the cells have entered S-phase. How this process is regulated and which upstream signals lead to SAGA recruitment or assembly at centromeric sites is unclear and provides many options for further investigations. As the results presented here indicate, the acetylation decreases in late S-phase, whereas the methylation persists. Cse4 histones are replaced at the point centromeres of budding yeast in early S-phase and are remodeled by the specific histone chaperone Scm3 (Camahort et al., 2007; Mizuguchi et al., 2007). It has been shown previously that newly synthesized Cse4 histones are incorporated into centromeric nucleosomes in early S-phase and remain stably associated throughout the cell cycle (Wisniewski et al., 2014). This could be an indication that the acetylation is removed enzymatically via an HDAC and leads to the suggestion that the Cse4K49 acetylation adopts a specific function either in structural alterations of the centromeric nucleosome or the specific binding of Ctf19 and perhaps more inner kinetochore components. It would be interesting to experimentally test this hypothesis. Therefore, a future goal will be to reveal whether K49 acetylation is actively deacetylated and to identify the responsible HDAC.

For a comprehensive understanding of the epigenetic regulation of chromosome segregation in yeast, it would also be interesting to learn which histone

methyltransferase (HMT) is responsible for the Cse4R37 methylation and whether there is also a corresponding demethylase. Although it has been assumed for a long time that histone methylation is a non-reversible process, the discovery of the histone arginine demethylase JMJD6 in mice, which is responsible for demethylation of histone residues H3R2 and H4R3, indicates that other methyl moieties might also be removed enzymatically (Bannister and Kouzarides, 2011; Chang et al., 2007). The investigation of the involvement of such chromatin modifying enzymes at the centromeric histone variant CENP-A could lead to a deeper understanding of the regulation of kinetochore attachment and chromosome segregation.

4.3.1. Biochemical interactions of Ctf19, Okp1/Okp1R164C and the N-terminus of Cse4

In an earlier study in this group, it was shown that the acetylation on Cse4K49 antagonizes the methylation on Cse4R37. As the results shown here demonstrate, the substitution of the single amino acid K49 to arginine leads to a complete recovery from the cell cycle defect in a *cbf1Δ cse4R37A* temperature sensitive mutant. This leads to the suggestion that the acetylation on this lysine displays an antagonistic function and might also be involved in the assembly of the kinetochore and proper chromosome segregation as was shown by genetic studies for the methylation on Cse4 (Samel et al., 2012). It is likely that histone modifications provide dynamic binding platforms or interrupt direct binding of diverse factors (Bannister and Kouzarides, 2011). With respect to the antagonistic phenotype described above and the hypothesis that Cse4R37 methylation acts as a positive regulator in kinetochore recruitment (Samel et al., 2012), it is likely that the acetylation on Cse4 acts as a negative regulator. Maybe Cse4K49 acetylation prevents the recruitment of linker components of the kinetochore, such as Ctf19, until other factors are recruited and assembled. This may ensure the successive and concerted assembly of kinetochore subunits during S-phase.

Because of the inconsistent results of the peptide-binding assay with Okp1 and the Okp1 mutant, it was not possible to draw conclusions regarding direct protein-protein interactions of the N-terminus of Cse4 and Okp1 (Figure 29). It is likely that Okp1 interacts with the N-terminal domain, either with the unacetylated or the acetylated

Cse4K49, as indicated by previous genetic interaction studies. It would be interesting to investigate direct biochemical interactions using peptide pull-down experiments with methylated or unmethylated Cse4R37, to see if there is a preference of Okp1 to one of these Cse4 peptides or maybe also to see whether there are other factors or components that might confer the PTM-specific binding and PTM-dependent assembly of the kinetochore or kinetochore subunits.

Ctf19 seems to be directly recruited to the centromere by the N-terminus of Cse4, and the recruitment is potentially dependent on the acetylation status of Cse4K49. Although these results have to be considered with caution, the data presented here support the hypothesis that K49 acetylation displays an inhibiting function in the recruitment process of kinetochore proteins. It was shown before that the subunits of the COMA complex Ctf19, Okp1 and Mcm21, are components of the linker layer of the yeast kinetochore. Further it was shown that this complex links CBF3, which directly binds the CDEIII element of the centromeric DNA, to further components of the centromere, Cbf1 and Cse4 (Ortiz et al., 1999). Whereas direct biochemical interaction of Cse4 and the COMA components was detected in a Yeast-2-hybrid assay, in this study, we could identify Ctf19 as an interaction partner of Cse4 via immunoprecipitation, and that the interaction is dependent on the acetylation of K49 in the N-terminus of Cse4. Taken together, these findings lead to the suggestion that the PTMs on the N-terminus of Cse4 are form a basis of the epigenetically regulated recruitment of kinetochore components.

4.4. A crosstalk between the PTMs on Cse4

It is also conceivable that there is a crosstalk between the methylation on Cse4R37 and the acetylation on K49. Histone modifications can have an effect on each other *in cis* or *in trans*. An *in cis* interplay between an arginine methylation and lysine acetylation has been described for the N-terminus of H4. The methylation of H4R3 facilitates the acetylation of different lysine residues in the H4 N-terminus. However, the hyperacetylation of H4 inhibits further methylation of H4 R3 by PRMT1 (Wang et al., 2001). One possibility is that both N-termini of two Cse4 molecules within a nucleosome interact with each other, suggesting that these two modifications are distributed to two Cse4 molecules and probably influence the stability of the

centromeric nucleosome. Here a two-hybrid analysis was performed to investigate if two N-terminal domains of Cse4 could interact, but such an interaction was not observed. This could hint at the PTMs of this tail also acting in crosstalk. Either the proposed *trans* interaction does not exist under physiological conditions, or the N-terminal domains are not posttranslationally modified in the experimental setting. As a result, it is possible that both PTMs on the N-terminal domain on Cse4 influence each other *in cis*, and not *in trans*. It would be possible to test this hypothesis for example with the use of methylated Cse4 peptides in a HAT assay using purified Gcn5. If a methylated peptide enhances *in vitro* Gcn5 activity, this would support the *in cis* hypothesis.

4.4.1. Secondary structure determinations of the N-terminal domain of Cse4

A secondary structure prediction based on the full-length Cse4 sequence showed a partially α-helical N-terminal tail, interrupted by loops (data not shown). This is in agreement with the structural data obtained from the CD spectroscopy (Figure 31). The long and flexible, partially unstructured N-terminal tail of Cse4 renders interactions with manifold interaction partners possible. On one hand, it is the target of histone-modifying enzymes, Gcn5 from the SAGA complex likely being one of them. On the other hand, this tail is involved in the recruitment of the kinetochore linker components, at least Ctf19 as suggested by direct protein-protein interactions revealed in this study. It would be interesting to investigate the N-terminal part of Cse4 by means of further structural approaches. It is possible that the N-terminus of Cse4 is a partially unstructured domain, which further folds upon binding to a ligand. This domain could form a complex with Ctf19. At first, it would be promising to investigate the folding of the N-terminal domain of Cse4 in the presence of Ctf19 via a titration experiment using CD spectroscopy. To do this, recombinant purified Ctf19 and the N-terminal domain of Cse4 isolated in this study could be used. It would be interesting to determine the folding kinetics of the flexible N-terminal Cse4 domain upon successively increasing concentration of it binding partner Ctf19. A more detailed analysis of a potential complex of both proteins could be based co-crystallization experiments and X-ray crystallographic analyses.

4.5. Conclusions

In this study, it was shown that the acetylation on lysine 49 of the centromeric histone H3 variant Cse4 depends on the histone acetyltransferase Gcn5. It was further found that the acetylation on Cse4K49 also depends on the transcriptional co-activator SAGA/SLIK, but not on the ADA complex. For the acetylation of Cse4K49, the involvement in the regulation of the kinetochore assembly was revealed by direct interactions with the kinetochore component Ctf19, which belongs to the COMA subcomplex of the CTF19 complex and to the linker layer of the kinetochore. Additionally, it was shown that the K49 acetylation increased in early S-phase and decreased in late S-phase, also indicating an involvement in chromosome segregation. With this study, our knowledge of the N-terminal domain of Cse4 and its function within the kinetochore has been expanded. These findings contribute to the understanding of the ways in which the centromeric regions function and highlight the epigenetic features of centromere identity and regulation. Due to the fact that the histone H3 variant is conserved in eukaryotes, it is conceivable that similar mechanisms exist in higher eukaryotes to ensure proper attachment of the kinetochore. The mechanism of chromosome segregation seems to be, at least in part, epigenetically regulated. The multiple PTMs on the histone tails of CENP-A species that have been identified so far lead to the suggestion that diverse enzymes are involved, which catalyze PTMs and lead to a highly complex network ensuring the faithful assembly of kinetochores and, consequently, chromosome segregation. Further insight into these processes could provide the basis of the development of new therapeutic approaches for, e.g., treating cancer, where defects in chromosome segregation contribute to malignancies by increasing genomic instability.

5. References

Ahmad, K., and Henikoff, S. (2002). The histone variant H3.3 marks active chromatin by replication-independent nucleosome assembly. Molecular Cell *9*, 1191-1200.

Allan, J., Hartman, P.G., Cranerobinson, C., and Aviles, F.X. (1980). The structure of histone-H1 and its location in chromatin. Nature *288*, 675-679.

Allard, S., Utley, R.T., Savard, J., Clarke, A., Grant, P., Brandl, C.J., Pillus, L., Workman, J.L., and Cote, J. (1999). NuA4, an essential transcription adaptor/histone H4 acetyltransferase complex containing Esa1p and the ATM-related cofactor Tra1p. Embo Journal *18*, 5108-5119.

Allshire, R.C., and Karpen, G.H. (2008). Epigenetic regulation of centromeric chromatin: old dogs, new tricks? Nature Reviews Genetics *9*, 923-937.

Aravamudhan, P., Felzer-Kim, I., and Joglekar, A.P. (2013). The Budding Yeast Point Centromere Associates with Two Cse4 Molecules during Mitosis. Current Biology *23*, 770-774.

Arents, G., and Moudrianakis, E.N. (1995). The histone fold - a ubiquitous architectural motif utilized in DNA compaction and protein dimerization. Proceedings of the National Academy of Sciences of the United States of America *92*, 11170-11174.

Avner, P., and Heard, E. (2001). X-chromosome inactivation: Counting, choice and initiation. Nature Reviews Genetics *2*, 59-67.

Bailey, A.O., Panchenko, T., Sathyan, K.M., Petkowski, J.J., Pai, P.J., Bai, D.L., Russell, D.H., Macara, I.G., Shabanowitz, J., Hunt, D.F.*, et al.* (2013). Posttranslational modification of CENP-A influences the conformation of centromeric chromatin. Proceedings of the National Academy of Sciences of the United States of America *110*, 11827-11832.

Baker, R.E., Fitzgeraldhayes, M., and Obrien, T.C. (1989). Purification of the yeast centromere binding-protein CP1 and a mutational analysis of its binding-site. Journal of Biological Chemistry *264*, 10843-10850.

Baker, R.E., Harris, K., and Zhang, K.M. (1998). Mutations synthetically lethal with cep1 target S-cerevisiae kinetochore components. Genetics *149*, 73-85.

Baker, S.P., and Grant, P.A. (2007). The SAGA continues: expanding the cellular role of a transcriptional co-activator complex. Oncogene *26*, 5329-5340.

Balasubramanian, R., Pray-Grant, M.G., Selleck, W., Grant, P.A., and Tan, S. (2002). Role of the Ada2 and Ada3 transcriptional coactivators in histone acetylation. Journal of Biological Chemistry *277*, 7989-7995.

Bandyopadhyay, S., Mehta, M., Kuo, D., Sung, M.-K., Chuang, R., Jaehnig, E.J., Bodenmiller, B., Licon, K., Copeland, W., Shales, M.*, et al.* (2010). Rewiring of Genetic Networks in Response to DNA Damage. Science *330*, 1385-1389.

Bannister, A.J., and Kouzarides, T. (2011). Regulation of chromatin by histone modifications. Cell Research *21*, 381-395.

Bansal, P.K., Abdulle, R., and Kitagawa, K. (2004). Sgt1 associates with Hsp90: an initial step of assembly of the core kinetochore complex. Molecular and Cellular Biology *24*, 8069-8079.

Barski, A., Cuddapah, S., Cui, K., Roh, T.-Y., Schones, D.E., Wang, Z., Wei, G., Chepelev, I., and Zhao, K. (2007). High-resolution profiling of histone methylations in the human genome. Cell *129*, 823-837.

Bedford, M.T., and Clarke, S.G. (2009). Protein Arginine Methylation in Mammals: Who, What, and Why. Molecular Cell *33*, 1-13.

Bednar, J., Horowitz, R.A., Grigoryev, S.A., Carruthers, L.M., Hansen, J.C., Koster, A.J., and Woodcock, C.L. (1998). Nucleosomes, linker DNA, and linker histone form a unique structural motif that directs the higher-order folding and compaction of chromatin.

Proceedings of the National Academy of Sciences of the United States of America *95*, 14173-14178.

Belotserkovskaya, R., Sterner, D.E., Deng, M., Sayre, M.H., Lieberman, P.M., and Berger, S.L. (2000). Inhibition of TATA-binding protein function by SAGA subunits Spt3 and Spt8 at Gcn4-activated promoters. Molecular and Cellular Biology *20*, 634-647.

Berger, A.B., Cabal, G.G., Fabre, E., Duong, T., Buc, H., Nehrbass, U., Olivo-Marin, J.C., Gadal, O., and Zimmer, C. (2008). High-resolution statistical mapping reveals gene territories in live yeast. Nature Methods *5*, 1031-1037.

Berger, S.L., Pina, B., Silverman, N., Marcus, G.A., Agapite, J., Regier, J.L., Triezenberg, S.J., and Guarente, L. (1992). Genetic isolation of ADA2 - a potential transcriptional adapter required for function of certain acidic activation domains. Cell *70*, 251-265.

Berndsen, C.E., and Denu, J.M. (2005). Assays for mechanistic investigations of protein/histone acetyltransferases. Methods *36*, 321-331.

Berndsen, C.E., and Denu, J.M. (2008). Catalysis and substrate selection by histone/protein lysine acetyltransferases. Current Opinion in Structural Biology *18*, 682-689.

Bhaumik, S.R., and Green, M.R. (2001). SAGA is an essential in vivo target of the yeast acidic activator Gal4p. Genes & Development *15*, 1935-1945.

Bian, C.B., Xu, C., Ruan, J.B., Lee, K.K., Burke, T.L., Tempel, W., Barsyte, D., Li, J., Wu, M.H., Zhou, B.O*., et al.* (2011). Sgf29 binds histone H3K4me2/3 and is required for SAGA complex recruitment and histone H3 acetylation. Embo Journal *30*, 2829-2842.

Biggins, S., and Murray, A.W. (2001). The budding yeast protein kinase Ipl1/Aurora allows the absence of tension to activate the, spindle checkpoint. Genes & Development *15*, 3118-3129.

Black, B.E., Foltz, D.R., Chakravarthy, S., Luger, K., Woods, V.L., and Cleveland, D.W. (2004). Structural determinants for generating centromeric chromatin. Nature *430*, 578-582.

Black, B.E., Jansen, L.E.T., Maddox, P.S., Foltz, D.R., Desai, A.B., Shah, J.V., and Cleveland, D.W. (2007). Centromere identity maintained by nucleosomes assembled with histone H3 containing the CENP-A targeting domain. Molecular Cell *25*, 309-322.

Blower, M.D., Sullivan, B.A., and Karpen, G.H. (2002). Conserved organization of centromeric chromatin in flies and humans. Developmental Cell *2*, 319-330.

Bodor, D.L., Valente, L.P., Mata, J.F., Black, B.E., and Jansen, L.E.T. (2013). Assembly in G1 phase and long-term stability are unique intrinsic features of CENP-A nucleosomes. Molecular Biology of the Cell *24*, 923-932.

Boeckmann, L., Takahashi, Y., Au, W.-C., Mishra, P.K., Choy, J.S., Dawson, A.R., Szeto, M.Y., Waybright, T.J., Heger, C., McAndrew, C*., et al.* (2013). Phosphorylation of centromeric histone H3 variant regulates chromosome segregation in Saccharomyces cerevisiae. Molecular Biology of the Cell *24*, 2034-2044.

Brown, C.E., Lechner, T., Howe, L., and Workman, J.L. (2000). The many HATs of transcription coactivators. Trends in Biochemical Sciences *25*, 15-19.

Brown, S.W. (1966). Heterochromatin. Science *151*, 417-&.

Brownell, J.E., and Allis, C.D. (1995). An activity gel assay detects a single, catalytically active histone acetyltransferase subunit in *Tetrahymena* macronuclei. Proceedings of the National Academy of Sciences of the United States of America *92*, 6364-6368.

Brownell, J.E., and Allis, C.D. (1996). Special HATs for special occasions: Linking histone acetylation to chromatin assembly and gene activation. Current Opinion in Genetics & Development *6*, 176-184.

Brownell, J.E., Zhou, J.X., Ranalli, T., Kobayashi, R., Edmondson, D.G., Roth, S.Y., and Allis, C.D. (1996). Tetrahymena histone acetyltransferase A: A homolog to yeast Gcn5p linking histone acetylation to gene activation. Cell *84*, 843-851.

Bui, M., Dimitriadis, E.K., Hoischen, C., An, E., Quenet, D., Giebe, S., Nita-Lazar, A., Diekmann, S., and Dalal, Y. (2012). Cell-Cycle-Dependent Structural Transitions in the Human CENP-A Nucleosome In Vivo. Cell *150*, 317-326.

Burke, D.J., and Stukenberg, P.T. (2008). Linking kinetochore-microtubule binding to the spindle checkpoint. Developmental Cell *14*, 474-479.

Butler, J.S., Koutelou, E., Schibler, A.C., and Dent, S.Y.R. (2012). Histone-modifying enzymes: regulators of developmental decisions and drivers of human disease. Epigenomics *4*, 163-177.

Cai, M.J., and Davis, R.W. (1989). Purification of a yeast centromere-binding protein that is able to distinguish single base-pair mutations in its recognition site. Molecular and Cellular Biology *9*, 2544-2550.

Cai, M.J., and Davis, R.W. (1990). Yeast centromere binding protein-Cbf1, of the helix-loop-helix protein family, is required for chromosome stability and methionine prototrophy. Cell *61*, 437-446.

Camahort, R., Li, B., Florens, L., Swanson, S.K., Washburn, M.P., and Gerton, J.L. (2007). Scm3 is essential to recruit the histone H3 variant Cse4 to centromeres and to maintain a functional kinetochore. Molecular Cell *26*, 853-865.

Camahort, R., Shivaraju, M., Mattingly, M., Li, B., Nakanishi, S., Zhu, D.X., Shilatifard, A., Workman, J.L., and Gerton, J.L. (2009). Cse4 Is Part of an Octameric Nucleosome in Budding Yeast. Molecular Cell *35*, 794-805.

Candau, R., Moore, P.A., Wang, L., Barlev, N., Ying, C.Y., Rosen, C.A., and Berger, S.L. (1996). Identification of human proteins functionally conserved with the yeast putative adaptors ADA2 and GCN5. Molecular and Cellular Biology *16*, 593-602.

Chang, B., Chen, Y., Zhao, Y., and Bruick, R.K. (2007). JMJD6 is a histone arginine demethylase. Science *318*, 444-447.

Cheeseman, I.M., Anderson, S., Jwa, M., Green, E.M., Kang, J.s., Yates, J.R., 3rd, Chan, C.S.M., Drubin, D.G., and Barnes, G. (2002). Phospho-regulation of kinetochore-microtubule attachments by the Aurora kinase Ipl1p. Cell *111*, 163-172.

Chen, Y.H., Baker, R.E., Keith, K.C., Harris, K., Stoler, S., and Fitzgerald-Hayes, M. (2000). The N terminus of the centromere H3-like protein Cse4p performs an essential function distinct from that of the histone fold domain. Molecular and Cellular Biology *20*, 7037-7048.

Cheung, W.L., Briggs, S.D., and Allis, C.D. (2000). Acetylation and chromosomal functions. Current Opinion in Cell Biology *12*, 326-333.

Choo, K.H.A. (2001). Domain organization at the centromere and neocentromere. Developmental Cell *1*, 165-177.

Chow, J.C., Yen, Z., Ziesche, S.M., and Brown, C.J. (2005). Silencing of the mammalian X chromosome. In Annual Review of Genomics and Human Genetics (Palo Alto: Annual Reviews), pp. 69-92.

Choy, J.S., Acuna, R., Au, W.-C., and Basrai, M.A. (2011). A Role for Histone H4K 16 Hypoacetylation in Saccharomyces cerevisiae Kinetochore Function. Genetics *189*, 11-U595.

Choy, J.S., Mishra, P.K., Au, W.C., and Basrai, M.A. (2012). Insights into assembly and regulation of centromeric chromatin in Saccharomyces cerevisiae. Biochimica Et Biophysica Acta-Gene Regulatory Mechanisms *1819*, 776-783.

Clarke, A.S., Lowell, J.E., Jacobson, S.J., and Pillus, L. (1999). Esa1p is an essential histone acetyltransferase required for cell cycle progression. Molecular and Cellular Biology *19*, 2515-2526.

Clarke, A.S., Samal, E., and Pillus, L. (2006). Distinct roles for the essential MYST family HAT Esa1p in transcriptional silencing. Molecular Biology of the Cell *17*, 1744-1757.

Corona, D.F.V., Clapier, C.R., Becker, P.B., and Tamkun, J.W. (2002). Modulation of ISWI function by site-specific histone acetylation. Embo Reports *3*, 242-247.

Costanzi, C., and Pehrson, J.R. (1998). Histone macroH2A1 is concentrated in the inactive X chromosome of female mammals. Nature *393*, 599-601.

Costanzo, M., Baryshnikova, A., Bellay, J., Kim, Y., Spear, E.D., Sevier, C.S., Ding, H.M., Koh, J.L.Y., Toufighi, K., Mostafavi, S.*, et al.* (2010). The Genetic Landscape of a Cell. Science *327*, 425-431.

Dalal, Y., Wang, H., Lindsay, S., and Henikoff, S. (2007). Tetrameric structure of centromeric nucleosomes in interphase Drosophila cells. Plos Biology *5*, 1798-1809.

Daniel, J.A., and Grant, P.A. (2007). Multi-tasking on chromatin with the SAGA coactivator complexes. Mutation Research-Fundamental and Molecular Mechanisms of Mutagenesis *618*, 135-148.

Daniel, J.A., Torok, M.S., Sun, Z.W., Schieltz, D., Allis, C.D., Yates, J.R., and Grant, P.A. (2004). Deubiquitination of histone H2B by a yeast acetyltransferase complex regulates transcription. Journal of Biological Chemistry *279*, 1867-1871.

De Wulf, P., McAinsh, A.D., and Sorger, P.K. (2003). Hierarchical assembly of the budding yeast kinetochore from multiple subcomplexes. Genes & Development *17*, 2902-2921.

Desai, A., Rybina, S., Muller-Reichert, T., Shevchenko, A., Hyman, A., and Oegema, K. (2003). KNL-1 directs assembly of the microtubule-binding interface of the kinetochore in C. elegans. Genes & Development *17*, 2421-2435.

Di Lorenzo, A., and Bedford, M.T. (2011). Histone arginine methylation. Febs Letters *585*, 2024-2031.

Dion, M.F., Altschuler, S.J., Wu, L.F., and Rando, O.J. (2005). Genomic characterization reveals a simple histone H4 acetylation code. Proceedings of the National Academy of Sciences of the United States of America *102*, 5501-5506.

Driscoll, R., Hudson, A., and Jackson, S.P. (2007). Yeast Rtt109 promotes genome stability by acetylating histone H3 on lysine 56. Science *315*, 649-652.

Dudley, A.M., Rougeulle, C., and Winston, F. (1999). The Spt components of SAGA facilitate TBP binding to a promoter at a post-activator-binding step in vivo. Genes & Development *13*, 2940-2945.

Dunleavy, E.M., Roche, D., Tagami, H., Lacoste, N., Ray-Gallet, D., Nakamura, Y., Daigo, Y., Nakatani, Y., and Almouzni-Pettinotti, G. (2009). HJURP Is a Cell-Cycle-Dependent Maintenance and Deposition Factor of CENP-A at Centromeres. Cell *137*, 485-497.

Earnshaw, W.C., and Rothfield, N. (1985). Identification of a family of human centromere proteins using autoimmune sera from patients with scleroderma. Chromosoma *91*, 313-321.

Eberharter, A., John, S., Grant, P.A., Utley, R.T., and Workman, J.L. (1998). Identification and analysis of yeast nucleosomal histone acetyltransferase complexes. Methods-a Companion to Methods in Enzymology *15*, 315-321.

Eberharter, A., Sterner, D.E., Schieltz, D., Hassan, A., Yates, J.R., Berger, S.L., and Workman, J.L. (1999). The ADA complex is a distinct histone acetyltransferase complex in Saccharomyces cerevisiae. Molecular and Cellular Biology *19*, 6621-6631.

Espelin, C.W., Kaplan, K.B., and Sorger, P.K. (1997). Probing the architecture of a simple kinetochore using DNA-protein crosslinking. Journal of Cell Biology *139*, 1383-1396.

Felsenfeld, G., and McGhee, J.D. (1986). Structure of the 30 nm chromatin fiber. Cell *44*, 375-377.

Finch, J.T., and Klug, A. (1976). Solenoidal model for superstructure in chromatin. Proceedings of the National Academy of Sciences of the United States of America *73*, 1897-1901.

Fischle, W., Tseng, B.S., Dormann, H.L., Ueberheide, B.M., Garcia, B.A., Shabanowitz, J., Hunt, D.F., Funabiki, H., and Allis, C.D. (2005). Regulation of HP1-chromatin binding by histone H3 methylation and phosphorylation. Nature *438*, 1116-1122.

Fitzgerald-Hayes (1987). Yeast centromeres (Yeast).

Foley, E.A., and Kapoor, T.M. (2013). Microtubule attachment and spindle assembly checkpoint signalling at the kinetochore. Nature Reviews Molecular Cell Biology *14*, 25-37.

Foltz, D.R., Jansen, L.E.T., Bailey, A.O., Yates, J.R., Bassett, E.A., Wood, S., Black, B.E., and Cleveland, D.W. (2009). Centromere-Specific Assembly of CENP-A Nucleosomes Is Mediated by HJURP. Cell *137*, 472-484.

Foltz, D.R., Jansen, L.E.T., Black, B.E., Bailey, A.O., Yates, J.R., and Cleveland, D.W. (2006). The human CENP-A centromeric nucleosome-associated complex. Nature Cell Biology *8*, 458-U477.

Franck, A.D., Powers, A.F., Gestaut, D.R., Gonen, T., Davis, T.N., and Asbury, C.L. (2007). Tension applied through the Dam1 complex promotes microtubule elongation providing a direct mechanism for length control in mitosis. Nature Cell Biology *9*, 832-U171.

Freidkin, I., and Katcoff, D.J. (2001). Specific distribution of the Saccharomyces cerevisiae linker histone homolog HHO1p in the chromatin. Nucleic Acids Research *29*, 4043-4051.

Fudenberg, G., and Mirny, L.A. (2012). Higher-order chromatin structure: bridging physics and biology. Current Opinion in Genetics & Development *22*, 115-124.

Furuyama, T., and Henikoff, S. (2009). Centromeric Nucleosomes Induce Positive DNA Supercoils. Cell *138*, 104-113.

Gachet, Y., Reyes, C., Courtheoux, T., Goldstone, S., Gay, G., Serrurier, C., and Tournier, S. (2008). Sister kinetochore recapture in fission yeast occurs by two distinct mechanisms, both requiring Dam1 and Klp2. Molecular Biology of the Cell *19*, 1646-1662.

Georgakopoulos, T., Gounalaki, N., and Thireos, G. (1995). Genetic-evidence for the interaction of the yeast transcriptional coactivator proteins Gcn5 and Ada2. Molecular & General Genetics *246*, 723-728.

Georgakopoulos, T., and Thireos, G. (1992). 2 distinct yeast transcriptional activators require the function of the Gcn5 protein to promote normal levels of transcription. Embo Journal *11*, 4145-4152.

Goffeau, A., Barrell, B.G., Bussey, H., Davis, R.W., Dujon, B., Feldmann, H., Galibert, F., Hoheisel, J.D., Jacq, C., Johnston, M.*, et al.* (1996). Life with 6000 genes. Science *274*, 546-&.

Goodman, R.H., and Smolik, S. (2000). CBP/p300 in cell growth, transformation, and development. Genes & Development *14*, 1553-1577.

Gordon, F., Luger, K., and Hansen, J.C. (2005). The core histone N-terminal tail domains function independently and additively during salt-dependent oligomerization of nucleosomal arrays. The Journal of biological chemistry *280*, 33701-33706.

Gottschling, D.E., Aparicio, O.M., Billington, B.L., and Zakian, V.A. (1990). Position effect at *Saccharomyces cerevisiae* telomeres - reversible repression of Pol-II transcription. Cell *63*, 751-762.

Grant, P.A., Duggan, L., Cote, J., Roberts, S.M., Brownell, J.E., Candau, R., Ohba, R., OwenHughes, T., Allis, C.D., Winston, F.*, et al.* (1997). Yeast Gcn5 functions in two multisubunit complexes to acetylate nucleosomal histones: Characterization of an Ada complex and the SAGA (Spt/Ada) complex. Genes & Development *11*, 1640-1650.

Grant, P.A., Eberharter, A., John, S., Cook, R.G., Turner, B.M., and Workman, J.L. (1999). Expanded lysine acetylation specificity of Gcn5 in native complexes. Journal of Biological Chemistry *274*, 5895-5900.

Green, M.R. (2000). TBP-associated factors (TAF(II)s): multiple, selective transcriptional mediators in common complexes. Trends in Biochemical Sciences *25*, 59-63.

Grewal, S.I.S., Bonaduce, M.J., and Klar, A.J.S. (1998). Histone deacetylase homologs regulate epigenetic inheritance of transcriptional silencing and chromosome segregation in fission yeast. Genetics *150*, 563-576.

Grewal, S.I.S., and Jia, S.T. (2007). Heterochromatin revisited. Nature Reviews Genetics *8*, 35-46.

Hagstrom, K.A., Liu, H., Yates, J.R., and Meyer, B.J. (2002). Helping chromosomes pack up and split: the role of condensin in mitotic and meiotic chromosome segregation. Molecular Biology of the Cell *13*, 311A-311A.

Han, J., Zhou, H., Horazdovsky, B., Zhang, K., Xu, R.-M., and Zhang, Z. (2007). Rtt109 acetylates histone H3 lysine 56 and functions in DNA replication. Science *315*, 653-655.

Hardwick, K.G., Weiss, E., Luca, F.C., Winey, M., and Murray, A.W. (1996). Activation of the budding yeast spindle assembly checkpoint without mitotic spindle disruption. Science *273*, 953-956.

Hauf, S., and Watanabe, Y. (2004). Kinetochore orientation in mitosis and meiosis. Cell *119*, 317-327.

Hebbes, T.R., Clayton, A.L., Thorne, A.W., and Cranerobinson, C. (1994). Core histone hyperacetylation co-maps with generalized DNAse-I sensitivity in the chicken beta-globin chromosomal domain. Embo Journal *13*, 1823-1830.

Heitz E (1928) Das Heterochromatin der Moose. Jahrb Wiss Botanik 69: 762–818.

Henikoff, S., Ahmad, K., and Malik, H.S. (2001). The centromere paradox: Stable inheritance with rapidly evolving DNA. Science *293*, 1098-1102.

Henry, K.W., Wyce, A., Lo, W.S., Duggan, L.J., Emre, N.C.T., Kao, C.F., Pillus, L., Shilatifard, A., Osley, M.A., and Berger, S.L. (2003). Transcriptional activation via sequential histone H2B ubiquitylation and deubiquitylation, mediated by SAGA-associated Ubp8. Genes & Development *17*, 2648-2663.

Henry, M.F., and Silver, P.A. (1996). A novel methyltransferase (Hmt1p) modifies poly(A)(+)-RNA-binding proteins. Molecular and Cellular Biology *16*, 3668-3678.

Heun, P., Erhardt, S., Blower, M.D., Weiss, S., Skora, A.D., and Karpen, G.H. (2006). Mislocalization of the Drosophila centromere-specific histone CID promotes formation of functional ectopic kinetochores. Developmental Cell *10*, 303-315.

Hoffman, C.S., and Winston, F. (1987). A 10-minute DNA preparation from yeast efficiently releases autonomous plasmids for transformation of *Escherichia coli*. Gene *57*, 267-272.

Horiuchi, J., Silverman, N., Pina, B., Marcus, G.A., and Guarente, L. (1997). ADA1, a novel component of the ADA/GCN5 complex, has broader effects than GCN5, ADA2, or ADA3. Molecular and Cellular Biology *17*, 3220-3228.

Huisinga, K.L., and Pugh, B.F. (2004). A genome-wide housekeeping role for TFIID and a highly regulated stress-related role for SAGA in Saccharomyces cerevisiae. Molecular Cell *13*, 573-585.

Huynh, V.A.T., Robinson, P.J.J., and Rhodes, D. (2005). A method for the in vitro reconstitution of a defined "30 nm" chromatin fibre containing stoichiometric amounts of the linker histone. Journal of Molecular Biology *345*, 957-968.

Imai, S., Armstrong, C.M., Kaeberlein, M., and Guarente, L. (2000). Transcriptional silencing and longevity protein Sir2 is an NAD-dependent histone deacetylase. Nature *403*, 795-800.

Janke, C., Ortiz, J., Lechner, J., Shevchenko, A., Magiera, M.M., Schramm, C., and Schiebel, E. (2001). The budding yeast proteins Spc24p and Spc25p interact with Ndc80p and Nuf2p at the kinetochore and are important for kinetochore clustering and checkpoint control. Embo Journal *20*, 777-791.

Jazwinski, S.M. (2013). The retrograde response: When mitochondrial quality control is not enough. Biochimica Et Biophysica Acta-Molecular Cell Research *1833*, 400-409.

Jenuwein, T., and Allis, C.D. (2001). Translating the histone code. Science *293*, 1074-1080.

Joglekar, A.P., Bloom, K., and Salmon, E.D. (2009). In Vivo Protein Architecture of the Eukaryotic Kinetochore with Nanometer Scale Accuracy. Current Biology *19*, 694-699.

Joglekar, A.P., Bouck, D.C., Molk, J.N., Bloom, K.S., and Salmon, E.D. (2006). Molecular architecture of a kinetochore-microtubule attachment site. Nature Cell Biology *8*, 581-585.

Keith, K.C., Baker, R.E., Chen, Y.H., Harris, K., Stoler, S., and Fitzgerald-Hayes, M. (1999). Analysis of primary structural determinants that distinguish the centromere-specific function of histone variant Cse4p from histone H3. Molecular and Cellular Biology *19*, 6130-6139.

Kent, N.A., Tsang, J.S.H., Crowther, D.J., and Mellor, J. (1994). Chromatin structure modulation in *Saccharomyces cerevisiae* by centromere and promoter factor 1. Molecular and Cellular Biology *14*, 5229-5241.

Khorasanizadeh, S. (2004). The nucleosome: From genomic organization to genomic regulation. Cell *116*, 259-272.

Kimura, A., Matsubara, K., and Horikoshi, M. (2005). A decade of histone acetylation: Marking eukaryotic chromosomes with specific codes. Journal of Biochemistry *138*, 647-662.

Kimura, K., Rybenkov, V.V., Crisona, N.J., Hirano, T., and Cozzarelli, N.R. (1999). 13S condensin actively reconfigures DNA by introducing global positive writhe: Implications for chromosome condensation. Cell *98*, 239-248.

Kitagawa, K., Skowyra, D., Elledge, S.J., Harper, J.W., and Hieter, P. (1999). SGT1 encodes an essential component of the yeast kinetochore assembly pathway and a novel subunit of the SCF ubiquitin ligase complex. Molecular Cell *4*, 21-33.

Koutelou, E., Hirsch, C.L., and Dent, S.Y.R. (2010). Multiple faces of the SAGA complex. Current Opinion in Cell Biology *22*, 374-382.

Kouzarides, T. (2007). Chromatin modifications and their function. Cell *128*, 693-705.

Kunitoku, N., Sasayama, T., Marumoto, T., Zhang, D.W., Honda, S., Kobayashi, O., Hatakeyama, K., Ushio, Y., Saya, H., and Hirota, T. (2003). CENP-A phosphorylation by Aurora-A in prophase is required for enrichment of Aurora-B inner centromeres and for kinetochore function. Developmental Cell *5*, 853-864.

Kuo, M.H., Brownell, J.E., Sobel, R.E., Ranalli, T.A., Cook, R.G., Edmondson, D.G., Roth, S.Y., and Allis, C.D. (1996). Transcription-linked acetylation by Gcn5p of histones H3 and H4 at specific lysines. Nature *383*, 269-272.

Kurdistani, S.K., Tavazoie, S., and Grunstein, M. (2004). Mapping global histone acetylation patterns to gene expression. Cell *117*, 721-733.

Laemmli, U.K. (1970). Cleavage of structural proteins during assembly of head of bacteriophage-T4. Nature *227*, 680-&.

Lander, E.S., Int Human Genome Sequencing, C., Linton, L.M., Birren, B., Nusbaum, C., Zody, M.C., Baldwin, J., Devon, K., Dewar, K., Doyle, M.*, et al.* (2001). Initial sequencing and analysis of the human genome. Nature *409*, 860-921.

Larschan, E., and Winston, F. (2001). The S-cerevisiae SAGA complex functions in vivo as a coactivator for transcriptional activation by Gal4. Genes & Development *15*, 1946-1956.

Lee, J.H., Cook, J.R., Pollack, B.P., Kinzy, T.G., Norris, D., and Pestka, S. (2000a). Hsl7p, the yeast homologue of human JBP1, is a protein methyltransferase. Biochemical and Biophysical Research Communications *274*, 105-111.

Lee, K.K., Sardiu, M.E., Swanson, S.K., Gilmore, J.M., Torok, M., Grant, P.A., Florens, L., Workman, J.L., and Washburn, M.P. (2011). Combinatorial depletion analysis to assemble the network architecture of the SAGA and ADA chromatin remodeling complexes. Molecular Systems Biology *7*.

Lee, K.K., and Workman, J.L. (2007). Histone acetyltransferase complexes: one size doesn't fit all. Nature Reviews Molecular Cell Biology *8*, 284-295.

Lee, T.I., Causton, H.C., Holstege, F.C.P., Shen, W.C., Hannett, N., Jennings, E.G., Winston, F., Green, N.R., and Young, R.A. (2000b). Redundant roles for the TFIID and SAGA complexes in global transcription. Nature *405*, 701-704.

Li, X.Z., Wu, L.P., Corsa, C.A.S., Kunkel, S., and Dou, Y.L. (2009). Two Mammalian MOF Complexes Regulate Transcription Activation by Distinct Mechanisms. Molecular Cell *36*, 290-301.

Lim, K., Ho, J.X., Keeling, K., Gilliland, G.L., Ji, X.H., Ruker, F., and Carter, D.C. (1994). 3-dimensional structure of *Schistosoma japonicum* glutathione-s-transferase fused with a 6-amino acid conserved neutralizing epitope of Gp41 from HIV. Protein Science *3*, 2233-2244.

Lingelbach, L.B., and Kaplan, K.B. (2004). The interaction between Sgt1p and Skp1p is regulated by HSP90 chaperones and is required for proper CBF3 assembly. Molecular and Cellular Biology *24*, 8938-8950.

Liu, S.T., Rattner, J.B., Jablonski, S.A., and Yen, T.J. (2006). Mapping the assembly pathways that specify formation of the trilaminar kinetochore plates in human cells. Journal of Cell Biology *175*, 41-53.

Luger, K. (2001). Nucleosomes: Structure and Function (Encyclopedia Of Life Sciences: Nature Publishing Group).

Luger, K., Rechsteiner, T.J., Flaus, A.J., Waye, M.M.Y., and Richmond, T.J. (1997). Characterization of nucleosome core particles containing histone proteins made in bacteria. Journal of Molecular Biology *272*, 301-311.

Maeder, D.L., and Bohm, L. (1991). The c-domain in the H1 histone is structurally conserved. Biochimica Et Biophysica Acta *1076*, 233-238.

Maeshima, K., Hihara, S., and Eltsov, M. (2010). Chromatin structure: does the 30-nm fibre exist in vivo? Current Opinion in Cell Biology *22*, 291-297.

Marcus, G.A., Silverman, N., Berger, S.L., Horiuchi, J., and Guarente, L. (1994). Functional similarity and physical association between Gcn5 and Ada2 - putative transcriptional adapters. Embo Journal *13*, 4807-4815.

Marmorstein, R., and Trievel, R.C. (2009). Histone modifying enzymes: Structures, mechanisms, and specificities. Biochimica Et Biophysica Acta-Gene Regulatory Mechanisms *1789*, 58-68.

Masison, D.C., and Baker, R.E. (1992). Meiosis in *Saccharomyces cerevisiae* mutants lacking the centromere-binding protein CP1. Genetics *131*, 43-53.

McMahon, S.B., Wood, M.A., and Cole, M.D. (2000). The essential cofactor TRRAP recruits the histone acetyltransferase hGCN5 to c-Myc. Molecular and Cellular Biology *20*, 556-562.

Meijsing, S.H., and Ehrenhofer-Murray, A.E. (2001). The silencing complex SAS-I links histone acetylation to the assembly of repressed chromatin by CAF-I and Asf1 in Saccharomyces cerevisiae. Genes & Development *15*, 3169-3182.

Meluh, P.B., Yang, P.R., Glowczewski, L., Koshland, D., and Smith, M.M. (1998). Cse4p is a component of the core centromere of Saccharomyces cerevisiae. Cell *94*, 607-613.

Miell, M.D.D., Straight, A.F., and Allshire, R.C. (2014). CENP-A octamers do not confer a reduction in nucleosome height by AFM Reply. Nature Structural & Molecular Biology *21*, 5-8.

Mizuguchi, G., Xiao, H., Wisniewski, J., Smith, M.M., and Wu, C. (2007). Nonhistone Scm3 and histones CenH3-H4 assemble the core of centromere-specific nucleosomes. Cell *129*, 1153-1164.

Moreno-Moreno, O., Torras-Llort, M., and Azorin, F. (2006). Proteolysis restricts localization of CID, the centromere-specific histone H3 variant of Drosophila, to centromeres. Nucleic Acids Research *34*, 6247-6255.

Morey, L., Barnes, K., Chen, Y.H., Fitzgerald-Hayes, M., and Baker, R.E. (2004). The histone fold domain of Cse4 is sufficient for CEN targeting and propagation of active centromeres in budding yeast. Eukaryotic Cell *3*, 1533-1543.

Nekrasov, V.S., Smith, M.A., Peak-Chew, S., and Kilmartin, J.V. (2003). Interactions between centromere complexes in Saccharomyces cerevisiae. Molecular Biology of the Cell *14*, 4931-4946.

Niewmierzycka, A., and Clarke, S. (1999). S-adenosylmethionine-dependent methylation in Saccharomyces cerevisiae - Identification of a novel protein arginine methyltransferase. Journal of Biological Chemistry *274*, 814-824.

Nishino, Y., Eltsov, M., Joti, Y., Ito, K., Takata, H., Takahashi, Y., Hihara, S., Frangakis, A.S., Imamoto, N., Ishikawa, T.*, et al.* (2012). Human mitotic chromosomes consist predominantly of irregularly folded nucleosome fibres without a 30-nm chromatin structure. Embo Journal *31*, 1644-1653.

Ortiz, J., Stemmann, O., Rank, S., and Lechner, J. (1999). A putative protein complex consisting of Ctf19, Mcm21 and Okp1 represents a missing link in the budding yeast kinetochore. Genes & Development *13*, 1140-1155.

Osada, S., Sutton, A., Muster, N., Brown, C.E., Yates, J.R., Sternglanz, R., and Workman, J.L. (2001). The yeast SAS (something about silencing) protein complex contains a MYST-type putative acetyltransferase and functions with chromatin assembly factor ASF1. Genes & Development *15*, 3155-3168.

Owen, D.J., Ornaghi, P., Yang, J.C., Lowe, N., Evans, P.R., Ballario, P., Neuhaus, D., Filetici, P., and Travers, A.A. (2000). The structural basis for the recognition of acetylated histone H4 by the bromodomain of histone acetyltransferase Gcn5p. Embo Journal *19*, 6141-6149.

Palmer, D.K., Oday, K., Wener, M.H., Andrews, B.S., and Margolis, R.L. (1987). A 17-kD centromere protein (CENP-A) copurifies with nucleosome core particles and with histones. Journal of Cell Biology *104*, 805-815.

Pandey, R., Muller, A., Napoli, C.A., Selinger, D.A., Pikaard, C.S., Richards, E.J., Bender, J., Mount, D.W., and Jorgensen, R.A. (2002). Analysis of histone acetyltransferase and histone deacetylase families of Arabidopsis thaliana suggests functional diversification of chromatin modification among multicellular eukaryotes. Nucleic Acids Research *30*, 5036-5055.

Patterton, H.G., Landel, C.C., Landsman, D., Peterson, C.L., and Simpson, R.T. (1998). The biochemical and phenotypic characterization of Hho1p, the putative linker histone H1 of Saccharomyces cerevisiae. Journal of Biological Chemistry *273*, 7268-7276.

Pchelintsev, N.A., McBryan, T., Rai, T.S., van Tuyn, J., Ray-Gallet, D., Almouzni, G., and Adams, P.D. (2013). Placing the HIRA Histone Chaperone Complex in the Chromatin Landscape. Cell Reports *3*, 1012-1019.

Pepenella, S., Murphy, K.J., and Hayes, J.J. (2014). Intra- and inter-nucleosome interactions of the core histone tail domains in higher-order chromatin structure. Chromosoma *123*, 3-13.

Pidoux, A.L., and Allshire, R.C. (2004). Kinetochore and heterochromatin domains of the fission yeast centromere. Chromosome Research *12*, 521-534.

Pikaart, M.I., Recillas-Targa, F., and Felsenfeld, G. (1998). Loss of transcriptional activity of a transgene is accompanied by DNA methylation and histone deacetylation and is prevented by insulators. Genes & Development *12*, 2852-2862.

Pina, B., Berger, S., Marcus, G.A., Silverman, N., Agapite, J., and Guarente, L. (1993). ADA3 - a gene, identified by resistance to GAL4-VP16, with properties similar to and different from those of ADA2. Molecular and Cellular Biology *13*, 5981-5989.

Pray-Grant, M.G., Schieltz, D., McMahon, S.J., Wood, J.M., Kennedy, E.L., Cook, R.G., Workman, J.L., Yates, J.R., and Grant, P.A. (2002). The novel SLIK histone acetyltransferase complex functions in the yeast retrograde response pathway. Molecular and Cellular Biology *22*, 8774-8786.

Richmond, T.J., and Davey, C.A. (2003). The structure of DNA in the nucleosome core. Nature *423*, 145-150.

Robinson, P.J.J., An, W., Routh, A., Martino, F., Chapman, L., Roeder, R.G., and Rhodes, D. (2008). 30 nm chromatin fibre decompaction requires both H4-K16 acetylation and linker histone eviction. Journal of Molecular Biology *381*, 816-825.

Robinson, P.J.J., and Rhodes, D. (2006). Structure of the '30 nm' chromatin fibre: A key role for the linker histone. Current Opinion in Structural Biology *16*, 336-343.

Sambrook, J., Fritsch, E.F., and Maniatis, T. (1989). Molecular Cloning: A Laboratory Manual. (Cold Spring Harbor Laboratory Press).

Samel, A., Cuomo, A., Bonaldi, T., and Ehrenhofer-Murray, A.E. (2012). Methylation of CenH3 arginine 37 regulates kinetochore integrity and chromosome segregation.

Proceedings of the National Academy of Sciences of the United States of America *109*, 9029-9034.

Sanchez-Perez, I., Renwick, S.J., Crawley, K., Karig, I., Buck, V., Meadows, J.C., Franco-Sanchez, A., Fleig, U., Toda, T., and Millar, J.B.A. (2005). The DASH complex and Klp5/Klp6 kinesin coordinate bipolar chromosome attachment in fission yeast. Embo Journal *24*, 2931-2943.

Santaguida, S., and Musacchio, A. (2009). The life and miracles of kinetochores. Embo Journal *28*, 2511-2531.

Santos-Rosa, H., Schneider, R., Bannister, A.J., Sherriff, J., Bernstein, B.E., Emre, N.C.T., Schreiber, S.L., Mellor, J., and Kouzarides, T. (2002). Active genes are tri-methylated at K4 of histone H3. Nature *419*, 407-411.

Schalch, T., Duda, S., Sargent, D.F., and Richmond, T.J. (2005). X-ray structure of a tetranucleosome and its implications for the chromatin fibre. Nature *436*, 138-141.

Scharfenberger, M., Ortiz, J., Grau, N., Janke, C., Schiebel, E., and Lechner, J. (2003). Nsl1p is essential for the establishment of bipolarity and the localization of the Dam-Duo complex. Embo Journal *22*, 6584-6597.

Schmitzberger, F., and Harrison, S.C. (2012). RWD domain: a recurring module in kinetochore architecture shown by a Ctf19-Mcm21 complex structure. Embo Reports *13*, 216-222.

Schneider, J., Bajwa, P., Johnson, F.C., Bhaumik, S.R., and Shilatifard, A. (2006). Rtt109 is required for proper H3K56 acetylation - A Chromatin mark associated with the elongating RNA polymerase II. Journal of Biological Chemistry *281*, 37270-37274.

Schueler, M.G., and Sullivan, B.A. (2006). Structural and functional dynamics of human centromeric chromatin. In Annual Review of Genomics and Human Genetics (Palo Alto: Annual Reviews), pp. 301-313.

Seitz (2004). Connecting the histone acetyltransferase complex SAS-I to the centromere in S. cerevisiae.

Sekulic, N., Bassett, E.A., Rogers, D.J., and Black, B.E. (2010). The structure of (CENP-A-H4)(2) reveals physical features that mark centromeres. Nature *467*, 347-U132.

Shen, X. (1995). Linker histones are not essential and affect chromatin condensation in vivo, L. Yu, J.W. Weir, and M.A. Gorovsky, eds. (Cell).

Sherman, F. (1991). Getting started with yeast. Methods in Enzymology *194*, 3-21.

Shogren-Knaak, M., Ishii, H., Sun, J.M., Pazin, M.J., Davie, J.R., and Peterson, C.L. (2006). Histone H4-K16 acetylation controls chromatin structure and protein interactions. Science *311*, 844-847.

Singer, M.S., Kahana, A., Wolf, A.J., Meisinger, L.L., Peterson, S.E., Goggin, C., Mahowald, M., and Gottschling, D.E. (1998). Identification of high-copy disrupters of telomeric silencing in Saccharomyces cerevisiae. Genetics *150*, 613-632.

Smith, E.R., Belote, J.M., Schiltz, R.L., Yang, X.J., Moore, P.A., Berger, S.L., Nakatani, Y., and Allis, C.D. (1998). Cloning of Drosophila GCN5: conserved features among metazoan GCN5 family members. Nucleic Acids Research *26*, 2948-2954.

Song, F., Chen, P., Sun, D., Wang, M., Dong, L., Liang, D., Xu, R.-M., Zhu, P., and Li, G. (2014). Cryo-EM Study of the Chromatin Fiber Reveals a Double Helix Twisted by Tetranucleosomal Units. Science *344*, 376-380.

Sreerama, N., and Woody, R.W. (2000). Estimation of protein secondary structure from circular dichroism spectra: Comparison of CONTIN, SELCON, and CDSSTR methods with an expanded reference set. Analytical Biochemistry *287*, 252-260.

Sterner, D.E., Belotserkovskaya, R., and Berger, S.L. (2002). SALSA, a variant of yeast SAGA, contains truncated Spt7, which correlates with activated transcription. Proceedings of the National Academy of Sciences of the United States of America *99*, 11622-11627.

Sterner, D.E., and Berger, S.L. (2000). Acetylation of histones and transcription-related factors. Microbiology and Molecular Biology Reviews *64*, 435-+.

Stoler, S., Keith, K.C., Curnick, K.E., and Fitzgeraldhayes, M. (1995). A mutation in CSE4, an essential gene encoding a novel chromatin-associated protein in yeast, causes chromosome nondisjunction and cell-cycle arrest at mitosis. Genes & Development *9*, 573-586.

Stoler, S., Rogers, K., Weitze, S., Morey, L., Fitzgerald-Hayes, M., and Baker, R.E. (2007). Scm3, an essential Saccharomyces cerevisiae centromere protein required for G(2)/M progression and Cse4 localization. Proceedings of the National Academy of Sciences of the United States of America *104*, 10571-10576.

Suka, N., Luo, K.H., and Grunstein, M. (2002). Sir2p and Sas2p opposingly regulate acetylation of yeast histone H4 lysine16 and spreading of heterochromatin. Nature Genetics *32*, 378-383.

Sullivan, B.A., and Karpen, G.H. (2004). Centromeric chromatin exhibits a histone modification pattern that is distinct from both euchromatin and heterochromatin. Nature Structural & Molecular Biology *11*, 1076-1083.

Sutton, A., Shia, W.J., Band, D., Kaufman, P.D., Osada, S., Workman, J.L., and Sternglanz, R. (2003). Sas4 and Sas5 are required for the histone acetyltransferase activity of Sas2 in the SAS complex. Journal of Biological Chemistry *278*, 16887-16892.

Sykes, S.M., Mellert, H.S., Holbert, M.A., Li, K., Marmorstein, R., Lane, W.S., and McMahon, S.B. (2006). Acetylation of the p53 DNA-binding domain regulates apoptosis induction. Molecular Cell *24*, 841-851.

Tang, Y., Luo, J., Zhang, W., and Gu, W. (2006). Tip60-dependent acetylation of p53 modulates the decision between cell-cycle arrest and apoptosis. Molecular Cell *24*, 827-839.

Tomonaga, T., Matsushita, K., Yamaguchi, S., Oohashi, T., Shimada, H., Ochiai, T., Yoda, K., and Nomura, F. (2003). Overexpression and mistargeting of centromere protein-A in human primary colorectal cancer. Cancer Research *63*, 3511-3516.

Trask, B.J., Allen, S., Massa, H., Fertitta, A., Sachs, R., Vandenengh, G., and Wu, M. (1993). Studies of metaphase and interphase chromosomes using fluorescence in-situ hybridization. Cold Spring Harbor Symposia on Quantitative Biology *58*, 767-775.

Trojer, P., and Reinberg, D. (2007). Facultative heterochromatin: Is there a distinctive molecular signature? Molecular Cell *28*, 1-13.

Turner, B.M. (1991). Histone acetylation and control of gene-expression. Journal of Cell Science *99*, 13-20.

Utley, R.T., Ikeda, K., Grant, P.A., Cote, J., Steger, D.J., Eberharter, A., John, S., and Workman, J.L. (1998). Transcriptional activators direct histone acetyltransferase complexes to nucleosomes. Nature *394*, 498-502.

Vermeulen, M., Eberl, H.C., Matarese, F., Marks, H., Denissov, S., Butter, F., Lee, K.K., Olsen, J.V., Hyman, A.A., Stunnenberg, H.G.*, et al.* (2010). Quantitative Interaction Proteomics and Genome-wide Profiling of Epigenetic Histone Marks and Their Readers. Cell *142*, 967-980.

Vernarecci, S., Ornaghi, P., Bagu, A., Cundari, E., Ballario, P., and Filetici, P. (2008). Gcn5p plays an important role in centromere kinetochore function in budding yeast. Molecular and Cellular Biology *28*, 988-996.

Verreault, A., Kaufman, P.D., Kobayashi, R., and Stillman, B. (1996). Nucleosome assembly by a complex of CAF-1 and acetylated histones H3/H4. Cell *87*, 95-104.

Wach, A., Brachat, A., Pohlmann, R., and Philippsen, P. (1994). New heterologous modules for classical or pcr-based gene disruptions in *Saccharomyces cerevisiae*. Yeast *10*, 1793-1808.

Wang, H.B., Huang, Z.Q., Xia, L., Feng, Q., Erdjument-Bromage, H., Strahl, B.D., Briggs, S.D., Allis, C.D., Wong, J.M., Tempst, P.*, et al.* (2001). Methylation of histone H4 at arginine 3 facilitating transcriptional activation by nuclear hormone receptor. Science *293*, 853-857.

Wang, J.P., Fondufe-Mittendorf, Y., Xi, L.Q., Tsai, G.F., Segal, E., and Widom, J. (2008). Preferentially Quantized Linker DNA Lengths in *Saccharomyces cerevisiae*. Plos Computational Biology *4*, 10.

Wang, L.A., Mizzen, C., Ying, C., Candau, R., Barlev, N., Brownell, J., Allis, C.D., and Berger, S.L. (1997). Histone acetyltransferase activity is conserved between yeast and human GCN5 and is required for complementation of growth and transcriptional activation. Molecular and Cellular Biology *17*, 519-527.

Wang, Y.C., and Burke, D.J. (1995). Checkpoint genes required to delay cell-division in response to nocodazole respond to impaired kinetochore function in the yeast *Saccharomyces cerevisiae*. Molecular and Cellular Biology *15*, 6838-6844.

Watanabe, M., Watanabe, D., Nogami, S., Morishita, S., and Ohya, Y. (2009). Comprehensive and quantitative analysis of yeast deletion mutants defective in apical and isotropic bud growth. Current Genetics *55*, 365-380.

Waterborg, J.H. (2000). Steady-state levels of histone acetylation in Saccharomyces cerevisiae. Journal of Biological Chemistry *275*, 13007-13011.

Wells, D., and McBride, C. (1989). A comprehensive compilation and alignment of histones and histone genes. Nucleic Acids Research *17*, R311-R346.

Westermann, S., Drubin, D.G., and Barnes, G. (2007). Structures and functions of yeast kinetochore complexes. In Annual Review of Biochemistry (Palo Alto: Annual Reviews), pp. 563-591.

Westermann, S., and Schleiffer, A. (2013). Family matters: structural and functional conservation of centromere-associated proteins from yeast to humans. Trends in Cell Biology *23*, 260-269.

Westermann, S., Wang, H.W., Avila-Sakar, A., Drubin, D.G., Nogales, E., and Barnes, G. (2006). The Dam1 kinetochore ring complex moves processively on depolymerizing microtubule ends. Nature *440*, 565-569.

Wigge, P.A., and Kilmartin, J.V. (2001). The Ndc80p complex from Saccharomyces cerevisiae contains conserved centromere components and has a function in chromosome segregation. Journal of Cell Biology *152*, 349-360.

Wilkins, B.J., Rall, N.A., Ostwal, Y., Kruitwagen, T., Hiragami-Hamada, K., Winkler, M., Barral, Y., Fischle, W., and Neumann, H. (2014). A Cascade of Histone Modifications Induces Chromatin Condensation in Mitosis. Science *343*, 77-80.

Williams, J.S., Hayashi, T., Yanagida, M., and Russell, P. (2009). Fission Yeast Scm3 Mediates Stable Assembly of Cnp1/CENP-A into Centromeric Chromatin. Molecular Cell *33*, 287-298.

Wisniewski, J., Hajj, B., Chen, J.J., Mizuguchi, G., Xiao, H., Wei, D., Dahan, M., and Wu, C. (2014). Imaging the fate of histone Cse4 reveals de novo replacement in S phase and subsequent stable residence at centromeres. Elife *3*, 38.

Workman, J.L. (2006). Nucleosome displacement in transcription. Genes & Development *20*, 2009-2017.

Wu, C.Y., Bassett, A., and Travers, A. (2007). A variable topology for the 30-nm chromatin fibre. Embo Reports *8*, 1129-1134.

Wu, P.Y.J., and Winston, F. (2002). Analysis of Spt7 function in the Saccharomyces cerevisiae SAGA coactivator complex. Molecular and Cellular Biology *22*, 5367-5379.

Xu, W.T., Edmondson, D.G., Evrard, Y.A., Wakamiya, M., Behringer, R.R., and Roth, S.Y. (2000). Loss of Gcn5/2 leads to increased apoptosis and mesodermal defects during mouse development. Nature Genetics *26*, 229-232.

Yang, X.J., Ogryzko, V.V., Nishikawa, J., Howard, B.H., and Nakatani, Y. (1996). A p300/CBP-associated factor that competes with the adenoviral oncoprotein E1A. Nature *382*, 319-324.

Yao, T.P., Oh, S.P., Fuchs, M., Zhou, N.D., Ch'ng, L.E., Newsome, D., Bronson, R.T., Li, E., Livingston, D.M., and Eckner, R. (1998). Gene dosage-dependent embryonic development and proliferation defects in mice lacking the transcriptional integrator p300. Cell *93*, 361-372.

Yi, C., Ma, M., Ran, L., Zheng, J., Tong, J., Zhu, J., Ma, C., Sun, Y., Zhang, S., Feng, W.*, et al.* (2012). Function and Molecular Mechanism of Acetylation in Autophagy Regulation. Science *336*, 474-477.

Yoda, K., Ando, S., Morishita, S., Houmura, K., Hashimoto, K., Takeyasu, K., and Okazaki, T. (2000). Human centromere protein A (CENP-A) can replace histone H3 in nucleosome reconstitution in vitro. Proceedings of the National Academy of Sciences of the United States of America *97*, 7266-7271.

Zeitlin, S.G., Shelby, R.D., and Sullivan, K.F. (2001). CENP-A is phosphorylated by Aurora B kinase and plays an unexpected role in completion of cytokinesis. Journal of Cell Biology *155*, 1147-1157.

Zeng, L., and Zhou, M.M. (2002). Bromodomain: an acetyl-lysine binding domain. Febs Letters *513*, 124-128.

Zhang, X., Wen, H., and Shi, X. (2012). Lysine methylation: beyond histones. Acta Biochimica Et Biophysica Sinica *44*, 14-27.

Zhou, Z., Feng, H.Q., Zhou, B.R., Ghirlando, R., Hu, K.F., Zwolak, A., Jenkins, L.M.M., Xiao, H., Tjandra, N., Wu, C.*, et al.* (2011). Structural basis for recognition of centromere histone variant CenH3 by the chaperone Scm3. Nature *472*, 234-237.

6. Appendix

6.1 Quantification of immunoprecipitation experiments

To validate the results of the immunoprecipitation experiments shown in the results section (Figures 10-12 and 14, 20 and 21, respectively), quantifications were carried out. In Figures 33-37, quantifications of all western blotting results of the immunoprecipitation experiments performed during this study are shown. The calculation of the intensities of the single western blotting bands was done using ImageJ. Input signals of the corresponding wild type control and the mutants were set to 1, and the signals of the indicated precipitations (Cse4K49ac, 3xHA-Cse4, and w/o antibody, respectively) were calculated relative to the input signals.

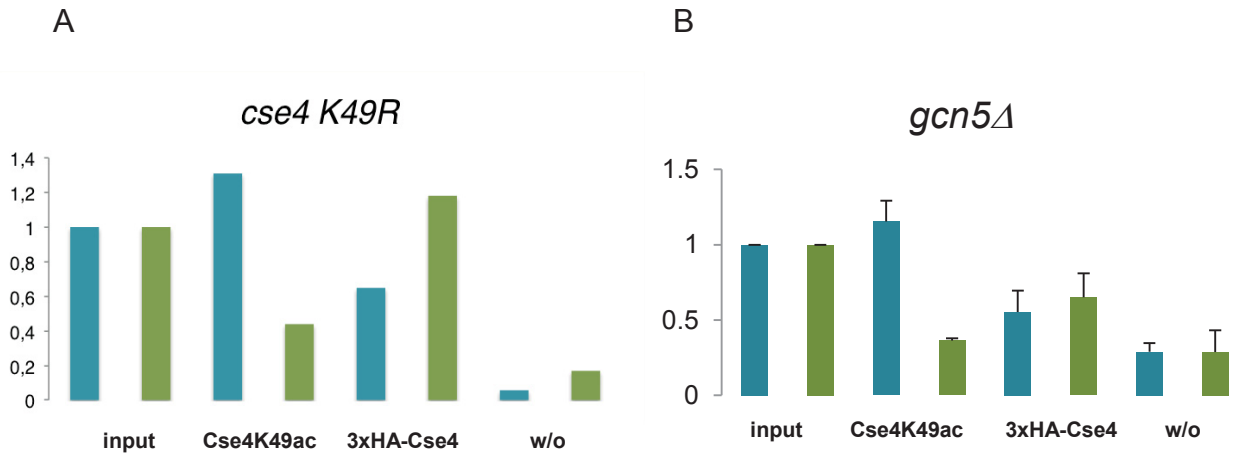

Figure 33: Identification of Gcn5 as the histone acetyltransferase that acetylates Cse4K49
A: Quantification of the western blotting analysis of immunoprecipitated 3xHA-Cse4K49ac in wild type (AEY2781) and 3xHA-Cse4K49R (AEY2960) showed reduced precipitated Cse4K49ac signal in Cse4K49R. Wild type signals are depicted in blue, mutants in green. **B**: Comparison of wild type (AEY2781) and *gcn5Δ* mutant (AEY5310) showed a considerably reduced acetylation level in the *gcn5Δ* mutant strain in comparison to wild type (three biological replicates;). From left to right: input controls of wild type and mutant; precipitated acetylated Cse4K49 of wild type and mutant; precipitated 3xHA-tagged Cse4; negative controls w/o antibody.

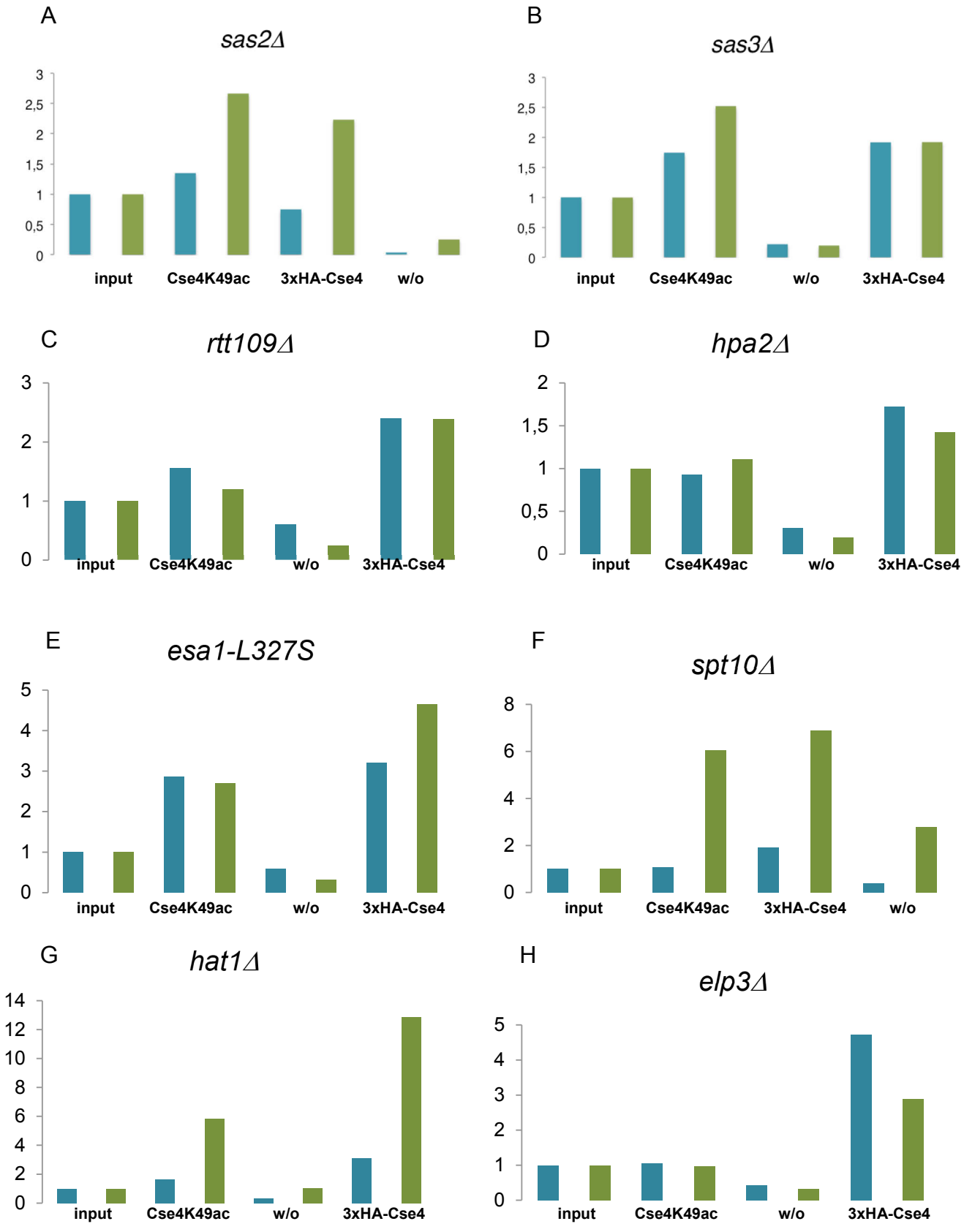

Figure 34: No influence of other histone acetyltransferases on Cse4K49ac.

Quantification of the western blotting analysis of immunoprecipitated acetylated Cse4K49 in wild type cells (AEY2781) and strains containing mutations in the HAT genes: *sas2Δ* (AEY5312), *sas3Δ* (AEY5300), *hpa2Δ* (AEY5308) and *rtt109Δ* (AEY5306) as shown in the results (Figure 11) and

elp3Δ (AEY5302), *hat1Δ* (AEY5314), *esa1-L327S* (AEY5316) and *spt10Δ* (AEY5304) (Figure 12). Wild type signals are depicted in blue, mutants in green. **A**: *sas2Δ* did not reduce the Cse4K49ac signal detected by immunoprecipitation. The deletion of *sas3Δ* (**B**) *rtt109Δ* **C**), *hpa2Δ* (**D**), *esa1-L327S* (**E**) and *elp3Δ* (**H**) did not lead to significantly decreased acetylation on Cse4K49. The increasing signals result from the very low input signals in the cases of *spt10Δ* (**F**) and *hat1Δ* (**G**). From left to right: input controls of wild type and mutant; precipitated acetylated Cse4K49 of wild type and mutant. Negative controls w/o antibody; precipitated 3xHA-tagged Cse4 in case of **B**, **C**, **D**, **E**, **G**, **H**; or in **A** and **F**, precipitated 3xHA-tagged Cse4 and w/o antibody controls.

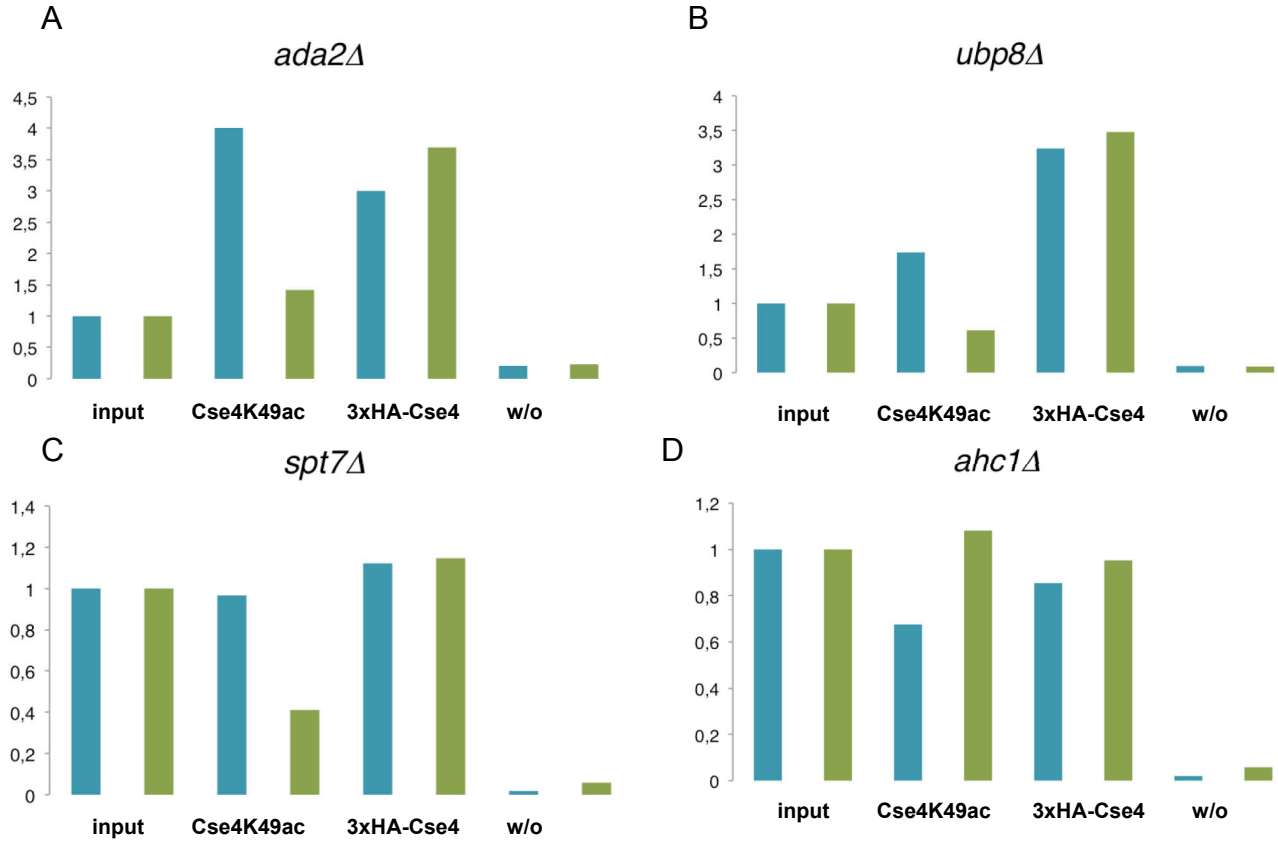

Figure 35: Decreased acetylation of Cse4K49 in SAGA mutants.

Quantification of the western blotting analysis of immunoprecipitated acetylated Cse4K49 in wild type cells (AEY2781) and SAGA/ADA complex mutants (Results: Figure 14). Wild type signals are depicted in blue, mutants in green. **A**: The mutation of *ADA2* (AEY5624) leads to a complete lack of precipitated acetylated Cse4K49. **B**: By deleting the ubiquitination SAGA subunit *UBP8* (AEY5538) no altered Cse4K49 acetylation could be detected by immunoprecipitation. **C**: The deletion of the architecture subunit *SPT7* (AEY5618) leads to significantly decreased acetylation of Cse4K49. **D**: The deletion of the ADA subunit *AHC1* (AEY5478) did not alter the amount of precipitated Cse4K49ac. From left to right: input controls of wild type and mutant; precipitated acetylated Cse4K49 of wild type and mutant; precipitated 3xHA-tagged Cse4; negative controls w/o antibody.

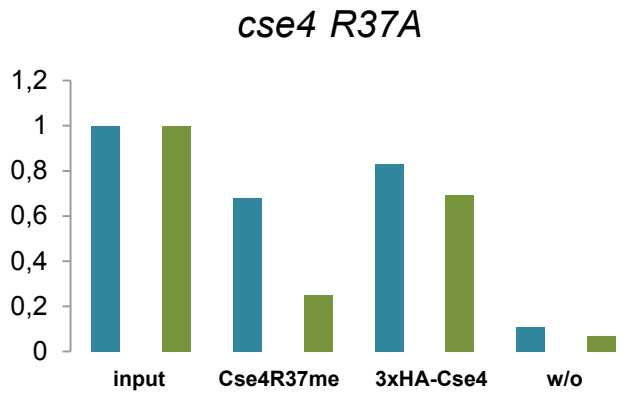

Figure 36: Immunoprecipitation of methylated Cse4R37

Quantification of the western blotting of the immunoprecipitated methylated Cse4R37, result is shown in Figure 21. A wild type Cse4 strain (AEY 2781) and a mutant *cse4R37A* strain (AEY 5040) were used for the immunoprecipitation experiment. Wild type signals are depicted in blue, mutants in green. The *cse4R37A* mutant showed a significantly decreased methylation signal in comparison to the wild type condition. From left to right: input controls of wild type and mutant; precipitated methylated Cse4R37 of wild type and mutant; precipitated 3xHA-tagged Cse4; negative controls w/o antibody.

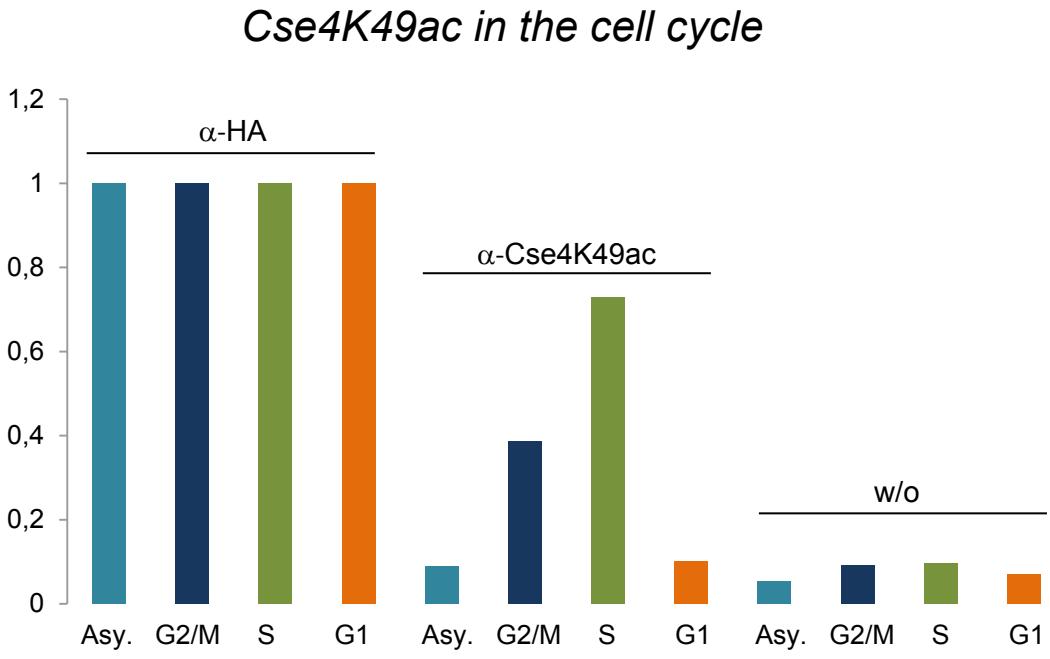

Figure 37: Cell-cycle dependence of Cse4K49 acetylation.

Quantification of the western blotting result of the cell cycle immunoprecipitation experiment (results, Figure 20). Yeast cells, which carry 3xHA-Cse4 on a plasmid in a *cse4Δ* background (AEY2781), were arrested in cell-cycle phases G1, S and G2/M, respectively, and acetylated Cse4K49 was immunoprecipitated (middle four bars). The turquoise bars show the population asynchronous cells` as control. G2/M phase cells are indicated in dark blue, S phase cells are shown in green and G1 cells

are shown in orange, respectively. As controls, equal amounts of lysates were used, and Cse4 was immunoprecipitated by the use of α-HA antibody (left four bars). HA levels of each cell-cycle phase was set to 1, and the acetylation on K49 of the corresponding cell-cycle phases were calculated relative to the HA levels. The second control was made without antibody incubation (right four bars). Acetylation on K49 of Cse4 increased in S-phase compared to G2/M-phase, G1-phase or asynchronous cells. Threefold replicates of this experiment were done.

6.2 FACS profiles of cell-cycle arrested yeast cells

For FACS analysis, 0.1 OD of yeast cells were harvested and stained in 50 µl PBS with propidium iodide (PPI). DNA contents of the samples were measured at a BD FACSCalibur or at a BD FACSAriaII and analyzed using FlowJo or Flowing Software. To control the arrest of yeast cells in different cell-cycle phases, or to follow the release of G1-arrested cells into S-phase, FACS analysis was used, shown in Figures 38 and 39.

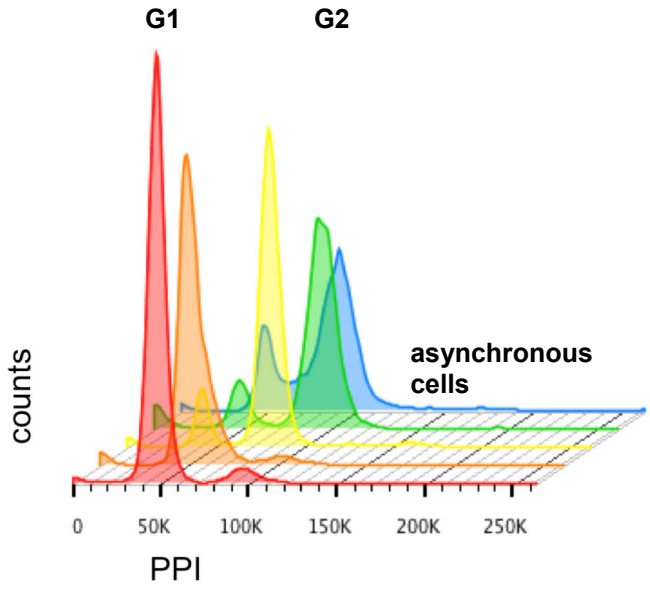

Figure 38: Yeast cells in S-phase progression

Illustrated is the FACS analysis of *bar1Δ* yeast cells (AEY5689) in the S-phase release experiment shown in the results in Figure 22. Cells were monitored throughout S-phase. Yeast cells were arrested in G1-phase and released with pronase into S-phase. S-phase progression was followed using FACS analysis after 0, 20, 40, 60min (red, orange, yellow and green). As control asynchronous cells were used (blue). Cells were stained with PPI.

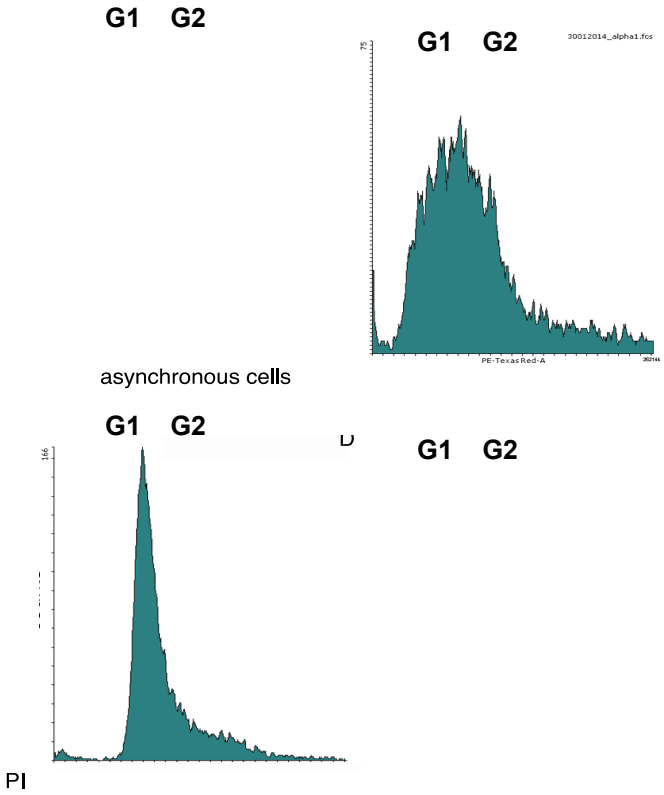

Figure 39: FACS analysis of arrested cells.

FACS profiles of arrested and propidium iodide (PPI) stained yeast cells (AEY 2781) of the indicated cell-cycle phases are depicted. Arrested cells were used for the immunoprecipitation cell cycle experiment shown in the results, Figure 20. **A**: asynchronous cells were used as control. **B**: G1-arrested cells, using nocodazole and α-factor. **C**: Using hydroxyurea, cells were arrested in S-phase. **D**: cells were arrested in G2/M-phase using nocodazole.